Quaternary Science Reviews 262 (2021) 106958

Contents lists available at ScienceDirect

Quaternary Science Reviews

journal homepage: www.elsevier.com/locate/quascirev

Glacial landforms and sediments (landsystem) of the Smoking Hills area, Northwest Territories, Canada: Implications for regional Pliocene – Pleistocene Laurentide Ice Sheet dynamics

D.J.A. Evans [a, *], I.R. Smith [b], J.C. Gosse [c], J.M. Galloway [b]

[a] Department of Geography, Durham University, South Road, Durham, DH1 3LE, England, UK
[b] Geological Survey of Canada, Calgary, Alberta, T2L 2A7, Canada
[c] Department of Earth and Environmental Sciences, Dalhousie University, Halifax, Nova Scotia, B3H 4R2, Canada

ARTICLE INFO

Article history:
Received 18 December 2020
Received in revised form
7 April 2021
Accepted 11 April 2021

Handling Editor: Giovanni Zanchetta

Keywords:
Smoking Hills
Polythermal ice sheet marginal landsystem
Ice stream flowsets
Pliocene glaciation
Glacitectonite
Interlobate ice-dammed lake
Cosmogenic nuclide burial dating

ABSTRACT

The Smoking Hills area in the western Canadian Arctic was purported to contain a regionally rare Quaternary stratigraphic section with multiple, local ice cap-derived tills and a long chronology constrained by palaeomagnetic markers. We present a fundamental revision of previous glacial and magnetostratigraphic interpretations based on detailed sedimentological and structural analyses of the main stratigraphic section and many new exposures, cosmogenic nuclide isochron burial dating, and a systematic reconstruction of the geomorphology and landscape evolution using a glacial landsystem approach. We demonstrate that the Smoking Hills area was fully glaciated during the last (Wisconsinan) glaciation. Previously reported tills ascribed to multiple glaciations represent instead a complex facies sequence of glacitectonic thrust stacking of Laurentide Ice Sheet (LIS) sourced diamictons, glacilacustrine and glacifluvial deposits, together with previously unidentified, poorly-consolidated Cretaceous bedrock rafts and deformed intraclasts. Much of this sedimentation and glacitectonic activity dates to the last (Wisconsinan) glaciation and can be reconciled with a polythermal ice sheet marginal landsystem signature, wherein ice-cored moraine belts are developed over subglacial bedforms (flutings) arranged in discrete flowsets. The flowsets record the complex interaction of ice streams nourished by ice flowing from three main sources: Great Bear Lake to the south, Amundsen Gulf (Franklin Bay) to the east and Liverpool Bay (Mackenzie Valley) to the southwest. Decoupling of the ice margins of these three ice sources gave rise to interlobate ice-dammed lake development over the lower Horton River area during final deglaciation. A cosmogenic $^{26}Al/^{10}Be$ isochron burial age of 2.9 ± 0.3 Ma (1σ, n = 4) from the lowermost glacial diamicton and glacitectonite sequence provides evidence of perhaps the earliest continental glaciation of this region. This deposit postdates, or is perhaps a later re-advance of the same initial glaciation that produced widespread glacitectonic disturbance of bedrock in preglacial valley networks and early glacifluvial and glacilacustrine deposits containing an ice wedge pseudomorph. Subsequent glaciations have largely removed or cannibalised pre-existing records to construct complex till and glacitectonite stacks that contain reworked organics with non-finite radiocarbon ages. One site preserves buried "old" glacier ice in which prominent ice wedges had formed during an interglacial permafrost phase and were then deformed down-flow by the LIS during the Wisconsinan glaciation.

1. Introduction and rationale

It has long been held that the Smoking Hills were only partially glaciated during the Late Wisconsinan (Mackay, 1958; Klassen, 1971; Dyke and Prest, 1987; Rampton, 1988; Mathews et al., 1989; Barendregt and Duk-Rodkin, 2004; Duk-Rodkin et al., 2004; Duk-Rodkin and Barendregt, 2011). Existence of more pervasive ice cover, and a regionally unique record of repeated glaciations (arising from a purported local Horton Ice Cap), dating back possibly as old as early Matuyama Chron (2.58 Ma), was described from a regionally unique Quaternary stratigraphic section reported to preserve 3–5 tills and various inter-till/interglacial deposits

* Corresponding author.
E-mail address: d.j.a.evans@durham.ac.uk (D.J.A. Evans).

https://doi.org/10.1016/j.quascirev.2021.106958

(Fulton and Klassen, 1969; Yorath et al., 1975; Barendregt and Duk-Rodkin, 2004; Duk-Rodkin et al., 2004; Duk-Rodkin and Barendregt, 2011). Correlations were made between these deposits and those on Banks Island, where similar arguments for restricted Late Wisconsinan Laurentide (continental) ice cover and the existence of multiple old glaciations had been made (cf. Vincent, 1983, 1990; Vincent et al., 1983; Barendregt and Vincent, 1990; Duk-Rodkin et al., 2004).

Fundamental revisions to the understanding of the Quaternary glacial history on Banks Island now refute the previously proposed chronostratigraphy and demonstrate that all of Banks Island was inundated by the Laurentide Ice Sheet (LIS) during the Late Wisconsinan (England et al., 2009; Lakeman and England, 2012, 2013, 2014; Evans et al., 2014; Vaughan et al., 2014). Carrying this into the broader regional context, evidence for pervasive glaciation and dynamic ice streaming in the western Canadian Arctic (Clark, 1997; Stokes et al., 2006, 2009, 2012) and from marine seismic and stratigraphic records (Batchelor et al., 2013a, b; 2014; MacLean et al., 2015; Lakeman et al., 2018), demonstrates that Late Wisconsinan LIS extended through Amundsen Gulf onto the Banks – Beaufort Shelf and shelf margin. This has progressively led to glaciological models and reconstructions that now imply by proxy the complete inundation of the Smoking Hills area by the Late Wisconsinan LIS (cf. Tarasov et al., 2012; Dalton et al., 2020 and references therein). The goal of this study was thus to return to the Smoking Hills in order to conduct a rigorous re-examination of the regional glacial landsystems and the chronostratigraphic record of Quaternary glaciations of the western Canadian Arctic. Regional geomorphological features were resolved using previously unavailable high resolution DEM imagery and cosmogenic nuclide burial dating was used to constrain proposed old glacial chronologies.

The Smoking Hills area was also reported to contain the southern-most occurrence of the Neogene fluvial Beaufort Formation (Yorath et al., 1975), although this was questioned by Mathews et al. (1989). Further, contradictory chronostratigraphic linkages between these "probable" Beaufort Formation plateau-cap deposits and a basal gravel sequence underlying the main Quaternary section (our section HR 1, discussed below) also needed to be addressed as it is critically linked to understanding the historic fluvial and glacial landscape evolution (cf. Mathews et al., 1989; Matthews and Ovenden, 1990; Duk-Rodkin and Hughes, 1994; Duk-Rodkin et al., 2004; Smith and Evans, 2018).

2. Study area and previous research

The Smoking Hills (69°15′N; 127°00′W) are a bedrock upland composed of poorly-consolidated Cretaceous strata that rise to ~380 m above sea level (asl; Fig. 1a, b, c). Upland areas of the Smoking Hills are deeply dissected by the Horton River and are bounded to the west by the Anderson River and to the east by Franklin Bay and Amundsen Gulf (Fig. 1a and b). River drainages illustrate strong rectilinear channel diversions that are not related to bedrock structure, but instead demonstrate the significant role glaciation(s) have played in altering their course (Mackay, 1958; Klassen, 1971; Rampton, 1988). The Horton River floodplain is renowned for its spectacular meander loops, one of which has broken through the coastal bluffs along Franklin Bay to form a large marine delta, cutting off the northern 100 km course of the river into Harrowby Bay (Fig. 1b; Mackay, 1958; 1981). The region is underlain by continuous permafrost, and treeline extends locally to approximately 69°N (further north along the lower slopes of the Horton River and its tributaries); terrain is otherwise blanketed by mixed shrub tundra and sedge meadow.

The area is most renowned as the site of spontaneously combusting mudrock (bocannes) of the Smoking Hills Formation, characterised by emissions of water vapour and sulphuric acid gases (Selwyn, 1877; Dawson, 1881; Crickmay, 1967; Mathews and Bustin, 1984; Grasby et al., 2019). Long known to Indigenous peoples, the first written record was by Sir John Richardson of the second Franklin overland expedition (Richardson, 1828), who accurately identified the cause as oxidation of abundant, finely disseminated pyrite, and the combustion of organic-rich shales (mudstones); analagous to the historical alum shale works along his native Yorkshire coast. Bocannes form only in the slumped material in landslides, suggesting that there is a critical mechanism of degrees of oxidation and/or the intermixing of strata required. Former and active bocanne sites are recognised by brightly-coloured brick red to orange clinker and paralava deposits, and are found throughout the extents of the Smoking Hills Formation bituminous member (Yorath et al., 1975; Yorath and Cook, 1981), extending from Franklin Bay west past the Anderson River (Fig. 1b). The landslide material is critical to the provision of matrix, as well as bedrock rafts, for the local clay-rich and very fine silt-rich tills.

Mackay (1958) made the first investigations of the regional Quaternary glacial history, examining aerial photographs over a large area, and focussing field investigations in areas south of Paulatuk. Reconnaissance Quaternary investigations in the Smoking Hills themselves were first conducted by Klassen (Fulton and Klassen, 1969; Yorath et al., 1969, 1975), who discovered and logged a unique Quaternary section (our HR 1) along a tributary of the Horton River. This section was reported to be 45 m thick, and was floored by fluvial sands and gravels, which were overlain by at least 3 tills. Klassen suggested that this site lay beyond the limits of the Late Wisconsinan glaciation, but made no chronostratigraphic division of the units he identified, reporting only that peat beds (later dated at >41 000 ^{14}C yr BP; GSC-1100; Lowdon et al., 1971) found below his uppermost till appeared to be at the same stratigraphic elevation (~205 m asl) as those recovered from a different section 1.6 km up a tributary valley that contained wood dating >38 100 ^{14}C yr BP (GSC-576; Lowdon et al., 1971). Klassen's section (HR 1) was then revisited by Vincent (1988, 1991; unpublished Geological Survey of Canada (GSC) field notebooks), where wood and other organic samples for palynological analyses were collected from the basal sand and gravel unit, 900 m up-stream of the main section. Results reported by Matthews and Ovenden (1990) suggest a Tertiary age for this basal sand and gravel unit (note that at that time the Pliocene Epoch ended at 1.8 Ma). Vincent (1988) conducted palaeomagnetic measurements on the stratigraphy, indicating a basal, magnetically normal till overlain by a magnetically reversed lacustrine deposit and till, and then a magnetically normal till at the top (in Duk-Rodkin et al., 2004; their Fig. 18). In 2004, this site was revisited by Duk-Rodkin and Barendregt (2011) where they conducted extensive palaeomagnetic sampling, indicating that the basal sand and gravel was reversely magnetized (interpreted to represent the Matuyama Chron; 0.78–2.58 Ma). They went on to state that these basal "pre-glacial" gravels were overlain by 3 magnetically reversed tills, separated by 2 silty-clay "lacustrine/interglacial" deposits (also reversely magnetized), which were then capped by a normally magnetized collection of lacustrine-palaeosol-mudflow deposits, in turn capped by a normally magnetized till (Brunhes Chron?; 0–0.78 Ma; Duk-Rodkin and Barendregt, 2011). They maintained that Canadian Shield erratics (i.e. granitic or gneissic material), indicative of a continental-style Laurentide glaciation, were only found scattered on the uppermost surface of the section (HR 1). In their absence, they argued that all underlying diamictons originated from a local "Horton Ice Cap" source (Melville Hills; Fig. 1a; Barendregt and Duk-Rodkin, 2004; Duk-Rodkin et al., 2004; Duk-Rodkin and Barendregt, 2011) and that Laurentide ice was responsible for depositing only the uppermost surface lag.

3. Methods

Geomorphological mapping was undertaken on ArcticDEM hillshade imagery (Porter et al., 2018), viewed under oblique and vertical perspectives using various illumination aspects and elevations, in combination with stereo aerial photographs and Google Earth imagery. This facilitated the identification of discrete debris assemblages and kettled terrain likely to be of glacial origin, streamlined landforms (flutings) of subglacial origin, major eskers of subglacial/englacial origin, and underfit or dry valleys considered to be of glacial meltwater or glacial lake spillway origins.

In order to verify the genetic origins of the Quaternary deposits, the stratigraphy and sedimentology of natural exposures were evaluated over a two week, helicopter-supported field program using standard procedures outlined in Evans and Benn (2004). Individual lithofacies are described in detail in vertical sediment logs and/or annotated photomosaics, which were compiled based on the identification of separate lithofacies according to bedding, texture, lithology and sedimentary structures. The lithofacies are described and classified according to a modified scheme of Eyles et al. (1983), incorporating additions proposed by Evans and Benn (2004), and Evans (2018).

Clast macrofabrics were measured in diamictons using 50 clasts per sample for the analysis of strain history and till genesis; each sample was confined to small areas within each lithofacies in order to accurately reflect local variability in sediment properties (cf. Benn, 2004a; Evans, 2018). Fabric data were plotted on spherical Gaussian weighted, contoured lower hemisphere stereonets, using Rockware™ software. Statistical analysis was undertaken using eigenvalues (S1–S3), based on the degree of clustering around three orthogonal vectors (V1–V3), presented in fabric shape ternary diagrams (Benn, 1994).

Debris modification and hence former geomorphic processes were evaluated using clast form analyses (shape and roundness), conducted on 50 clasts at field sections concurrent with clast macrofabric measurements and undertaken on granitic, gneissic and other igneous/metamorphic lithologies. Surface features such as striae and faceting were also noted for each sample because they are diagnostic indicators of glacial abrasion (cf. Sharp, 1982; Krüger, 1984; Benn, 2004b). Clast form analyses were also conducted on 50 of the largest clasts (>16 mm diameter) recovered from ~28 kg (5 gallon pail) bulk samples of diamict and "Beaufort Formation" plateau gravel deposits, collected for heavy indicator mineral studies (Smith and Evans, 2018).

Analysis of the clast form data followed the procedures outlined in Benn (2004b) and involved: a) calculation of the C40 index (the

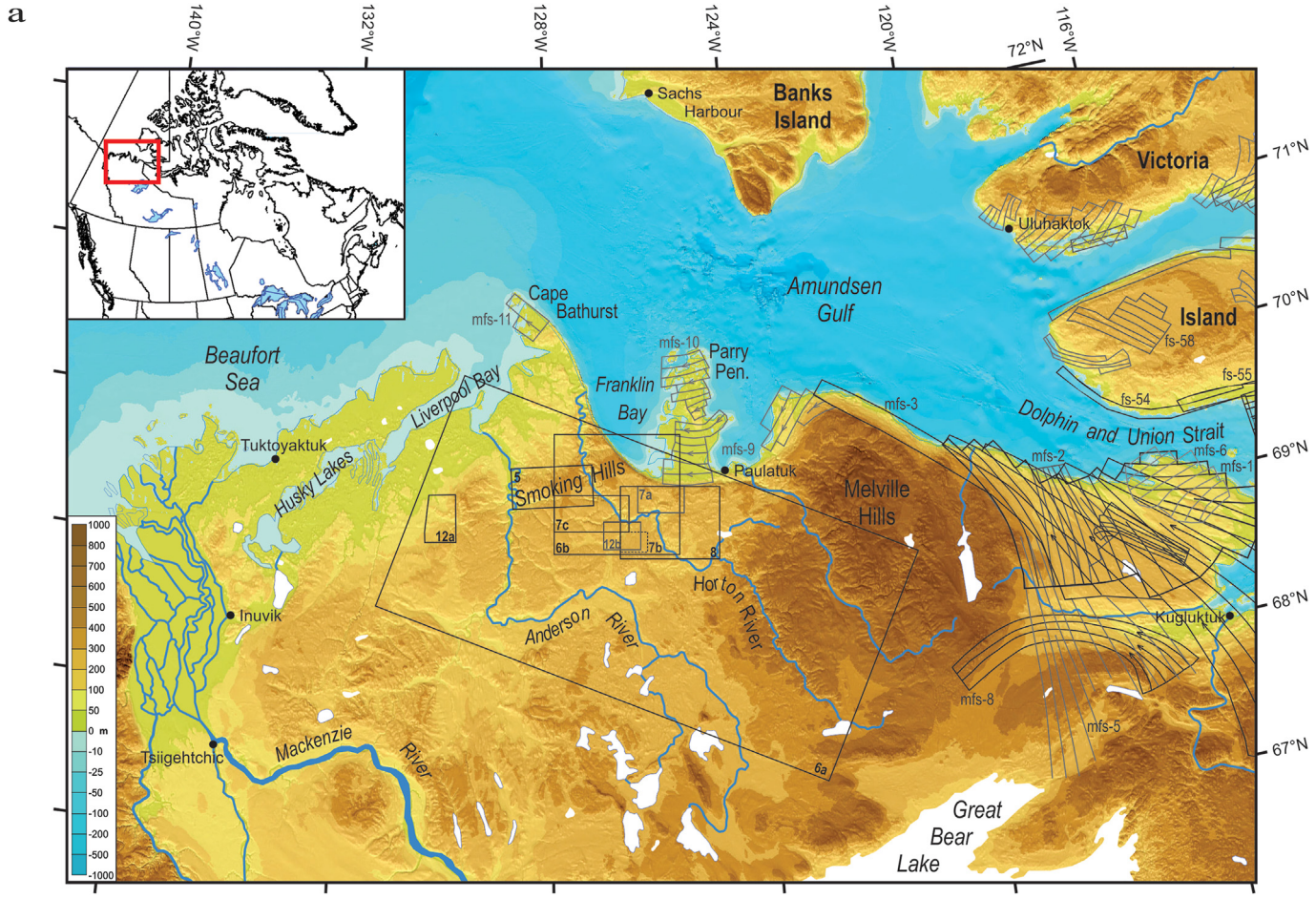

Fig. 1. a) Location map of the Smoking Hills study area, northwestern Arctic Canada. Regional ice stream flow-sets and labels reproduced from Stokes et al. (2006). Location of figures outlined by boxes. Basemap image from IBCAO topographic and bathymetric model (Jakobsson et al., 2012); b) location map with regional bedrock geology; extent of granitic Canadian Shield terrain indicated in pink in upper left index map. Historical ice margin reconstructions illustrated by coloured lines; c) oblique ArcticDEM image looking southeast across the field area. This view shows the incised nature of the Horton River as it crosses the Smoking Hills upland surface in the middle distance, a stretch of the river labelled the "Horton Gap" by Mathews et al. (1989), and their "swale" valley that we instead correlate with a prominent meltwater channel flowing westward from an Amundsen Gulf (Franklin Bay) ice mass, and a second meltwater channel (MWC) trending northward. Inset maps show study area location in Canada. (For interpretation of the references to colour in this figure legend, the reader is referred to the Web version of this article.)

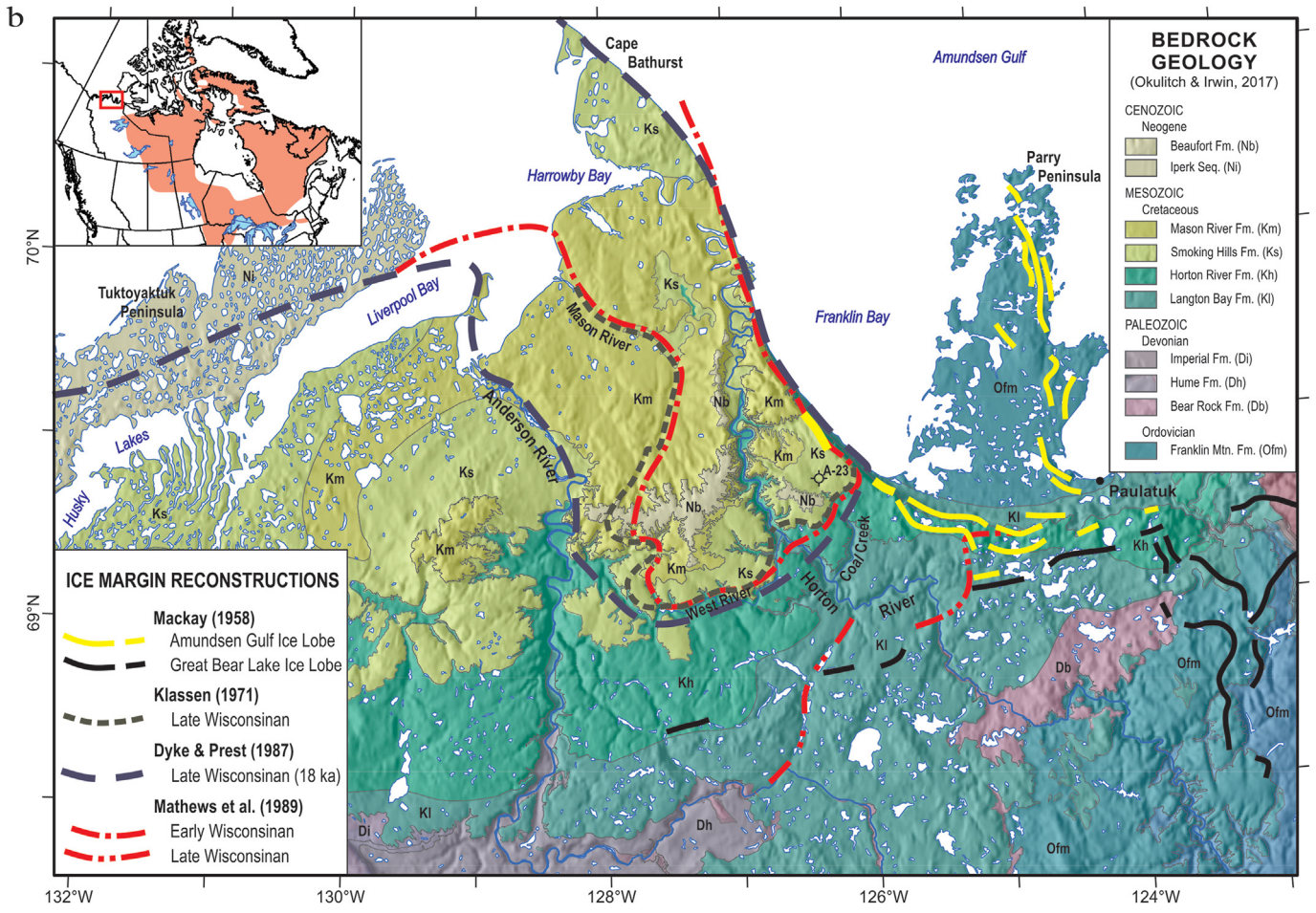

Fig. 1. (*continued*).

percentage of clasts with a C:A axis ratio of <0.4; Benn and Ballantyne, 1993); b) clast roundness (Powers, 1953), used to calculate the RA summary index (percentage of angular and very angular clasts within a sample; Benn and Ballantyne, 1993), and the RWR summary index (percentage of rounded and well-rounded clasts; Benn et al., 2004; Lukas et al., 2013); and c) mean roundness (AvR), based upon a numerical classification of Powers roundness as VA = 0 to WR = 5 (cf. Spedding and Evans, 2002; Evans, 2010). Co-variance plots (Benn and Ballantyne, 1994) were used to compare clast form results with different glacial sediment types from the Canadian High Arctic, all based on similar lithologies (Supplementary data S1).

Clast lithologies were documented in the field or were observed under a microscope using oxalic acid-washed clast samples recovered from bulk samples. While rare far-travelled erratics were recognised (e.g. Canadian Shield-derived granitic material), most lithologies reflected regional bedrock compositions which are summarized based on Yorath et al. (1969, 1975), Yorath and Cook (1981), Okulitch and Irwin (2017), and Rainbird (2019a, b). Cretaceous bedrock in the Smoking Hills area is composed generally of poorly consolidated shale, siltstone, mudstone and sandstone, and would have contributed little clast material within diamicts other than minor sandstone and concretionary ironstone and limestone, but likely make up a significant component of diamict matrices. Regional Devonian strata would have provided variably coloured siltstones, sandstones, shale and limestone. The Ordovician strata exposed on Parry Peninsula and southeast of Smoking Hills (Fig. 1b) would have sourced black, grey and red chert, dark grey-green argillite, shale, sandstone, quartzite, quartz, limestone and dolomite. A host of other lithologies, including diabase dykes and sills occur in areas of the Coppermine Arch, situated immediately east of Fig. 1b (Rainbird, 2019a, b), and granitic, gneissic and other igneous/metamorphic lithologies originating from areas of the exposed Canadian Shield (see index map on Fig. 1b). While lithology counts are based on 50 clast sample sizes, scans were made of the entire >2 mm bulk sample clasts in order to identify the presence of rare Canadian Shield erratic lithologies, important in consideration of regional ice-flow reconstructions.

Samples of diamicton matrix were also collected from exposed sections for physical sedimentological characterization and chemical analysis. Samples were processed at the GSC Sedimentology Laboratory (Ottawa, ON) according to standard GSC procedures (McClenaghan et al., 2013; Supplementary data S2).

Samples of interpreted bedrock rafts collected from section HR 1 were analyzed for palynology at the GSC Palynological Laboratory (Calgary, AB) in order to help resolve their nature and age. Palynological samples were prepared using standard procedures, including acid maceration with HCl and HF, and oxidative treatment with Schulze's solution (Traverse, 2007). Resulting slurries were permanently mounted on glass microscope slides using liquid bioplastic. Pollen and spores were counted and identified to the lowest possible taxonomic level in un-sieved preparations using a transmitted light Olympus BX61 microscope at 400x and 1000× magnification under oil immersion. The −20 μm fraction was also scanned for age-diagnostic angiosperm taxa.

Small shell fragments of unknown marine bivalve mollusc species (n = 1–9; 3–14 mm long; ≤0.21 g in mass) were identified in all but one of the diamicton samples (18SUV502) from section HR 1, but in none of the plateau gravel samples. A juvenile gastropod was also recovered from the uppermost diamicton sample (18SUV512). Vincent (1988) also noted shell fragments in till from this section. Five mollusc shell fragments from 3 of the diamicton samples (5, 7 and 36 m depth) and the gastropod were submitted for radiocarbon dating in order to potentially provide finite limiting ages for the various diamictons (Supplementary data S3). Samples had been oxalic acid-washed during processing of the bulk sample gravel fractions in order to remove iron staining. Additional acid leach and physical scraping of discoloured outer material was undertaken by the A. E. Lalonde AMS Laboratory (Ottawa, ON). A sample of the inner core of a rooted tree stump from a glacially rafted deposit in our section HR 4 (discussed below) was also submitted for radiocarbon dating.

Cosmogenic nuclide burial dating was undertaken on collections of quartz sandstone/quartzite/crystalline cobbles and density separates of quartz-rich sand from several diamictons and the basal gravel unit in section HR 1, and the basal gravel in our section HR 2 (discussed below). The units sampled are currently buried under a cover of at least 20 m (bulk density ~2.1 g cm^{-3}) and receive less than 1% of the surface production (even less when ice covered) and therefore are effectively shielded. We analyzed ten samples from deeper than 35.5 m below the 229 m asl upper surface in section HR 1, and one sample from 20 m depth in HR 2 with surface elevation 230 m asl (Supplementary data S4). The deepest samples in both sections are from a lithostratigraphically-correlated gravel, so their burial ages are assumed to be equivalent. Although the sampled units are deeply buried, the region has undergone multiple glaciations including the last, and therefore it is possible that the diamicts accumulated over many glacial-interglacial periods with unknown amounts of erosion and re-deposition of the samples that we collected. Recognizing that the depositional history of the samples was not ideal for either simple burial or isochron burial dating (cf. Gosse and Philips, 2001; Balco and Rovey, 2008), we sampled cobbles and sand samples to attempt both burial dating methods. Larger quartz sandstone/quartzite cobbles were dug from sites in and around (40 cm vertical) the location of each bulk diamict sample and the basal sand and gravel units. Quartz sand separates were produced by Overburden Drilling Management (ODM; Ottawa, ON) during processing of samples for recovery of heavy indicator minerals (Supplementary data S4). Samples were submitted to CRISDal Lab (Dalhousie University) for processing of accelerator mass spectrometer (AMS) targets. Quartz purification included crushing, grinding, and sieving of cobbles and pebbles with masses of multiple cobbles to ensure sufficient quartz for digestion (some cobbles had less than 20% quartz; Supplementary data S4, Table S4.1). Analytical procedures are outlined in Supplementary data S4.

Two cosmogenic isotope burial dating approaches were used to determine the duration of time since the buried units were deposited: (i) *simple burial dating*, and (ii) *isochron burial dating*. Both approaches use measurements of ^{10}Be and ^{26}Al in buried quartz sediment. *Simple burial dating* is used when it can be assumed that burial was relatively rapid (i.e. shielding from cosmic rays took less than 10% of the total burial duration) and when there is only one burial duration. If the quartz sample experienced multiple discrete burial and exposure events, the grains would not have the assumed surface production ratio of $^{26}Al/^{10}Be$ prior to the ultimate burial, and the apparent burial age would over-estimate the last burial duration of interest. The ^{26}Al and ^{10}Be measured in the shielded quartz grains is assumed to have been produced prior to deposition, and because shielding is assumed instantaneous, there is no post-depositional production, and the $^{26}Al/^{10}Be$ rate decreases at a rate controlled by their decay rates (Supplementary data S4). Quartz from individual cobbles or amalgamated quartz sand can be used. Their concentrations are typically plotted on a $^{26}Al/^{10}Be$ vs log normalized ^{10}Be concentration plot and a most probable age is determined by convolving the probability distribution function for all samples. *Isochron burial dating* is based on defining a best fit curve through all samples on a ^{26}Al vs ^{10}Be plot (e.g. Erlanger et al., 2012). The difference between its slope and 6.75 production ratio is proportional to burial duration. This method is useful in the

instance where shielding was neither instantaneous nor complete, in which case there will be a positive y-intercept (^{26}Al). We use a program provided by D. Granger (cf. Erlanger et al., 2012) which provides a recursive correction for post-depositional production based on the ^{26}Al intercept value. Both methods require a sufficient buildup of ^{10}Be and ^{26}Al to survive decay during burial, otherwise the large uncertainty controlled by counting statistics during their AMS measurement would prohibit an age calculation. In instances where clast ratios vary significantly (owing to measurement error or geological process), where burial histories may involve thick erosion events, or where the source regions are eroding quickly and therefore pre-depositional concentrations of one or both of the isotopes are low, it may not be correct to assume that post-depositional production explains the computed y-intercept. As this may be the case here, the approach benefitted from deeply shielded samples.

4. Results

4.1. Geomorphology

4.1.1. Modern processes and forms

The modern and historical geomorphology of the study area (Fig. 2) is important to review at this juncture because it has significant implications for later interpretations of the Quaternary glacial geology. Deeply incised river valleys and dense networks of steep-walled tributary valleys and locally developed badlands (Fig. 2a and b) are the products of intensive fluvial and glacifluvial erosion of poorly-lithified Cretaceous bedrock.

The depth and continued rapid rate of fluvial incision of this landscape gives rise to widespread large landslides, which are rotational and translational in character (Fig. 2c and d) and, due to the nature of the bedrock, often quickly disaggregate, developing into debris flows downslope (Fig. 2f and g). This process is critical to the initiation of bocannes (Fig. 2c, f, g). As debris flows progress downslope, new bocannes form as the bedrock material is progressively churned and exposed (Fig. 2g).

Field observations of active layer detachment slides and retrogressive thaw flow slides triggered by melting of buried ground ice and glacier ice are widespread and are also responsible for the movement of large volumes of Quaternary deposits into valley floors (Fig. 2e, h). In combination, the various landslides of the Smoking Hills area result in the amalgamation of bedrock masses and Quaternary deposits forming partial valley fills. This process was likely also prevalent in preglacial and interglacial valleys, and as will be discussed, is important in comprehending various glacigenic depositional and tectonic features seen in this study.

4.1.2. "Beaufort Formation" plateau gravels

4.1.2.1. Description and previous interpretations. Gravelly sediments that form flat-lying to gently inclined summits on higher terrain between the main river channels (Fig. 1b (unit Nb), 3) were considered by Yorath et al. (1969, 1975) to be probable Beaufort Formation deposits. The Beaufort Formation (Miocene to Pliocene-Pleistocene) forms a prominent accretionary wedge of unconsolidated sediment fringing the western islands of the Canadian Arctic Archipelago. It thickens westwards into the Beaufort Sea and was considered to have formed by rivers flowing generally northwestward across what was then a contiguous arctic coastal plain (Tozer, 1956, 1960, 1960; Craig and Fyles, 1960, 1965, 1965; Thorsteinsson, 1961; Thorsteinsson and Tozer, 1962; Hills, 1969; Kuc and Hills, 1971; Miall, 1979; Vincent, 1983, 1990, 1990; Fyles, 1990; Devaney, 1991; Fyles et al., 1994; Williams et al., 2008). The type locality occurs on Prince Patrick Island, and was described by Tozer (1956) as comprising cross-bedded quartz sand and well-rounded fine to medium gravel, containing much unlithified and uncarbonized fossil wood. Several other terrace gravels, interbedded silt, and organic detritus-rich and peat bed sites on Melville, Axel Heiberg and Ellesmere islands, and on the mainland northeast of Inuvik, bordering the Mackenzie River, are now considered contemporaneous deposits, or Beaufort-equivalents *sensu lato* (Thorsteinsson, 1961; Tozer, 1970; Balkwill and Bustin, 1975; Wilson, 1976; Norris, 1981; Yorath and Cook, 1981; Bustin, 1982; Hodgson et al., 1984; Fyles, 1989, 1990, 1990; Fyles et al., 1994; Davies et al., 2014).

In the Horton River area, Yorath et al. (1969, 1975) reported a uniform 2.5–3 m thick unconsolidated gravel and sand deposit, on plateau surfaces between the Anderson and Horton rivers and between the Horton River and Franklin Bay. They characterized these as being composed of low-angle sandy foreset beds with a wide range of palaeocurrents, but predominantly a northwesterly transport direction, with clast lithologies of mainly quartzite, dolomite, and black chert pebbles and cobbles, and small wood fragments and humic materials. These deposits were reported to form a flat, featureless plain (Fig. 3a), with exposures along a north to south transect at elevations between 183 and 335 m asl (Yorath et al., 1975). Based largely on lithological and sedimentological comparisons with descriptions of the Beaufort Formation on Banks Island (Thorsteinsson and Tozer, 1962), Yorath et al. (1969, 1975) suggested that these Smoking Hills plateau-cap deposits were probably correlative.

Our clast lithological data from six sites of gravelly sediments on the uplands (Fig. 4a) reveal a dominance of chert, sandstone, quartzite, quartz, and dolomite with rare clasts of ironstone and Canadian Shield-derived granitic clasts, similar to those reported by Mathews et al. (1989). Additionally, our clast form data (Fig. 4a) reveal that the gravel is similar in geomorphic provenance to that of High Arctic glacifluvial and till control samples, especially with respect to RA, RWR and AvR values (Fig. 4b; Supplementary data S1). Additionally, numerous boulder and cobble-sized clasts display surface striations and bullet-shaped/faceted forms indicative of subglacial wear patterns (Fig. 3e).

Evidence of other ancient channel forms in the area include that reported by Mathews et al. (1989), who describe a 145 m thick buried channel fill of "sandy and locally pebbly sediment with rare plant fragments" overlying Cretaceous bedrock at the Arco Smoking Hills A-23 well site (Figs. 1b; 69.36833°N; 126.34167°W). Our re-examination of both the petroleum well log and the archival washed cuttings questions aspects of their interpretation. From surface down to 330' (100 m) the cuttings are mostly subangular to angular lithic sand and gravel-sized ($\leq$1.2 cm diameter) sandstone (multiple colours and grain sizes) and black and red chert. Lithologies such as dolomite, limestone and ironstone are unrecognized, but may be present in small amounts. Part of the angularity of the larger fragments likely reflects the drilling process. However, the overall nature of the material is characteristic of well cuttings of glacial diamict washed over a shaker table, i.e., there is not the degree of rounding expected in a far-travelled fluvial deposit, as might be suspected for an ancient buried channel crossing the upper plateau surface. Between 100 and 145 m depth, the chip records reveal more fine grained quartz sand, coal/bitumen, rare plant and shell fragments, shale and siltstone material characteristic of a mix of Mason River and other local Cretaceous bedrock material (Yorath et al., 1975). So, rather than a buried channel, the A-23 well site, which is situated about 200 m away from the confluence of 2 streams, appears to coincide with a 145 m combined colluvial and glacial valley fill, possibly a hummocky ridge.

Mathews et al. (1989) also identified what they called the "swale" as a broad erosional valley (~275-200 m asl; Fig. 1c), suggesting it was likely a major tributary, if not the original head of the

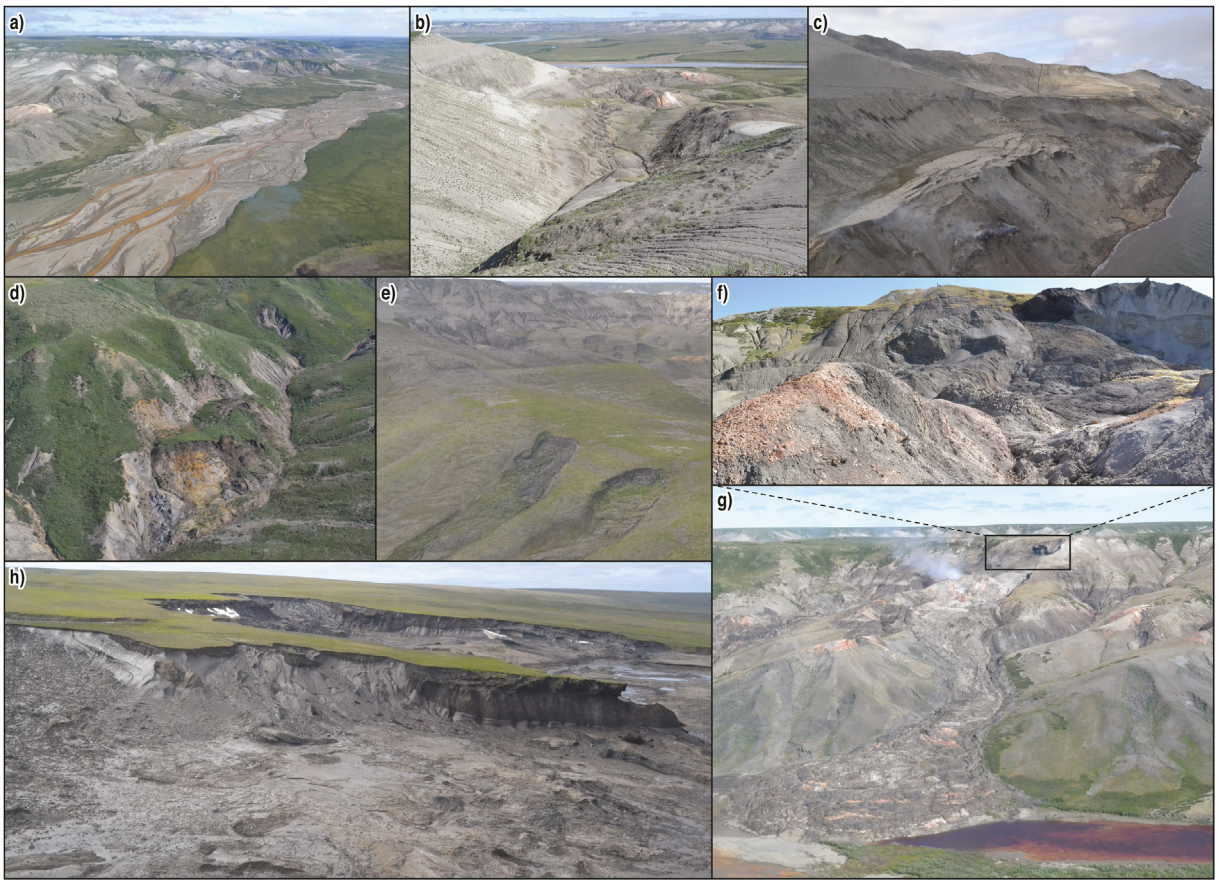

Fig. 2. Examples of the modern and historical geomorphology of the study area: a) braided river floodplain and adjacent badlands (West River); b) steep-walled tributary valleys and gullied bedrock with localised badlands (west of Horton River); c) translational to rotational landslide in Cretaceous bedrock overlain by Quaternary deposits on the Franklin Bay coast; bocannes in the lower slopes; d) small translational landslide that has delivered fragmented bedrock blocks and Quaternary deposits to the floor of a small Horton River tributary valley; e) active layer detachments slides west of Franklin Bay; f) large translational landslide developed below a Smoking Hills Formation headwall exposure (lower Horton River); g) landslide in f (above) that has disaggregated downslope and developed into a debris flow. Note the development of active and former bocanne sites marked by colourful clinker deposits; h) extensive retrogressive thaw flow slides triggered by active layer detachments and exposure of buried glacier ice, visible in the headwalls of failure scarps, west of Franklin Bay.

lower Horton Valley. Based on review of ArcticDEM imagery (Porter et al., 2018) and field investigations we question this interpretation. Instead we argue that the larger valley form was created by glaciers funnelling westward from Franklin Bay, and that the most prominent feature of "the swale" is an ice-contact glacial spillway which has deeply incised the bedrock landscape 40–100 m below the 200 m asl level. A second ice-contact spillway in the same general area, flows northward, sub-parallel to the Franklin Bay coast (Fig. 1c; MWC).

4.1.2.2. Interpretation. The Tertiary (Neogene) fluvial (probable Beaufort Formation) origin of Yorath et al.'s (1969, 1975) "plateau-cap fluvial sediments" is questionable for several reasons. First, Mathews et al. (1989), in a palynological study of gravel deposits at two sites along the plateau rim, recognised a Pleistocene interglacial flora, placing them much younger than the age range previously proposed for Beaufort Formation deposits. They also note the absence of pollen of hardwoods, typically associated with Beaufort Formation sediments in the Arctic Islands (Hills, 1969). Second, clast form data and the presence of faceted and striated clasts strongly suggest a glacifluvial input, whereby local tills have been transported short distances (Figs. 3e and 4b). Third, Mathews et al. (1989) indicated that the lateral extent of the plateau-cap sediments was difficult to ascertain, and that precise delimitation beyond that originally proposed by Yorath et al. (1975) would require much more detailed mapping. Indeed, Klassen (1971) did not identify these upland gravel deposits on his surficial geology map of the area, characterizing the cover instead as bedrock and hummocky terrain (till and in parts gravel). Our comprehensive fieldwork demonstrates that the aerial extent of these plateau gravel deposits, particularly along the broad western arc extending from Horton River to Anderson River, and also the arc extending eastward of the Horton River, is considerably less than was illustrated by Yorath et al. (1975; Figs. 1b (unit Nb), 5). Where pervasive cover was depicted in the western arc, we found instead widespread weathered residuum of Mason River bedrock and a discontinuous veneer, locally up to blanket cover (>2 m thick), of thermokarsted glacial sediments, both of which have been in places glacially streamlined. Within the western arc, actual glacifluvial sand and gravel deposits are isolated (2–5 m thick), and include terraces prograding not only northwestward, but also southwestward as a series of descending kame terraces fed by ice-contact streams cutting laterally across slope (Fig. 5, white arrow). In the eastern arc (east of Horton River; Fig. 1b), similar features trend southeast into the West River and Coal Creek basins. The aerial extents mapped by Yorath et al. (1975) largely mimic the bounds of more indurated ferruginous shale beds of the middle member and siliceous and ferruginous shale beds of the lower member of the Mason River Formation (Yorath et al., 1975), particularly along the more dissected north margin of the western arc (Fig. 5). It appears

Fig. 3. Plateau gravel deposits ("Beaufort Formation") and landforms: a) typical orange-stained gravel cover (5–10 m thick) overlying pale Mason River Formation grey shale and mudstone; view looking north, Horton River at right; b) ground view of gravel surface; sample site 18SUV018; c) and d) typical exposures and clast sizes; note, d) shows collection of pebbles, cobbles, and small boulders (beside pail) from a sieved (<2 mm) sample collection – 18SUV522; e) glacially faceted quartzite clast with surface striae. (For interpretation of the references to colour in this figure legend, the reader is referred to the Web version of this article.)

that the "softer" texture of this weathered bedrock residuum on aerial photographs and the ArcticDEM imagery (Fig. 5) largely conforms to the bounds delineated by these resistant beds. Along the southern margin of the western arc, the bounds of the lower member resistant beds also broadly parallel the geological contact between the Mason River and Smoking Hills formations, supporting a topographic (resistant bed) association.

The extents of thick (5 to ≤20 m), orange-stained gravel and

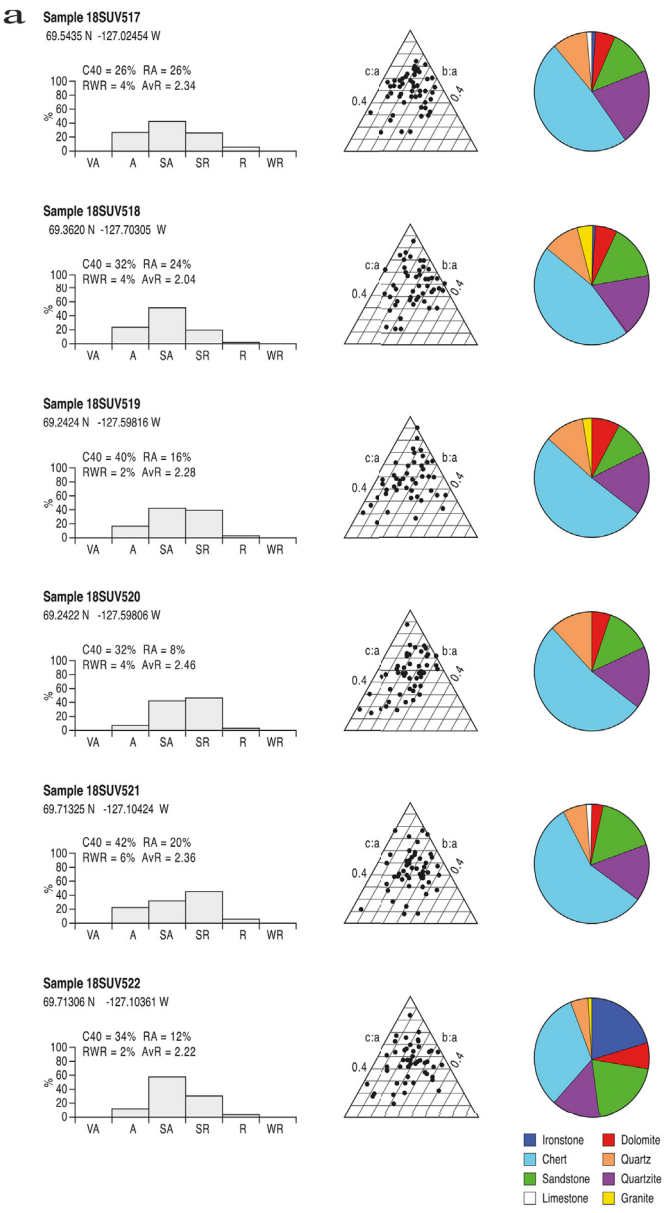

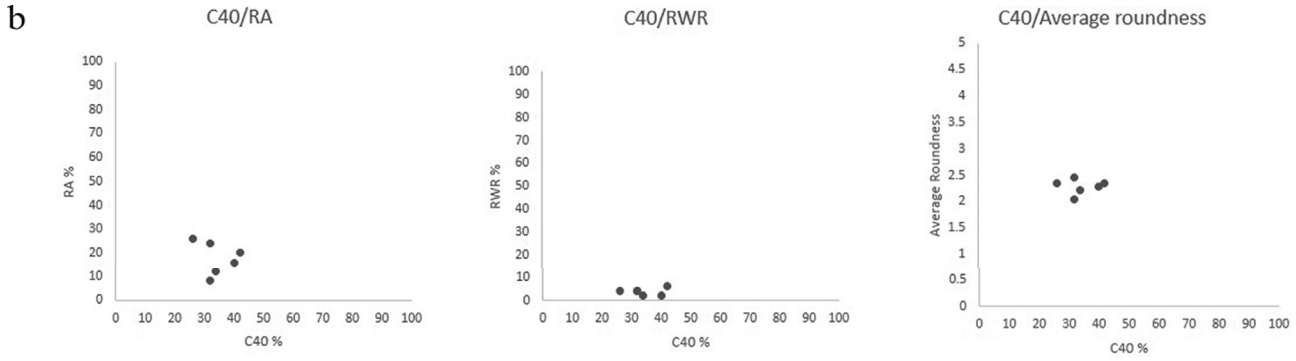

Fig. 4. Plateau gravel deposit ("Beaufort Formation") clast form and lithology data: a) roundness data histograms, clast shape ternary plots and clast lithology pie charts; b) co-variance graphs for the clast form data.

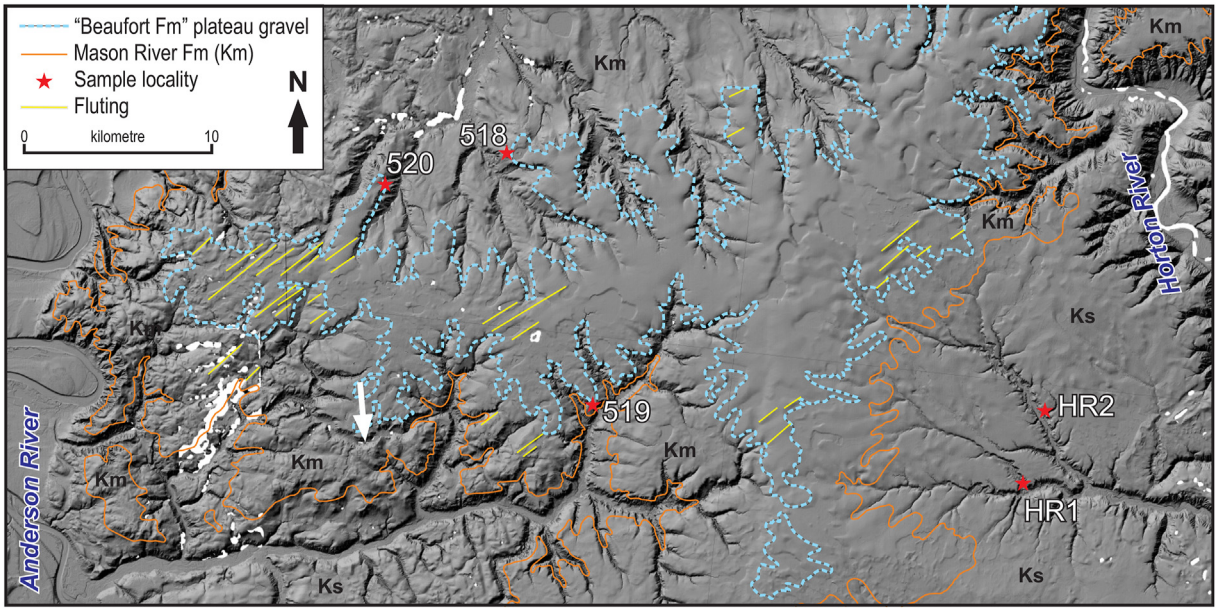

Fig. 5. Extents of the western arc of probable "Beaufort Formation" plateau gravel delineated by Yorath et al. (1975) and those of the Mason River (Km) – Smoking Hills (Ks) formations geological contact (Okulitch and Irwin, 2017). Many of the crenulated northern margins are defined by more indurated Mason River beds. Sites 518 (see Figs. 3b) and 520 mark sample sites from isolated glacifluvial terraces accordant with a southward retreating ice margin. Site 519 marks a kame terrace, one of several preserved at different elevations along these south-facing slopes. These, and lateral meltwater channels (e.g. white arrow) that cut laterally across interfluves, record a southward and descending glacier profile. Base image is an ArcticDEM hillshade model (Porter et al., 2018).

sand paralleling the west side of the Horton River valley, north of the western arc (Figs. 3 and 5), are closer to those demarcated by Yorath et al. (1975), but even here deposits are more discontinuous and laterally less extensive (again apparently including the resistant Mason River Formation beds). Similar gravel deposits are also found along the eastern edge of the Horton River valley in the area opposite the western arc (Mathews et al., 1989). It is readily apparent to us that the gravel deposits bordering the lower Horton River valley geomorphologically correspond to ice-contact kame and outwash terrace deposits, prograding northwestward (Figs. 1b and 3).

Yorath et al.'s (1969, 1975) plateau cap gravels have also, we argue (Smith and Evans, 2018), been incorrectly contextually linked with gravel deposits at the base of section HR 1 that lies at much lower altitudes in the landscape (172–178 m asl) compared to 280–340 m asl for "Beaufort Formation" extents 15–20 km northwest of this site (Fig. 5; Fulton and Klassen, 1969; Vincent, 1988, 1991; Matthews and Ovenden, 1990; Duk-Rodkin and Hughes, 1994; Barendregt and Duk-Rodkin, 2004; Duk-Rodkin et al., 2004; Duk-Rodkin and Barendregt, 2011). Faceted and rare striated clasts were found by us in the basal gravels at the HR 1 and HR 2 sections (and others in this drainage basin). Also, while it may not require direct glacifluvial deposition, the lithological makeup of these basal gravels requires glacial transport of erratic bedrock materials from the east and, at a minimum, local fluvial reworking of glacial materials. We will argue below that the basal gravels at sections HR 1 and 2 must have infilled pre-existing valleys that drained eastward into a proto Horton River, and that the plateau ("Beaufort Formation") gravels are instead a much later (and unrelated) glacial deposit.

4.1.3. Glacial geomorphology

4.1.3.1. Description and previous interpretations. The glacial landforms identified at a regional scale (Fig. 6a and b) comprise two major components; hummocky ice-cored terrain, and fluted or streamlined terrain. The hummocky ice-cored terrain comprises broadly arcuate assemblages of discontinuous hummocky ridge chains and intervening, mostly water-filled, depressions (Fig. 7). The outermost (distal) edge of each arcuate hummock assemblage is demarcated by distinctly more continuous, sharp-crested and narrower ridges (Fig. 7d). Outwash fans emanate from the outermost hummocky moraine arcs and coalesce to form linear, terraced sandar in adjacent valleys; a prominent example of such terraced outwash occurs at the re-entrant between the Franklin Bay and Horton River hummocky moraine arcs (Fig. 8). Within the hummocks, more continuous and locally sinuous ridges are conspicuous where their crests are orientated obliquely to those of hummocky ridge chains. These features are interpreted as eskers, especially where they converge on, or coincide with, large meltwater channels.

A retrogressive thaw flow slide in the lower Anderson River area exposes a ~250 m wide, 8 m high headwall of debris-rich, stratified ice facies and provides important information on the role and persistence of buried glacier ice in the study region (section AR 2; Fig. 9; 69.02901°N; −128.23679°W). This ice is entirely characteristic of buried glacier ice (cf. Kaplyanskaya and Tarnogradskiy, 1986; Astakhov and Isayeva, 1988; Astakhov et al., 1996; Ingólfsson and Lokrantz, 2003; Murton et al., 2004, 2005; Lacelle et al., 2007) and the stratification is cross-cut by numerous vertical ice wedges that have been deformed towards the northwest (obliquely down valley; see discussion below).

A large number of valleys with underfit streams, and some unusual regional drainage patterns, have been interpreted as the products of glacial meltwater, or the diversion of fluvial drainage by glacier ice margins. The lower Horton River and the Horton Gap, because of their unusual pathway, incised perpendicularly through the Smoking Hills uplands and lying sub-parallel to the Franklin Bay coast (Figs. 1c, 6b and 10), has traditionally been regarded as a glacially diverted course, formed at least partially between uncoupling Great Bear Lake/Liverpool Bay and Amundsen Gulf ice lobes (Mackay, 1958; Mathews et al., 1989; Brown et al., 2011).

A prominent assemblage of inset sinuous meltwater channels

(that incise east to west; ~217 m asl at the western side of the main channel) coincides with a hummocky moraine arc in the lower Horton River, immediately downstream from the confluence with the West River (Fig. 11). Mackay (1958) and Mathews et al. (1989) associated this system of channels with a large single, sinuous abandoned channel that cuts across a relatively low part of the upland between the Horton Gap and the West River valley to the southwest (hereby named the "West River interfluve channel", WRIC; Figs. 6b and 7c), constituting what they regarded as a former ice limit in an unglaciated enclave/re-entrant between the Great Bear Lake/Liverpool Bay and Amundsen Gulf ice margins. Flow through the WRIC was southward as the channel descends from ~212 m asl at its north end to 180 m asl at its south. Detailed topographic and geomorphic analysis using the ArcticDEM imagery (Porter et al., 2018) reveals that the sinuous channels on the east side of Horton River formed south to north along an impounding ice margin, indicating that these features mark the local uncoupling of southeastward retreating Great Bear Lake ice (forming the prominent inset hummocky moraine arcs), and northward retreating cold-based or possibly stagnating Amundsen Gulf ice that formed extensive uplands cored by buried glacial ice (Figs. 2h, 6b and 10).

Prominent depositional terraces occur on the valley sides of the Horton River immediately south of the Horton Gap at altitudes of ca. 200 and 160 m (Figs. 6b and 11a, c). Several exposures through deposits at these elevations reveal thick sequences (≤20 m) of rhythmically bedded sands, silts and clays, containing zones of climbing ripple drift, convolute lamination, and localised dropstone clusters, indicative of glacilacustrine sedimentation.

4.1.3.2. Interpretation. The hummocky ice-cored and streamlined terrain assemblages observed in the study region have been previously interpreted as moraine belts and employed to demarcate regional ice sheet marginal positions (Fig. 1b; Mackay, 1958; Klassen, 1971; Rampton, 1981; Vincent, 1984; Hughes, 1987; Rampton, 1988; Mathews et al., 1989), representative of either glacial stages and/or readvances. The moraine patterns we observe are interpreted to display ice recession and uncoupling of two major ice margins (see inferred ice margins on Fig. 6b), one receding northeastwards into Franklin Bay and the other receding south and eastwards towards Great Bear Lake. A third recessional sequence forms inset moraine arcs in the Mason River drainage basin and relates to the receding margin of the Liverpool Bay (Mackenzie lobe) ice.

Areas of fluted or streamlined terrain occur between the hummocky moraine arcs (Fig. 12) and have been previously interpreted as subglacial bedforms (Mackay, 1958; Hughes, 1987; Rampton, 1988; Stokes et al., 2006, 2009; Brown et al., 2011). Orientation patterns represent ice flowsets (*sensu* Clark, 1997) that occupy and emanate from the 3 different basins discussed above (Fig. 6a and b).

An important characteristic of the streamlined landforms is the occurrence of kettle holes in many examples (e.g. Fig. 7a), where it is clear that underlying ice has melted out. These hummocky assemblages often contain exposures of buried glacier ice in the headwalls of widespread retrogressive thaw flow slides, activated by modern climate warming (Fig. 2h; cf. Segal et al., 2016; Rudy et al., 2017; Kokelj et al., 2020). Buried ice underlying surficial materials is documented more regionally in seismic shothole drillers' log records (Smith and Lesk-Winfield, 2012). The widespread occurrence of retrogressive thaw flow slides, has been used to propose ice-cored moraine development at a regional scale for arcuate assemblages of discontinuous ridge chains and intervening depressions (cf. St-Onge and McMartin, 1995, 1999; Dyke and Savelle, 2000; Dyke and Evans, 2003; Evans, 2009). Where such

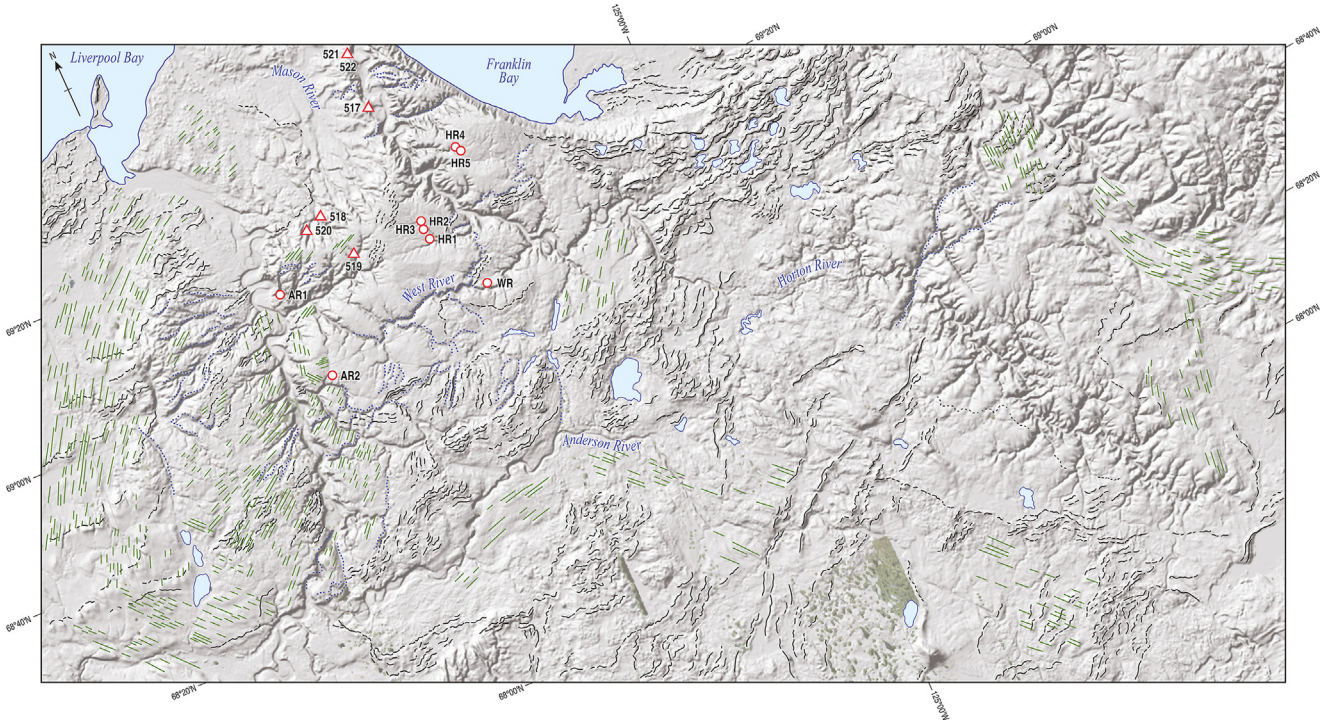

Fig. 6. Geomorphology maps annotated atop hillshaded ArcticDEM maps: a) the broader study region extending from the Melville Hills uplands west through the Horton and Anderson river drainage basins to Franklin and Liverpool bays. Black lines represent moraine ridges, green lines portray subglacially streamlined terrain (fluting and drumlin flowsets) and blue dashed lines represent selected major meltwater channels. Stratigraphic sections are located by numbered circle symbols. Plateau gravel samples are shown with triangle symbols. Green shaded areas in south of image are unresolved data patches in ArcticDEM; b) detailed map of the lower Horton River and Smoking Hills area. (For interpretation of the references to colour in this figure legend, the reader is referred to the Web version of this article.)

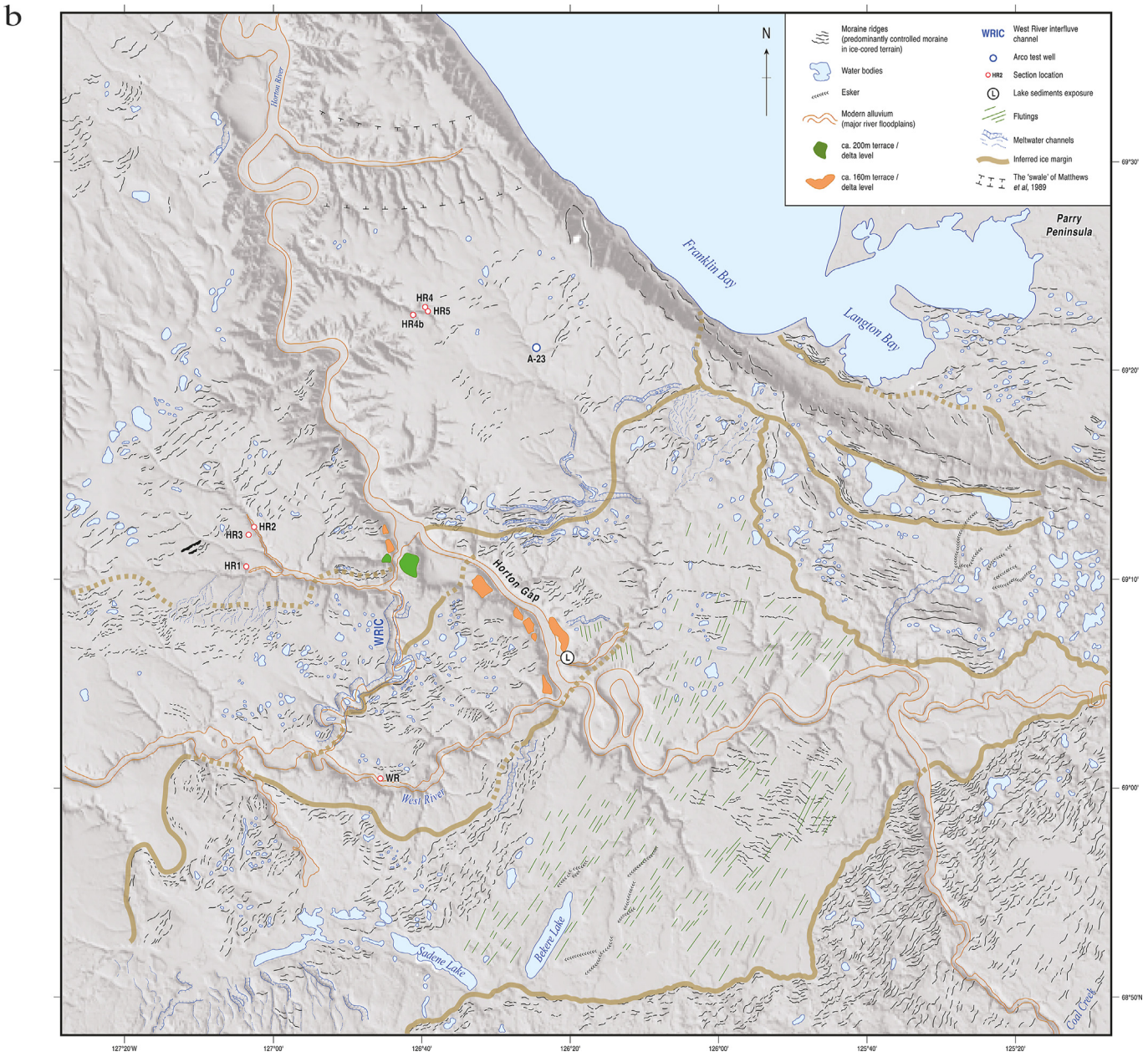

Fig. 6. (*continued*).

features develop at modern glacier margins they are termed "moraine mound complexes" (cf. Glasser and Hambrey, 2003) and they can be seen to relate directly to the formation of controlled moraine on debris-charged, polythermal and polar ice margins (Evans, 2009). Hence the moraine arcs that record the last phase of ice recession from the region represent polythermal or possibly cold/polar glacier margins. The occurrence of more continuous, sharp crested ridges at the outer margins of individual hummocky controlled moraine arcs appear to represent the limit of readvances by debris-charged snouts, because they resemble push moraines rather than supraglacial deposits (cf. Dyke and Evans, 2003). The outwash fans emanating from the outermost hummocks within the ice-cored moraine clearly have been fed by meltwater produced by the melting of ice cores and are hence supraglacial in origin. As such these glacifluvial outwash landforms constitute hochsandur fans (*sensu* Heim, 1983, 1992; Krüger, 1997; Kjaer et al., 2004), which have previously been associated with debris-covered temperate glaciers in Iceland but as they are proglacial depo-centres fed directly by supraglacial streams, it should not be surprising to observe them in large numbers around controlled moraine margins in cold polythermal settings.

In contrast to the ice-cored moraines, the areas of glacially streamlined terrain attest to subglacial sliding/deformation or temperate basal ice conditions (cf. Dyke and Evans, 2003) and regionally record multiple ice flow directions (cf. Mackay, 1958; Hughes, 1987; Rampton, 1988; Stokes et al., 2006, 2009; Brown et al., 2011). Together, the two landform components represent a landsystem imprint of sequentially less extensive and increasingly polythermal, lobate ice sheet margin retreat (cf. Dyke and Evans, 2003). The regional pattern of subglacial flowsets record ice stream operation over the region when ice flow units from the different source areas were coalescent but alternately dominant; this interpretation incorporates shear directional indicators in multiple tills as presented below. These overprinted flow events

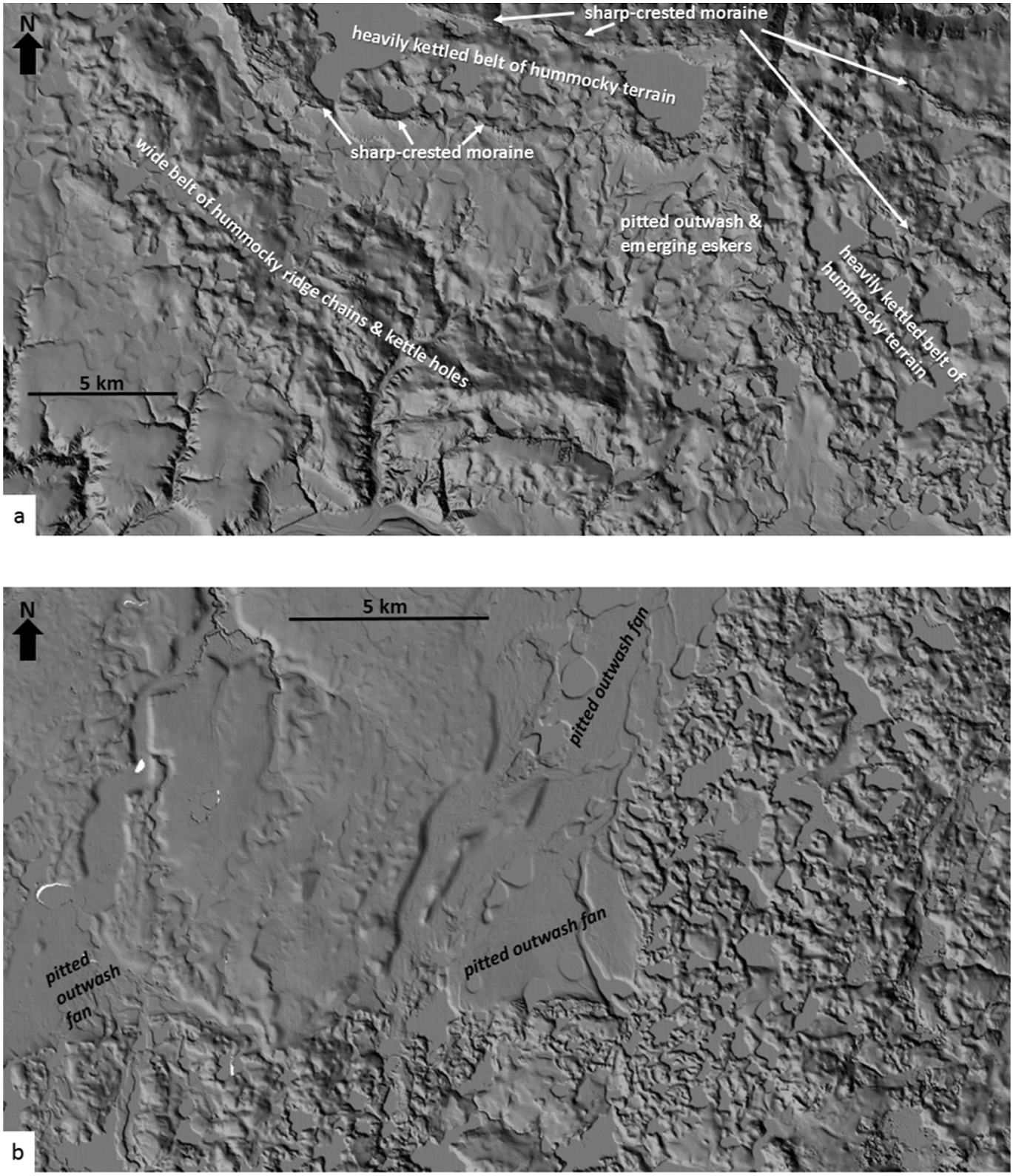

Fig. 7. Hummocky ice-cored terrain and associated features. See Fig. 1a for figure locations: a) ArcticDEM hillshade image of inset sequence of broadly arcuate assemblages of discontinuous hummocky ridge chains and intervening, mostly water-filled depressions related to the recession of an ice margin northwards into southern Franklin Bay; b) ArcticDEM hillshade image of a prominent, heavily-kettled margin and an assemblage of discontinuous hummocky ridge chains with kettled outwash fans emanating from re-entrants in the former ice margin. Ice recession was towards the south and southeast; c) ArcticDEM hillshade image of heavily kettled assemblage of discontinuous hummocky ridge chains trending across the upland (interfluve) between the West River and the Horton River at Horton Gap (ice recession towards southeast). The large, sinuous and abandoned channel ("West River interfluve channel", WRIC) runs along and partially through the hummock belt, descending north to south; d) aerial photograph stereo-triplicate of an example of a relatively continuous, sharp-crested and narrower ridge lying at the distal edge of an arcuate hummock assemblage south of Franklin Bay (A13784 147–149).

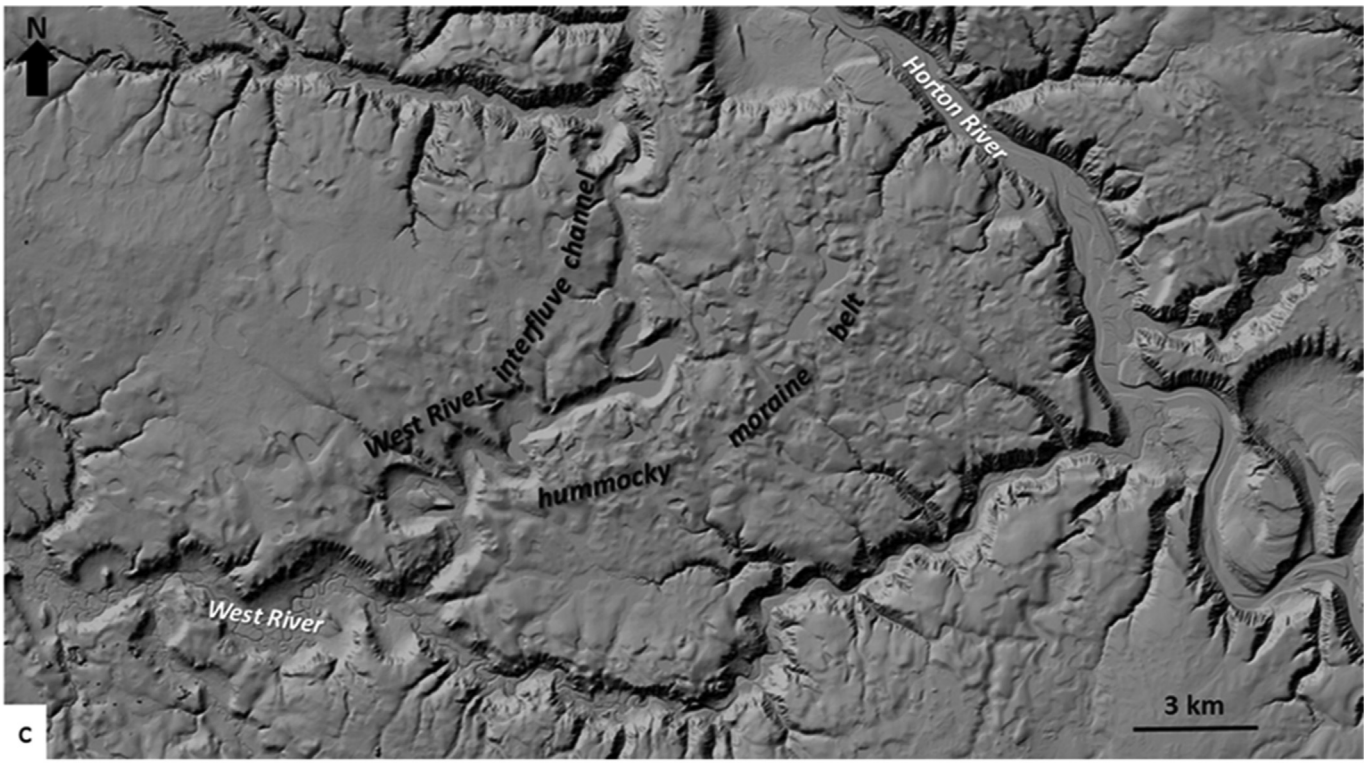

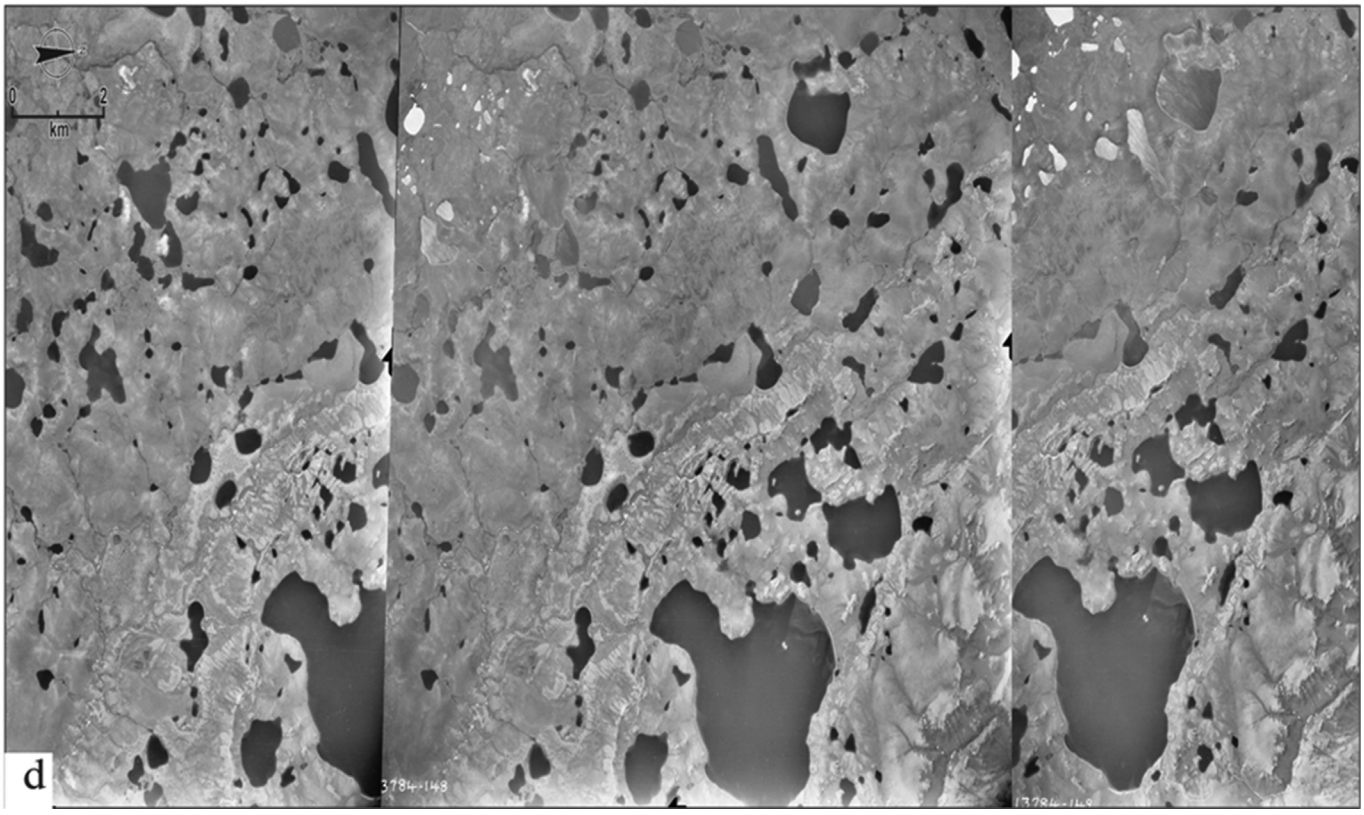

Fig. 7. (*continued*).

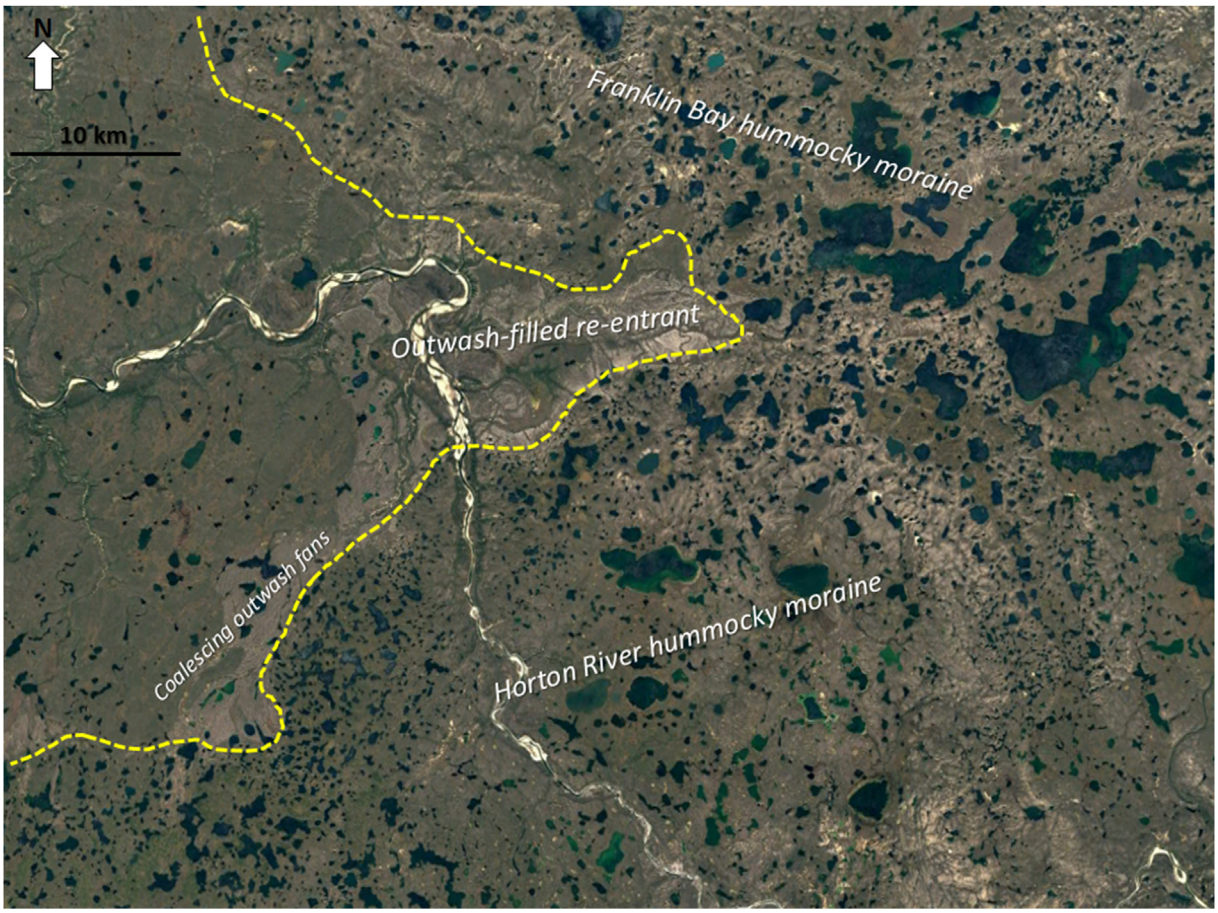

Fig. 8. Annotated Google Earth image of outwash fans emerging from kettled hummocky moraine and coalescing to form linear, terraced sandar (see also Figs. 1a and 6b for location).

include a phase of coalescence and vigorous flow northwestward toward the mouth of Amundsen Gulf (cf. Stokes et al., 2006; Brown et al., 2011), as well as west-southwesterly flow during Amundsen Gulf ice dominance and northeasterly flow during Liverpool Bay ice dominance (see Discussion for a regional reconstruction using all data sources). Kettled/pitted flutings (Fig. 9a) are similar to the ice-cored drumlins reported from recently deglaciated forelands in Iceland (cf. Schomacker et al., 2006; Evans et al., 2007), where such features are related to repeated glacier surges over buried snout remnants in regions of sporadic permafrost. In areas of continuous permafrost, such as the Smoking Hills region, the occurrence of melting ice beneath subglacial bedforms argues for the preservation of large areas of former LIS margins, entombed within permafrost (Rampton, 1988; St-Onge and McMartin, 1995; Dyke and Evans, 2003; Lacelle et al., 2018; Coulombe et al., 2019) and then overrun by the continued glacier advance. This is consistent with the Anderson River site (AR 2; Figs. 6a and 9), where deformation of formerly vertical ice wedges in an oblique down-valley direction, is aligned with streamlined landforms and other ice flow directional indicators in the immediate vicinity. Subglacial deformation and shear, usually associated with underlying till deposits (Evans, 2018), was in this case carried into the underlying relict glacial ice to form permafrost glacitectonite (Astakhov et al., 1996; Waller et al., 2009).

This buried old glacier ice site may well be unique in the record it preserves. In Arctic Canada, only sites in Yukon have demonstrated preservation of "old" (pre-Late Wisconsinan) ice wedges and massive segregated ice (cf. Lacelle et al., 2007; Froese et al., 2008). Pending future detailed field investigation, the following is proposed as a reconstruction of the Anderson River site. At some point prior to the last (Wisconsinan) glaciation, a large mass of clast-rich, foliated glacier ice stagnated, becoming buried below an insulating carapace of glacial sediment. Local permafrost conditions led to the formation of vertical ice wedges (present forms estimated $\leq$6 m deep, and 1.5 m in maximum width). The site then experienced a warming, leading to a thickening of the active layer, resulting in a prominent thermal unconformity with an undulatory basal contact that truncated the upper parts of ice wedges across the entire slump exposure (Fig. 9). We have insufficient information to assess whether the thermal unconformity formed in a subaerial environment, or whether it actually records subglacial thermal erosion from a "warm-based" ice sheet. However, subsequent to (or coeval with) the thermal unconformity, all of the ice wedges were deformed obliquely down-valley, in parallel with the adjacent pitted flutings that are accordant with reconstructed Late Wisconsinan ice flow (Figs. 6a and 9). One larger ice wedge is particularly intriguing, as it appears to show evidence of an initial thermal unconformity, then larger-scale simple drag folding, together with the surrounding buried glacial ice, followed by continued thermal erosion of the upper parts of the now horizontally deformed wedge structure (Fig. 9c and d). Although the overriding glacier ice deformed the ice wedges and created flutings, its thermal characteristics were not conducive to complete melting of the underlying "old" glacier ice. Instead, it became coupled with the near-surface ice to form a shearing interface (glacitectonite; Astakhov et al., 1996; Waller et al., 2009; Evans, 2018), within which

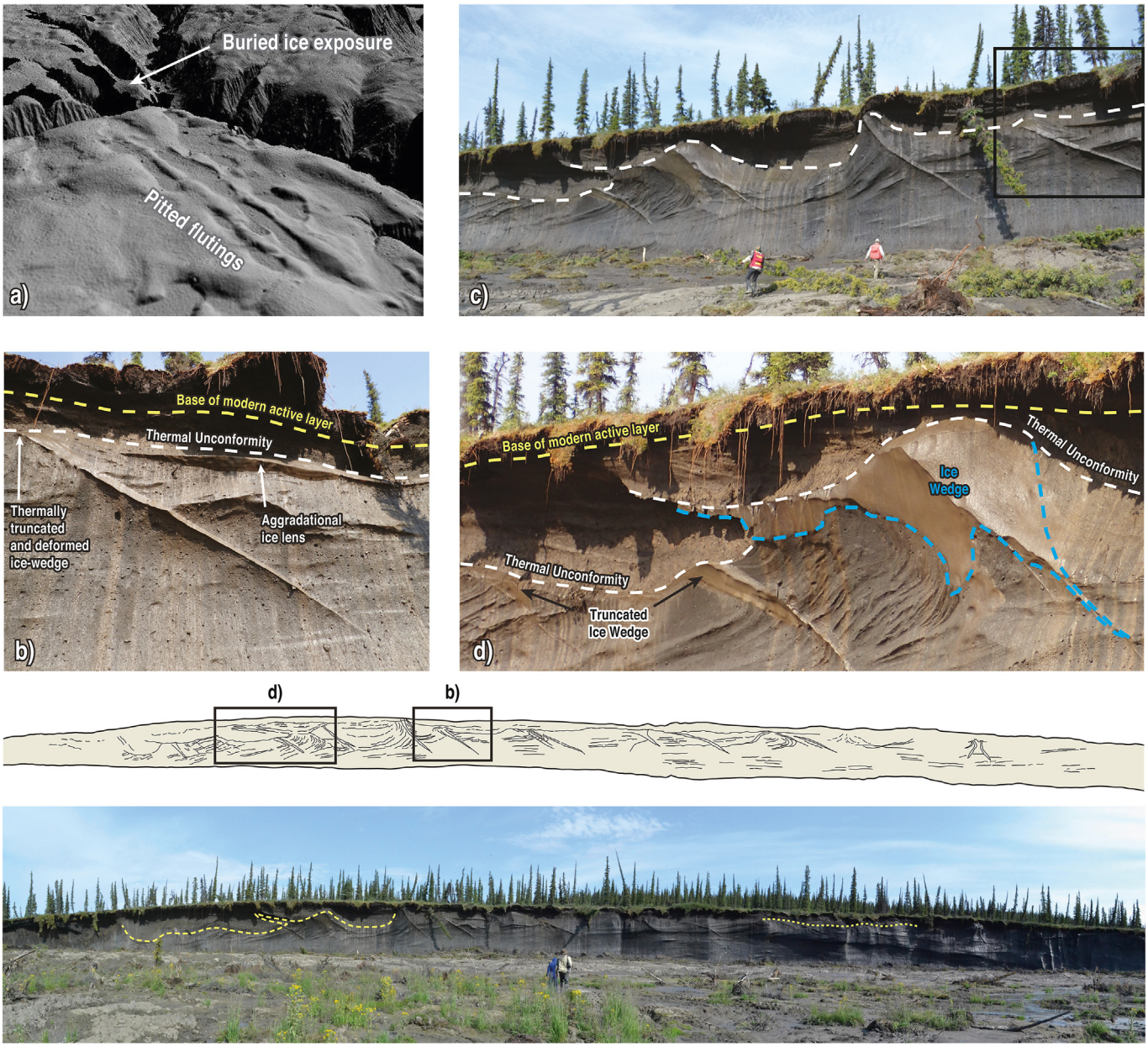

Fig. 9. Buried, pre-Late Wisconsinan glacier ice exposure in the lower Anderson River area (site AR 2 in Fig. 6a). Lower panoramic photo and sketch shows the broader architecture (~8 m high, 250 m across), with yellow broken line highlighting a thermal unconformity. Upper detailed photographs are from the boxed areas illustrated on the sketch. a) annotated ArcticDEM hillshade image showing oblique, southward looking view of two adjacent pitted flutings (3 km long) just north of the buried ice exposure; b) exposure of 6 m long, thermally truncated ice wedge deformed down-flow; base of thermal unconformity coincides with aggradational ice lens formed later as permafrost aggraded upwards into overlying debris (NRCan photo #2020-947); c) exposure of 5 thermally truncated and deformed ice wedges (including that in Fig. 9b – outlined by box); d) detail of widest (~1.5 m) ice wedge seen, and the anti-clockwise deformation of the ice wedge and thermal unconformity, up and over the thermal unconformity boundary and 2 ice wedges to the left (northwest; NRCan photo #2020-948). (For interpretation of the references to colour in this figure legend, the reader is referred to the Web version of this article.)

streamlining (flute construction) was undertaken, thereby explaining ice-core melt-out in the adjacent pitted flutings. Post-deformation, horizontal aggradational ice lenses (cf. Mackay, 1972; Burn, 1988, Fig. 9b) mark both sediment accumulation over the upper surface and a vertical migration of the base of the active layer upwards. No syngenetic upward ice wedge or ice veinlet growth was observed above any of the deformed ice wedges (cf. Mackay, 1990).

Meltwater channels in the region document ice-marginal drainage as a consequence of the development of cold-based glacier sub-marginal conditions (cf. Dyke, 1993) and associated with widespread controlled moraine construction during deglaciation. The westerly ice-marginal drainage from the multiple, inset sinuous meltwater channels and hummocky moraine in the lower Horton River (Fig. 11a and b) across to the West River interfluve channel (WRIC; Figs. 6b and 7c), as proposed by Mathews et al. (1989), would imply that the Horton River valley either did not exist or had been filled with sediment; otherwise drainage would have been northwards and not through the WRIC. However, the presence of fluvial gravel sequences at the base of sections HR 1 and 2 (~170 m asl) clearly indicate that streams in this side valley were draining eastward into a northward flowing proto-Horton River channel below the level of the sinuous meltwater channels and the WRIC. Hence, it seems most likely that the WRIC is a glacial

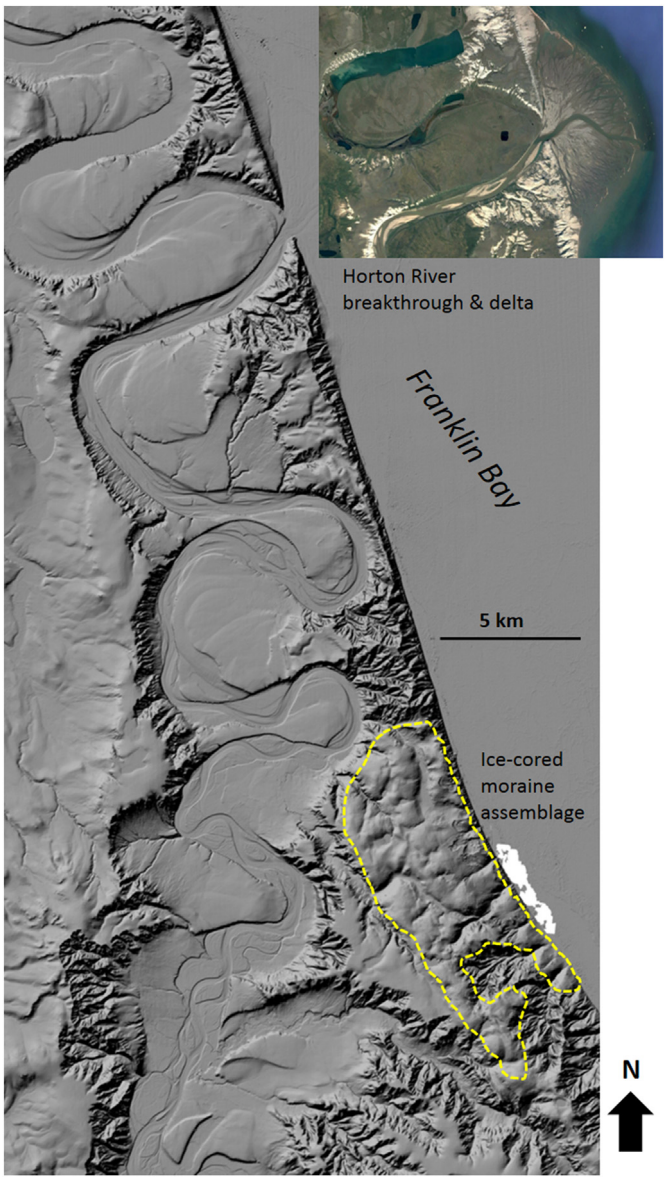

Fig. 10. ArcticDEM hillshade image showing the meanders of the lower Horton River and its unusual incised pathway along the uplands lying sub-parallel to the Franklin Bay coast, through which the river has created a breach to form the Horton delta (Google Earth image inset). Also demarcated is an area of ice-cored hummocky moraine that gives rise to the extensive retrogressive thaw flow slides and buried glacier ice exposures above Franklin Bay (see Fig. 2h).

lake spillway, albeit between two prominent ice margins, the southernmost of which is defined by a hummocky moraine belt, an interpretation that would explain a single drainage pathway and its altitude in relation to glacilacustrine deposits in terraces up to 200 m asl south of Horton Gap (Figs. 6b and 11c). To the north, the lower Horton River valley had to have been blocked by either Amundsen Gulf (Franklin Bay) or a confluence of Amundsen Gulf and Liverpool Bay ice margins (see Discussion for a regional reconstruction).

4.2. Sediments and stratigraphy

4.2.1. Section HR 1 (69.199407°N; −127.021966°W)

4.2.1.1. Description. First reported by Klassen (Fulton and Klassen, 1969), this exposure occurs along a river cut bank stretching >1 km along an unnamed western tributary to the lower Horton River (Figs. 5 and 6a) and reveals a thickness of up to 58 m of unconsolidated deposits and bedrock intraclasts (rafts). Our vertical profile log is a composite of a new lithostratigraphic analysis of the previously reported main section as well as a more accessible and better preserved part of the upper stratigraphy located 100 m upstream (Figs. 6 and 13).

Lithofacies (LF) 1–3 comprise a sequence of flat-lying gravel units containing organic lenses (Figs. 13 and 14a-c), overlying Smoking Hills Formation bedrock (containing conspicuous yellow jarosite beds ($KFe_3(OH)_6(SO_4)_2$); Yorath et al., 1975). The ≤3 m thick planar and horizontally bedded gravels and cobble lags of LF1 display strong northeastward imbrication (~26°) and an overall eastward-draining thalweg, and coarsen upwards to an erosional contact with the overlying, ≤1 m thick, matrix-supported gravels and boulder gravels of LF2. These are in turn conformably overlain by LF3, which comprises a ≤4 m thick, fining upwards sequence of massive and horizontally bedded gravels to planar bedded sands with gravel lags. Clast form data from LF1 and 2 reveal low angularity (RA = 0; AvR = 2.76) and low to medium C40 values (26 and 44%, respectively), as well as important numbers of striated clasts (8–16%) and some large faceted boulders.

Overlying LF1-3 is up to 50 m of diamicton with bedrock intraclasts (rafts), classified as LF4 but sub-divided according to internal structure and texture as well as relationships with the thickest and most laterally extensive rafts (Fig. 13). The lowest part of LF4 comprises 0.4–1.2 m thick beds of dark grey (5Y 4/1) massive or pseudo-laminated, matrix-supported diamicton (highly fissile in its upper 0.20 m), separated by ≤ 0.75 m thick intraclasts of poorly-consolidated Cretaceous mudstone, siltstone, or sandstone that pinch and swell laterally and in places pinch out completely (Fig. 14d). This sequence is classified LF4a and is separated from underlying LF3 by a 1.25 m thick mélange zone. This mélange comprises two sub-zones: i) a lower 1.1 m zone of deformed planar-bedded sands and silts that display cross-cutting reverse and normal faults (reidel shears) and attenuated or pinched beds; and ii) an upper zone (0.15 m thick) of highly deformed sands and silts displaying no recognizable internal bedding or bedforms and cross-cut by densely-spaced, anastomosing partings/fractures. The two sub-zones respectively resemble the mélange types Mt I and Mt IV of Cowan (1985; cf. Evans, 2018, Fig. 14e). The top of LF4a is separated from overlying LF4b by a ≤3 m thick and laterally continuous intraclast of laminated mudstone. This mudstone is friable and displays prominent rhythmic laminations of alternating clay and fine silt lamina (Fig. 14f). The clay lamina display weak lithification, while the silt lamina display generally none. Numerous spheroidal selenite (gypsum) concretions (≤25 cm diameter) occur within this mudstone and it is also characterised by densely spaced anastomosing partings/fractures, giving it a prominent fissility. Selenite was identified by Yorath et al. (1975) to occur in the upper beds of the Horton River Formation and in the lower Smoking Hills Formation. Palynological analyses of this rafted bedrock identify it as Albian in age, confirming a Horton River Formation classification (Supplementary data S5). The Horton River Formation outcrops extensively immediately east and south of this site (Fig. 1b). Clast macrofabrics from lower and upper LF4a reveal mean lineation azimuths of 064° (S_1 = 0.72) and 111° (S_1 = 0.58), respectively (Fig. 13). Clast form data indicate a vertical contrast in roundness between lower and upper LF4a, with the RA increasing from 4 to 26% and AvR decreasing from 2.50-1.94. Striated clasts in LF4a range from 4 to 14%.

The mudstone raft is overlain by the thickest diamicton within LF4, which is ≤ 28.3 m thick, greyish brown to dark greyish brown (2.5Y 5/2; 10 YR 4/2) and classified as LF4b. It is composed of pseudo-laminated to massive and in places highly fissile, matrix-

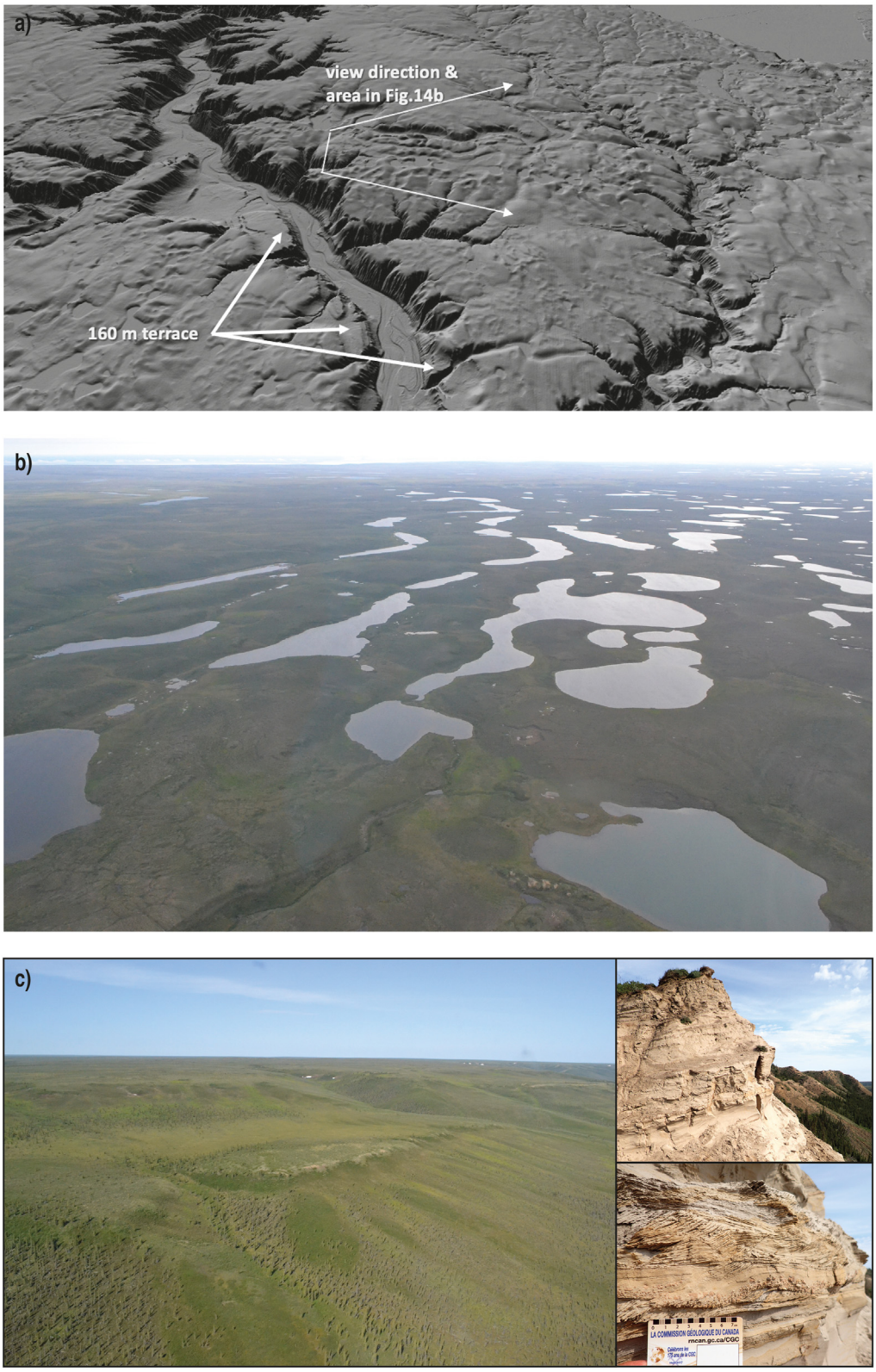

Fig. 11. Meltwater and glacial lake features of the lower Horton River: a) oblique northward view ArcticDEM hillshade image, and b) helicopter view from the west of the prominent inset sinuous meltwater channels; c) evidence of glacial lake sedimentation in the lower Horton River valley: main image shows prominent depositional terrace at 160 m asl located immediately south of the Horton Gap; inset images show details of exposures through rhythmically bedded sands, silts and clays, climbing ripple drift and dropstones (see Fig. 6b, site L, for location).

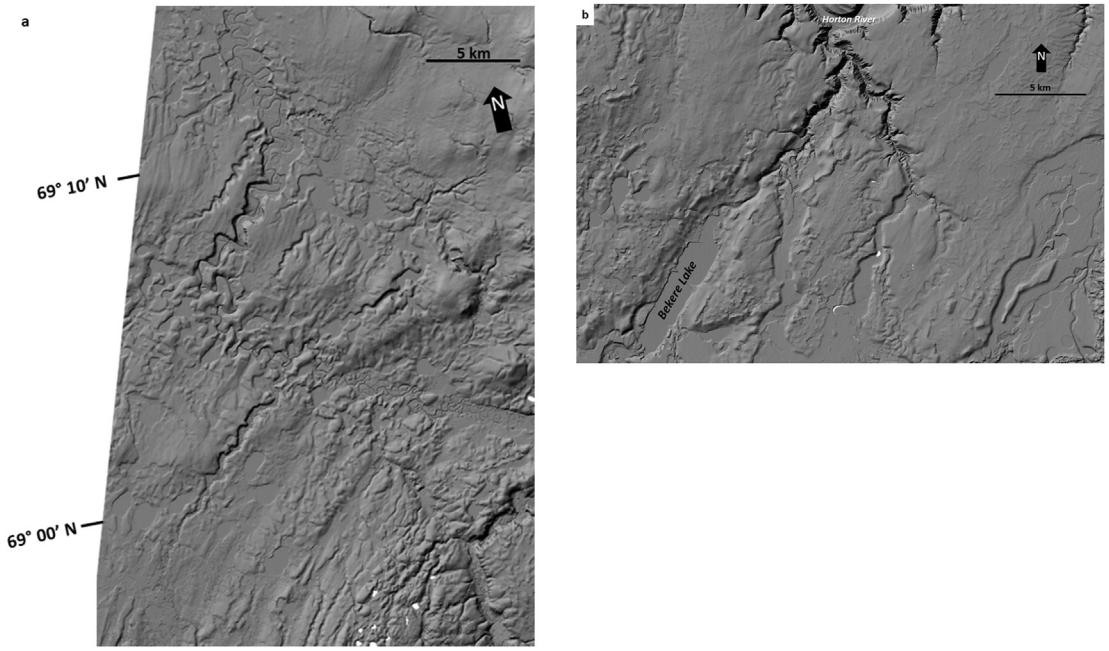

Fig. 12. ArcticDEM hillshade images showing typical fluted terrain of the study region. See Fig. 1a for locations: a) streamlined bed of the former Liverpool Bay ice stream between Husky Lakes and the lower Anderson River; b) subtle streamlining of the former bed of the Amundsen Gulf ice lobe produced during its incursion into the Bekere Lake area, southwest of the Horton River.

supported diamicton, with pseudo-lamination occurring in the basal 8 m and upper 6 m (Fig. 13). The basal contact with the underlying mudstone raft is erosional and cross-cuts the rhythmic laminations, which themselves are attenuated and pinched to form boudinage typical of a Type I mélange (*sensu* Cowan, 1985; cf. Evans, 2018, Fig. 14g). The basal 8 m of LF4b is clast poor (<5% by weight) and appears pseudo-laminated or banded because of internal sub-horizontal structures, which comprise partings, stringers and wisps of black and light grey coloured mudstone, and dense fissility (Fig. 15). Above this pseudo-laminated zone is a 13 m thick zone of massive, matrix-supported diamicton (Dmm), within which clasts are predominantly small pebble-sized (4–65 mm) and sparsely distributed. The matrix is largely a dark grey to black sandy-silt, with high (~40%) very-fine silt and clay (<8 μm) contents (Fig. 13b, Supplementary data S2). A clast macrofabric from the base of this Dmm zone reveals a mean lineation azimuth of 070° (S_1 = 0.50) and with clast form characteristics (RA = 30%; C40 = 38%; AvR = 2.06; 6% striated clasts) similar to those of the upper part of underlying LF4a. The uppermost 6 m of LF4b appears pseudo-laminated but, unlike the basal 8 m, it is less fissile and contains downward-tapering, sand-filled clastic dykes up to 1.7 m long. A clast macrofabric from this area of LF4b displays a mean lineation azimuth of 266° (S_1 = 0.58) and contains an unusually high number (28%) of striated clasts (Fig. 13).

The uppermost boundary of LF4b is characterised by a 1.2 m thick zone of interbedding with an overlying large intraclast/bedrock raft. This zone comprises Dmm with truncated sand dykes lying either side of brecciated sandstone with a mudstone matrix. Combinations of poorly-consolidated sandstone and mudstone rafts are then repeated in an overlying 6 m of stacked units displaying various styles of mixing and deformation and separated by erosional, and in places faulted, contacts (Fig. 16). The mudstone and sandstone rafts appear interbedded in at least two, less deformed units, indicating that this is their primary stratigraphic relationship. A further 1 m thick unit of grey-coloured, cross-bedded sand displays numerous low angled reverse (thrust) faults, indicative of westerly-directed stress. This sand appears to be entirely unlithified and could be derived from local bedrock or simply be unconsolidated sediments of unknown derivation. Where deformed, the mudstone and sandstone interbedding displays a range of mélange patterns from Types I through to IV (*sensu* Cowan, 1985; cf. Evans, 2018). Within the main exposure, this bedrock raft unit is thickest (6 m) at the eastern edge, and thins to ~2 m at the western side.

The 6 m thick sandstone and mudstone raft is extensively truncated by a ≤30 cm thick poorly-lithified shale/mudstone that has a broad Late Jurassic to late Albian palynological age (Horton River or Langton Bay formations; see Supplementary data S5), and the overlying LF4c, which comprises a pseudo-laminated (banded) to massive, matrix-supported diamicton (Dml/Dmm) with few, small clasts (4–7% by weight) and wood fragments (Figs. 16 and 17). Pseudo-lamination is imparted by colour banding, especially prominent due to the contrasts between discontinuous bands, stringers and wisps of dark grey to black mudstone-rich and light to dark brown sand-rich material; this is effectively an almost homogenised Type IV mélange (*sensu* Cowan, 1985; cf. Evans, 2018). Clast macrofabrics taken from the lower, middle and upper parts of LF4c indicate a consistent east-northeasterly dipping signature (053–086°; S_1 = 0.58–0.66) with sub-angular clast form characteristics (RA = 40–50%; C40 = 34–36%; AvR = 1.68–1.76) and small numbers (2–6%) of striated clasts (Fig. 13).

The uppermost 2 m of section HR 1 is characterised by a convolute bedded mélange composed of highly contorted lenses and pods of diamicton and poorly-sorted gravel. These deposits are manifest on the land surface as patterned ground features such as non-sorted hummocks and sorted to non-sorted polygons.

Clast lithological samples (Fig. 13b) reveal a dominance of chert in all diamictons (samples CL1-CL5) and in the gravels of LF1 (sample CL6). Note, clasts classified as chert contain a small percentage of grey-green argillites which are not easily distinguished and share similar colour and fracture patterns to regional chert bedrock. Also prominent are sandstone and quartzite and a vertical

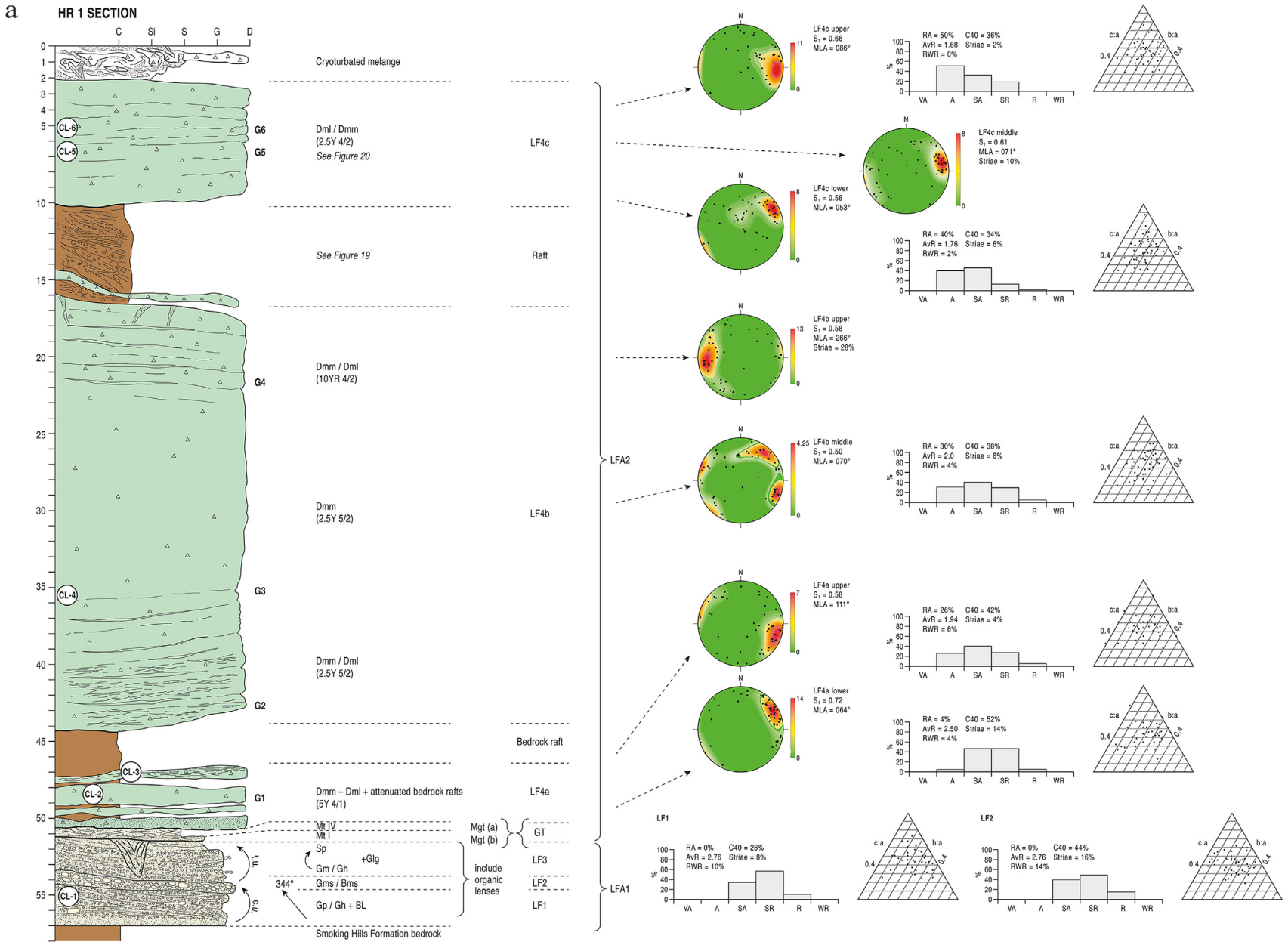

Fig. 13. Vertical (composite) profile log of section HR 1 with relevant data: a) lithofacies types and classifications, clast macrofabric and form data; b) basic log with clast lithological, geochemical and grain size data (see also Supplementary data 2) for the diamictons and basal sandy-gravel. For data plotting conventions see methods section. Labels CL1-CL6 and G1-G6 are locations of clast lithological and geochemical samples, respectively (see Supplementary data S2).

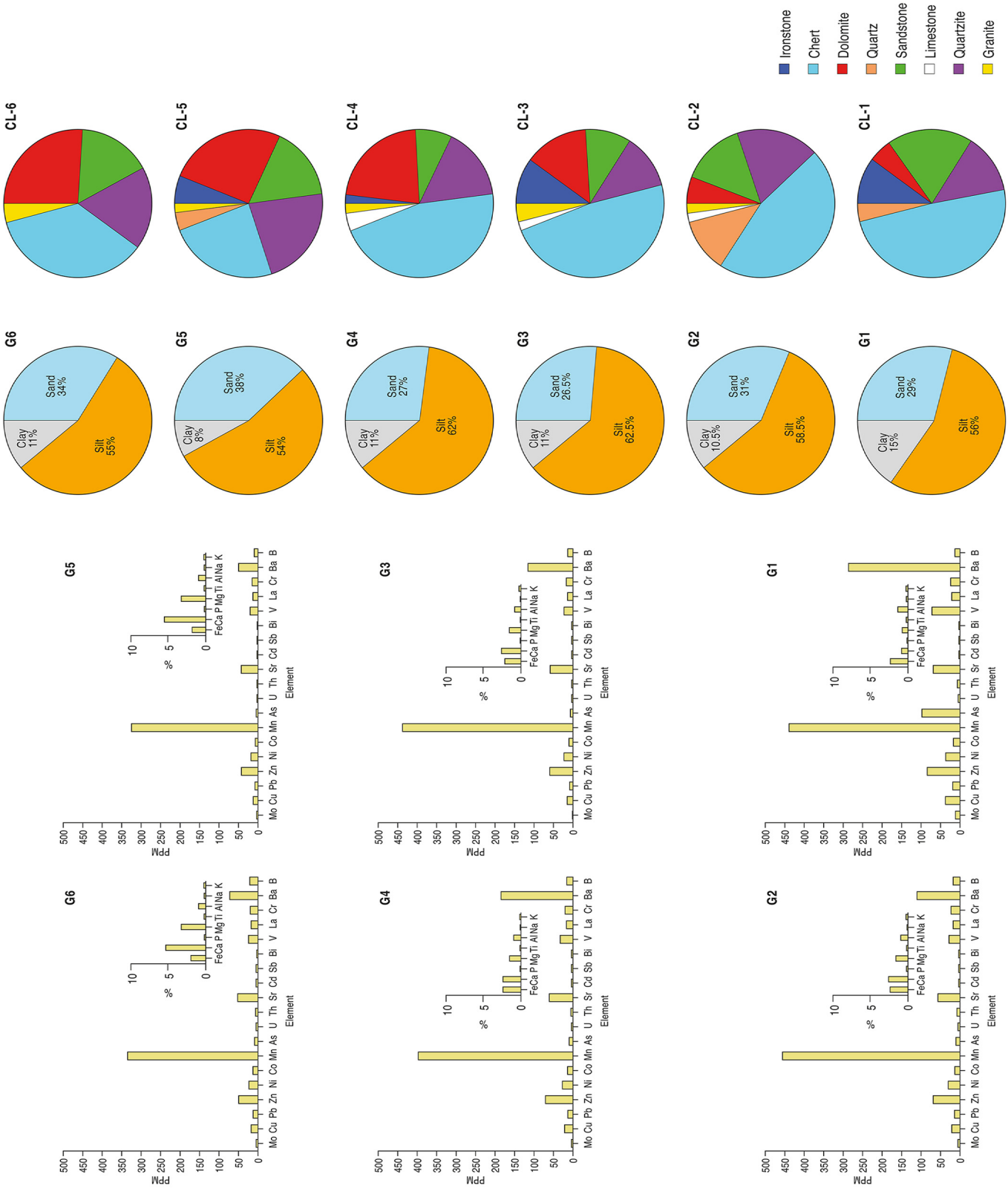

Fig. 13. (*continued*).

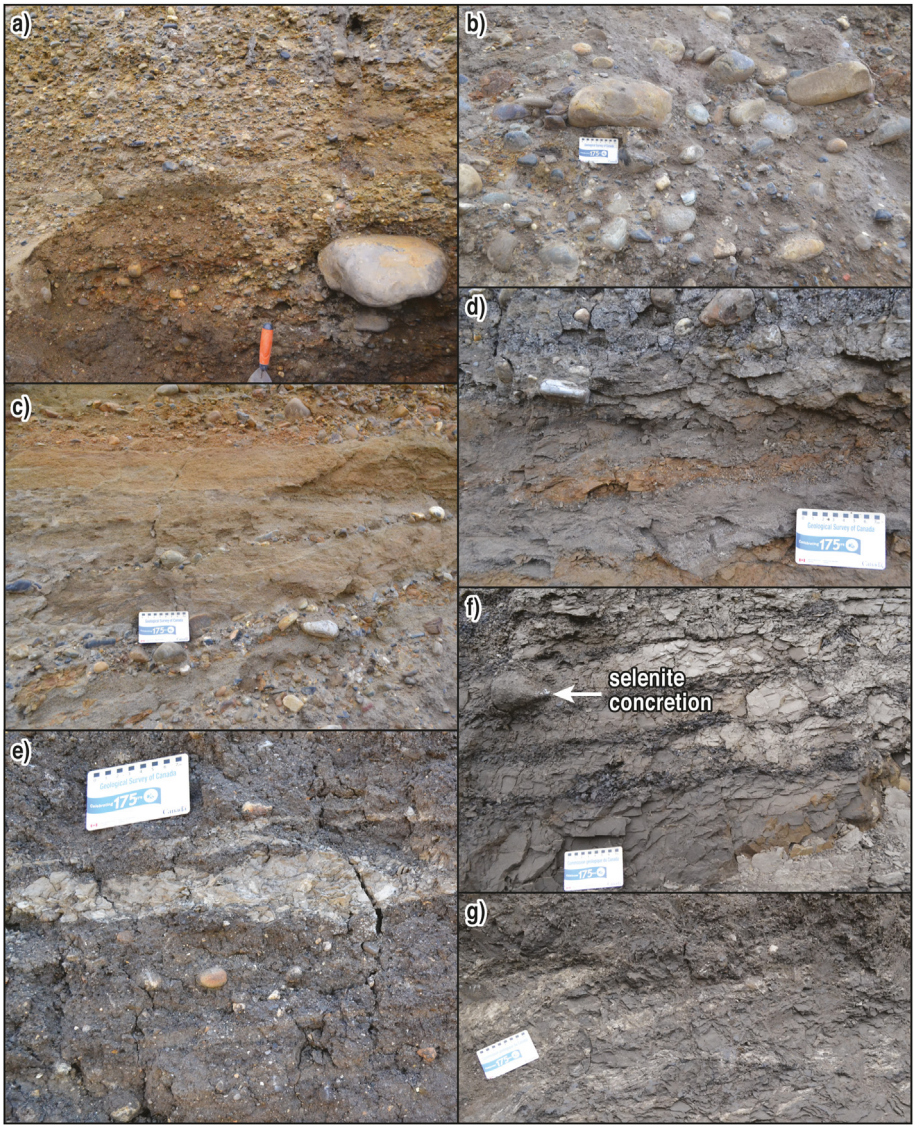

Fig. 14. Characteristics of lithofacies types LF1-4b: a) LF1, showing large, faceted outsized boulder; b) LF2 matrix-supported cobble to boulder gravel, with imbrication indicative of a palaeocurrent flowing towards the northwest; c) upper LF3, showing nature of upward fining and gravel lag horizons; d) contact between the base of LF4a and underlying mélange types IV and I; e) LF4a, showing attenuated bedrock rafts within pseudo-laminated diamicton (Dml); f) laminations in poorly-consolidated mudrock (bedrock) raft lying between LF4a and 4b, showing spheroidal selenite (gypsum) concretion and densely fissile structure; g) contact between mudrock raft and overlying LF4b, showing attenuation and boudinage of mudrock laminations to form zone of Type I mélange.

increase in dolomite. Lithologies noticeably absent from the LF1 gravels but apparent in small quantities ($\leq$1 and up to 2%) in all the overlying diamictons are granitic material and limestone. Duk-Rodkin et al. (2004) and Duk-Rodkin and Barendregt (2011) maintain that granites are only found in the very uppermost till veneer (overlying what we have described as a cryoturbated mélange) and as surface boulders. Vincent (1988), however, also noted the presence of granitic (and gabbroic) erratic material in both the lowermost 10 m of diamicton (our LF4a + lower LF4b), and through the upper diamictons (LF4c). As discussed, clast content of the diamictons, particularly larger pebble and cobble-sized material are sparse through much of this thick stratigraphic section. Our clast lithology compilations have benefitted from those conducted previously by the bulk sediment sieving and oxalic acid pre-treatments, which has enabled the inspection of larger populations of finer pebble and even granule-sized (2–4 mm) material. Without question though, Canadian Shield-derived granitic clasts occur sparsely in all diamicton samples overlying the basal sands and gravels (grouped into lithofacies association LFA1; Fig. 13b).

The geochemical signatures of the diamictons (G1-G6, Fig. 13b, Supplementary data S2) indicate mostly subtle differences between lithofacies, but of note is the relatively higher concentration of most trace metals in lower LF4a compared to the overlying diamictons (e.g. Mo, Cu, Zn, As, U, Cd, Sb, V, Ba). This constitutes an abrupt vertical change in geochemical signature, with samples at various heights in lithofacies LF4b being virtually indistinguishable. High metal concentrations are characteristic of the local Smoking Hills Formation bedrock (Grasby et al., 2019) which immediately floors this stratigraphic section. The uppermost diamicton (LF4c) is distinguishable by its relatively higher calcite and dolomite content (and accordingly, higher Ca and Mg contents), grain sizes characterised by relatively higher sand and lower very fine silt/clay (<8 μm), and a conspicuously lighter colour (2.5Y 4/2) compared to the underlying darker grey-black diamictons (Supplementary data S2).

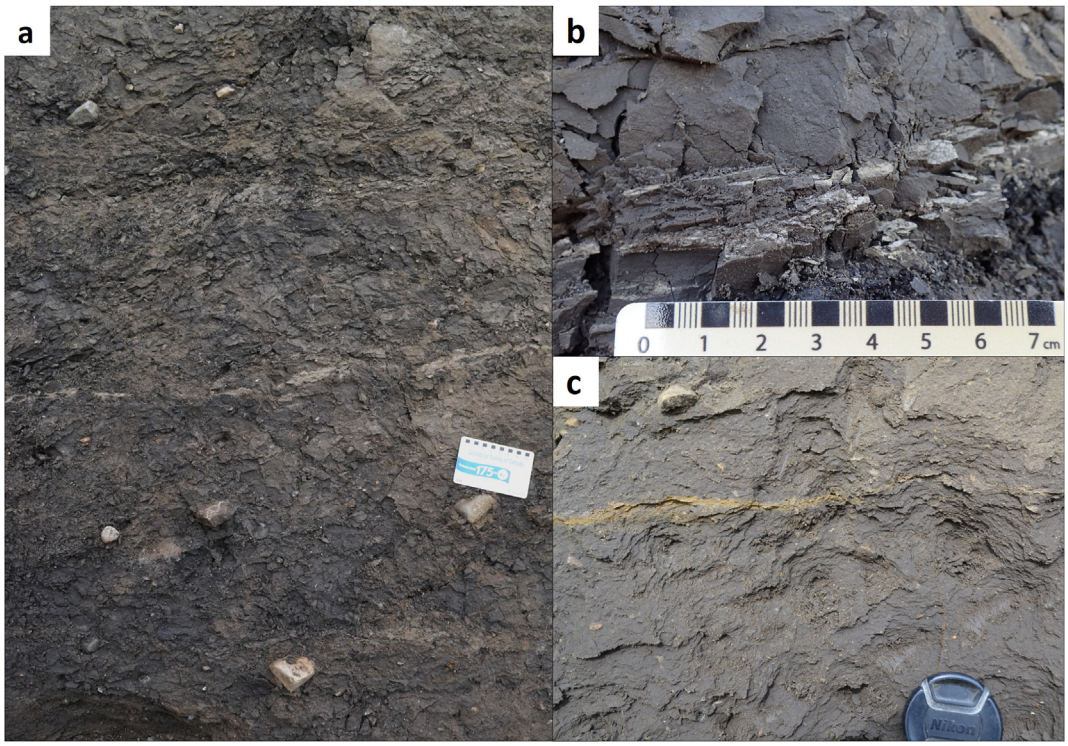

Fig. 15. Characteristics of LF4b: a) uppermost part (40–41 m) of lower zone of pseudo-lamination; b) typical complex, multi-layered wisps/stringers of light coloured mudstone (bedrock) at the base of the middle Dmm (38–40 m); c) light brown coloured, fine sandy (sandstone?) stringer within densely fissile Dmm (42–43 m). (For interpretation of the references to colour in this figure legend, the reader is referred to the Web version of this article.)

4.2.1.2. Interpretation. Section HR 1 is the thickest and most complex stratigraphic exposure in the study area. Strikingly, our identification of extensive unconsolidated Cretaceous bedrock intraclasts (rafts), boudinage, and numerous thin, often attenuated layers of poorly consolidated bedrock throughout this section has not been identified previously (Fig. 18). Klassen (1968, unpublished GSC field notebook – reported in Duk-Rodkin et al., 2004) identified a ~1.5 m thick bed of laminated clay interbedded with light grey silt, which likely correlates with a prominent bedrock raft (44–47 m depth; Figs. 13a, 14f and 18), and also a ~2 m thick layer of brown, fissile silt, overlain by dark grey clay with thin interbeds of peat that correlates to parts of our uppermost bedrock raft (10–16 m depth; Figs. 13a and 18). Klassen, however, did not affix relative chronostratigraphic interpretations to these deposits. In all subsequent studies, the unconsolidated bedrock components that we identify have either been overlooked, or have been incorrectly classified as various inter-till/interglacial, lacustrine, palaeosol, mudflow, and fluvial overbank deposits (Fig. 18; Vincent, 1988, 1991; Barendregt and Duk-Rodkin, 2004; Duk-Rodkin et al., 2004; Duk-Rodkin and Barendregt, 2011). Similarly, large rafts of poorly consolidated bedrock were not identified in historical accounts of stratigraphic sections on Banks Island either (cf. Evans et al., 2014; Vaughan et al., 2014).

Based upon the new observations presented, the various lithofacies reported here are grouped into two lithofacies associations, LFAs 1 and 2. LFA1 comprises LF 1–3 in which gravel-bed river deposits are manifest as cross-bedded gravels and sands, gravel lags and matrix-supported gravels and boulder gravels (Figs. 13 and 14a, b). The grain size variability in these deposits, especially the coarsening-upward sequence of LF1, capped by the poorly sorted boulder gravels of LF2 and then followed by the fining upwards sequence in LF3, is typical of rapidly changing discharge. The predominantly planar to horizontal nature of the cross-bedding is indicative of superimposed bars, which were occasionally truncated by the sediment gravity flow deposits (Gms/Bms) of hyperconcentrated flows. Rare outsized boulders are likely to have been emplaced by fragmented river icings (aufeis), onto which bank collapses can introduce anomalously large clasts (Mathews et al., 1989; Fyles et al., 1994). Organic lenses within LFA1 were likely introduced in a similar allochthonous way, either by bank collapse and/or fluvial erosion through pre-existing deposits. The clast forms of LF 1 and 2 are slightly more rounded and more blocky than those of our High Arctic glacifluvial reference sediments (Fig. 19, Supplementary data S1) but the occurrence of 8–16% striated clasts as well as significant numbers of faceted forms and more blocky shapes indicate that glacigenic deposits were being reworked and transported short distances to the site. For reasons discussed (lithology, imbrication, elevation, continuity with other basal gravel units), we reject the notion that LFA1 is Beaufort Formation gravels (*sensu stricto*), and instead argue that these are either glacifluvial deposits, or are "local" fluvial deposits that reworked proximal glacial deposits. The depth of landscape incision, northeastwards imbrication of clasts, and occurrences at several sites up and down-valley of HR 1 within the present drainage basin suggests a meandering thalweg that carried eastward down-valley towards a proto-lower Horton River drainage. There is no geomorphic or sedimentological evidence to suggest a buried channel draining north or west across the bedrock divide into a proto-Anderson River from this site. Fundamentally, the Cretaceous strata that encircles and underlies this drainage basin (Figs. 1b and 5) cannot be considered the source of the majority of clast lithologies in LFA1. Instead, the LFA1 deposits conform best to glacifluvial outwash from an ice margin advancing from the south-southeast.

Also important in reconstructing the palaeoenvironmental history of this site is an ice wedge pseudomorph in LF3, reported by Duk-Rodkin and Barendregt (2011) but covered by colluvium

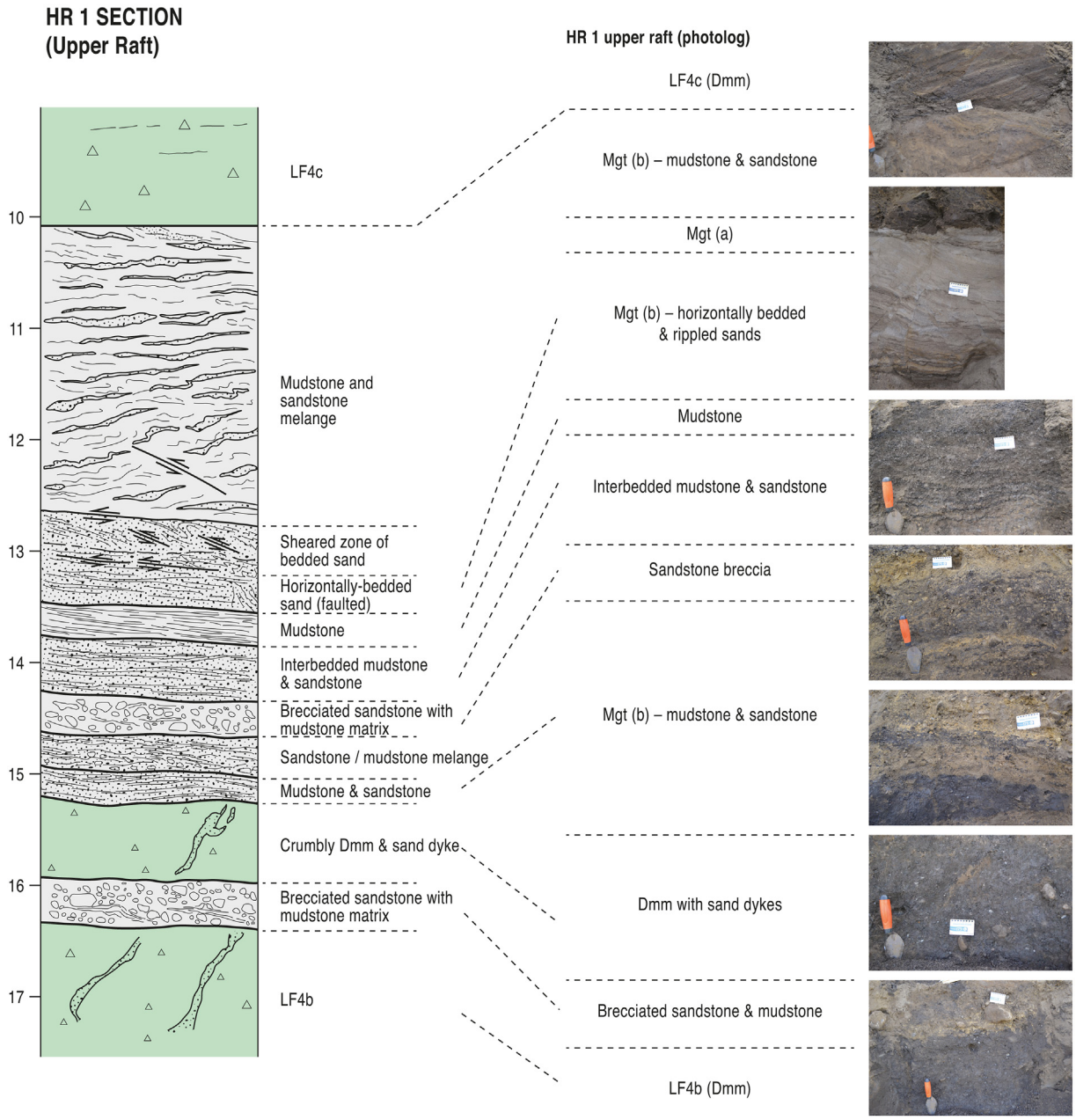

Fig. 16. Details of the upper raft in section HR 1: left) vertical profile log showing lithofacies characteristics; right) vertical photo log (not to scale) of the main lithofacies characteristics.

during this investigation. This feature indicates a period of permafrost conditions after the deposition of LFA1. This feature was truncated by the development of the mélange zone at the top of LF3, and was indicated by Duk-Rodkin to be infilled by diamictic material (pers. comm., 2020).

LFA2 comprises LF4 and all its enclosed bedrock intraclasts as well as the mélange zone (Mt I and IV) that has been created by the deformation of the top of LF3. The two sub-zones of the mélange are interpreted as glacitectonites (Mgt; *sensu* Evans et al., 2006; Evans, 2018), with Mt I and Mt IV representing the Type B (Mgt (b)) and Type A (Mgt (a)) glacitectonite classifications of Benn and Evans (1996), based on the intensity of deformation and preservation of parent sedimentary structures. Glacitectonite production occurred during the emplacement of overlying LF4a, which is interpreted as a subglacial traction till (*sensu* Evans et al., 2006; Evans, 2018) within which rafts of mudstone, shale, siltstone, and sandstone bedrock have been attenuated after their incorporation into the subglacial deforming layer (i.e. glacitectonic slices of Boulton et al., 2001) and subject to prolonged and/or intensive shear to produce pseudo-lamination (Dml). Less deformed bedrock rafts separating LF4a-b diamictons, which in themselves range from massive to pseudo-laminated and fissile, indicate that a range of strain signatures are recorded in LFA2. The range of raft attenuation, from the internally stacked 6 m thick upper raft (Fig. 16) to the stringers and wisps of the pseudo-laminated diamictons (Fig. 17), is indicative of a deformation continuum from bedrock cannibalisation to homogenization (Hicock and Dreimanis, 1992a, b; Kozarski and Kasprzak, 1994; Evans, 2000a, b, 2018).

The raft attenuation through to pseudo-lamination within the diamictons of LFA2, together with zones of dense fissility and

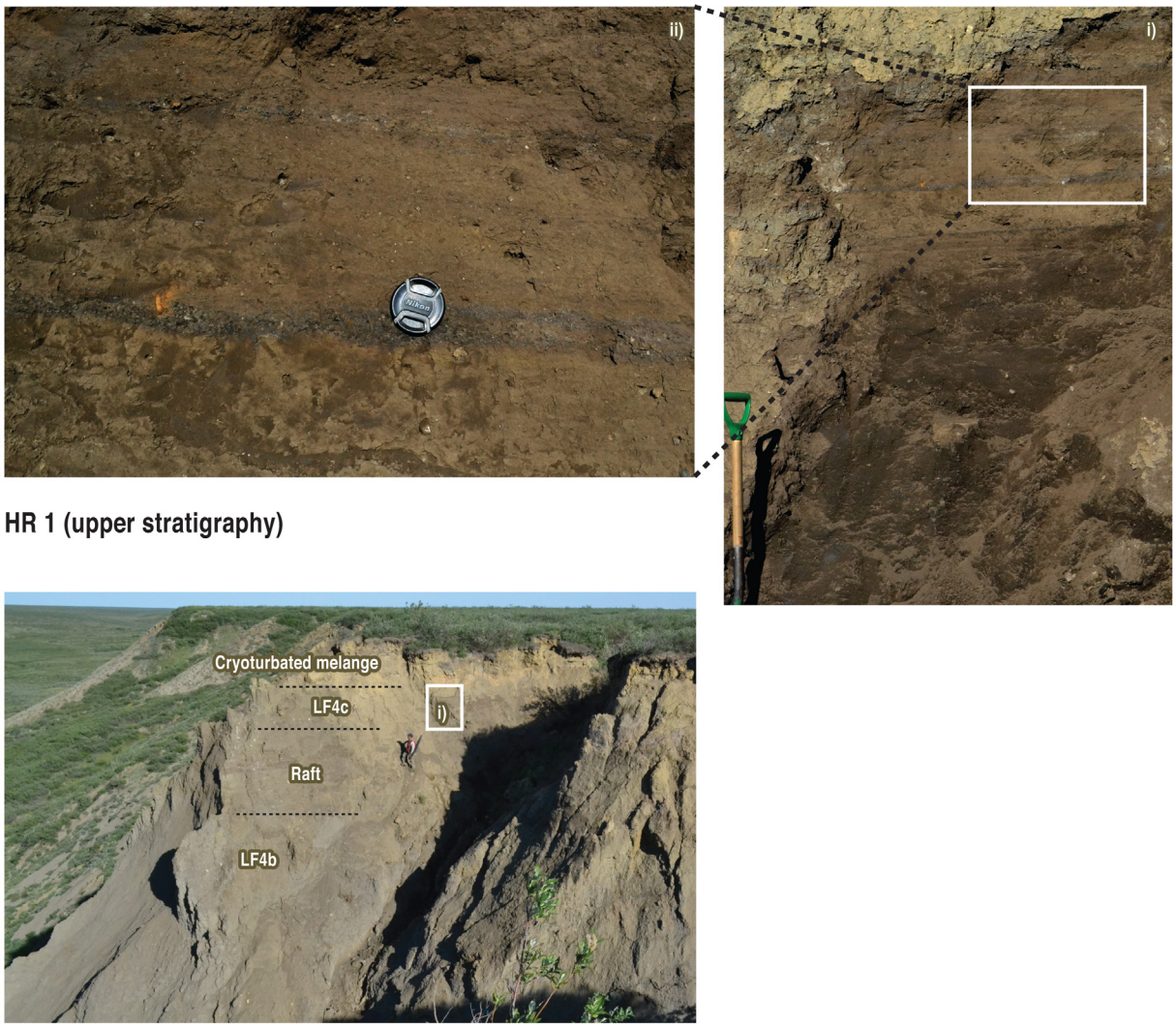

Fig. 17. Details of the upper stratigraphy at section HR 1 based upon a more accessible outcrop located c.100 m west of the main section face. Inset photographs show the pseudo-laminated (banded) and clast-poor nature of LF4c.

consistently well-orientated clast macrofabrics, are all indicative of subglacial traction till origins (Evans, 2018 and references therein). With the exception of the fabric from the middle of LF4b, all macrofabric strengths plot within the envelopes of known subglacial traction tills (upper and lower till envelopes on Fig. 20), with lower LF4a displaying a strength similar to fissile B horizons. Orientations display consistently shallow ENE or ESE dips, with the exception of upper LF4b, which gently dips westerly. These trends demonstrate that glacial shear stress was predominantly directed from east to west throughout the emplacement of the sedimentary sequence. The shallow westerly dip in upper LF4b could represent a progressive shift in ice flow direction from an Amundsen Gulf lobe to a Great Bear/Liverpool Bay lobe. It could also reflect localised modification of an easterly oriented clast fabric brought on by the emplacement/ploughing of the large bedrock raft above.

Clast form data from LFA2 show similar shapes but higher angularity to those of High Arctic tills (Fig. 19; Supplementary data S1), although this may simply be reflective of relative lithic comminution characteristics. A clear vertical trend exists in clast form co-variance in LFA2 (Fig. 19), with an increase in RA values (i.e. decreasing roundness). This increasing angularity indicates that the influence of the immediate substrate (basal gravels of LF1) was sequentially diluted after the emplacement of LF4a (till), which had clearly cannibalised LF1 clasts during glacier overriding. Such increasing or anomalously elevated angularity trends in tills have been equated to quarrying in areas of hard bedrock (Evans et al., 2016; Evans, 2018), and conforms to glacial erosion of harder regional Ordovician and Devonian strata (Fig. 1b). This is reflected also in the appearance of granitic material and limestone and an increase in dolomite in the tills. Limestone clasts, present in the LF4a and 4b diamicts, are absent in the LF4c units where dolomite percentages in the diamicton fines (<0.63 mm) are at their highest (Supplementary data S2). Both the upper two diamicton samples (G5, G6, Fig. 13; Supplementary data S2) contained only 15 clasts each >1.6 cm diameter; all the rest used in the clast lithology compilations were >0.8 cm diameter, and all such sized clasts recovered were included in the lithic analyses. Scans of the gravel <0.8 cm revealed no recognizable limestone fragments. The relative abundance of ironstone, and to a lesser degree, sandstone, in LFA1 are perhaps the strongest indicator of the incorporation of local bedrock clasts. However, that the clast compositions are otherwise so broadly similar between the lower gravels and all the overlying diamictons, further argues for glacifluvial deposition of the basal gravel, arising from glaciers traversing the same bedrock terrain,

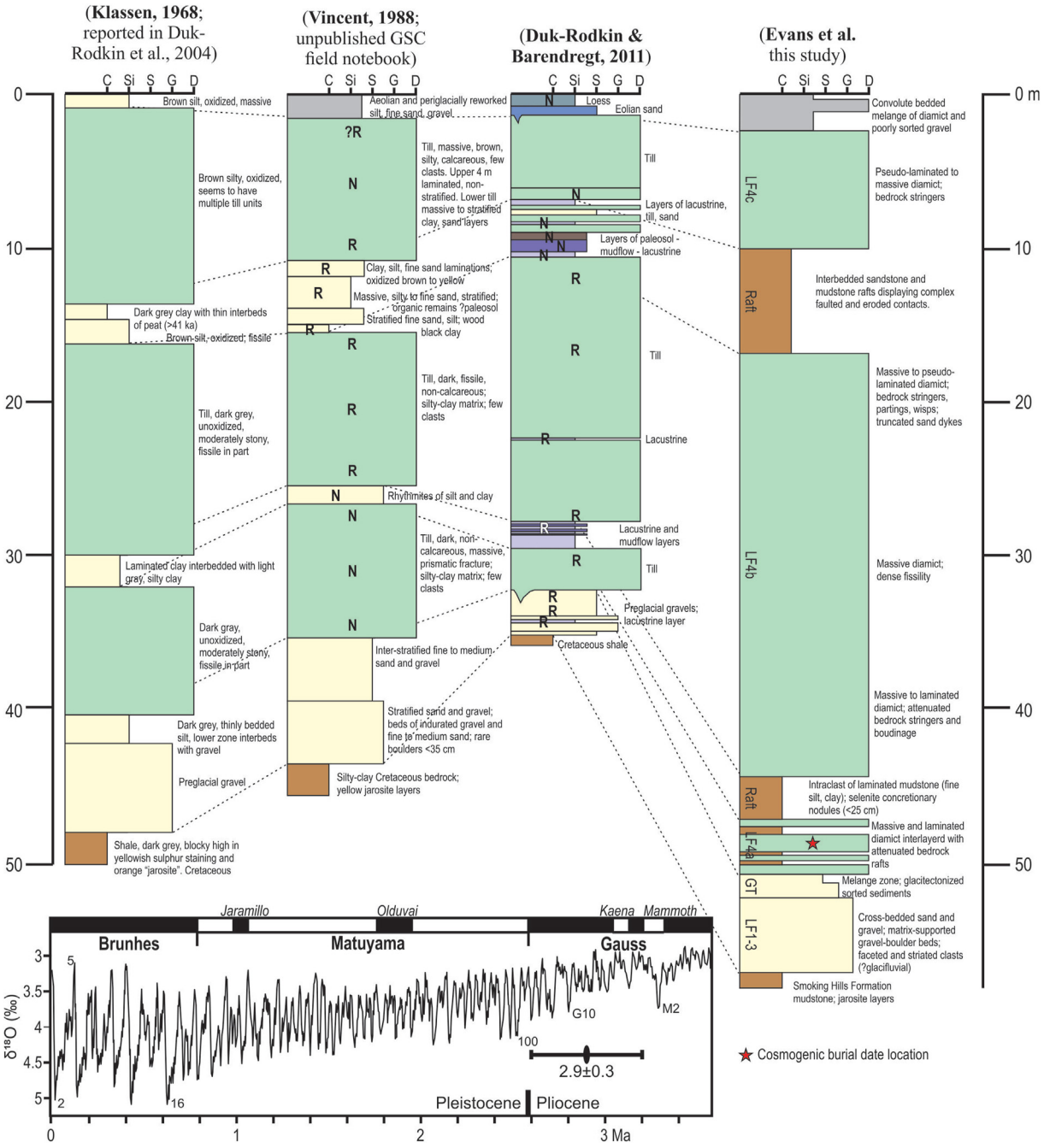

Fig. 18. Historical lithostratigraphic logs of section HR 1. Klassen's original 1968 field log was reconstructed and presented by Duk-Rodkin et al. (2004), while Vincent's 1988 log is our reconstruction from his field notebook account and his reported palaeomagnetic measurements. Stratigraphic correlations between logs are made in accordance with our revised sedimentological interpretations, and units are linked based on specific correlative sedimentological descriptions (e.g. rhythmites of silt and clay) and photographs, discounting previous genetic descriptions. Below, the stacked marine $\delta^{18}O$ isotopic record of Lisiecki and Raymo (2005) for the last 3.6 Ma is plotted alongside the palaeomagnetic chart of normal and reversed polarity chrons and subchrons. Our cosmogenic nuclide isochron burial age for LF4a (47.5 m depth; discussed below) is plotted at 2.9 ± 0.3 Ma.

east and south of this basin as all subsequent glaciations.

The change in geochemical signature between LF4a and both overlying diamictons (LF4b and LF4c; Supplementary data S2) is likely an indication of a higher concentration of Smoking Hills Formation bedrock in the till matrix of LF4a. Once the Smoking Hills Formation was covered or sealed off by a developing till sheet, it would have been increasingly difficult for ice to cannibalise the bedrock substrate. This is reflected also in the higher clay (<4 μm) contents of the lower diamicts (Supplementary data S2), which is further diluted in the matrix of the upper diamict (LF4c) likely due to its amalgamation with the sandy materials of the underlying upper bedrock raft (Fig. 16). Additionally, a higher bedrock content within the matrix of LF4a is reflected in its dark grey colour and multiple attenuated mudstone rafts overlying and partially derived from an underlying bedrock glacitectonite.

The convolute-bedded mélange that caps the HR 1 section is of postglacial periglacial origin. This is demonstrated by its surface representation as patterned ground features especially, but also by the enclosed convolution structures, which are indicative of cryoturbation.

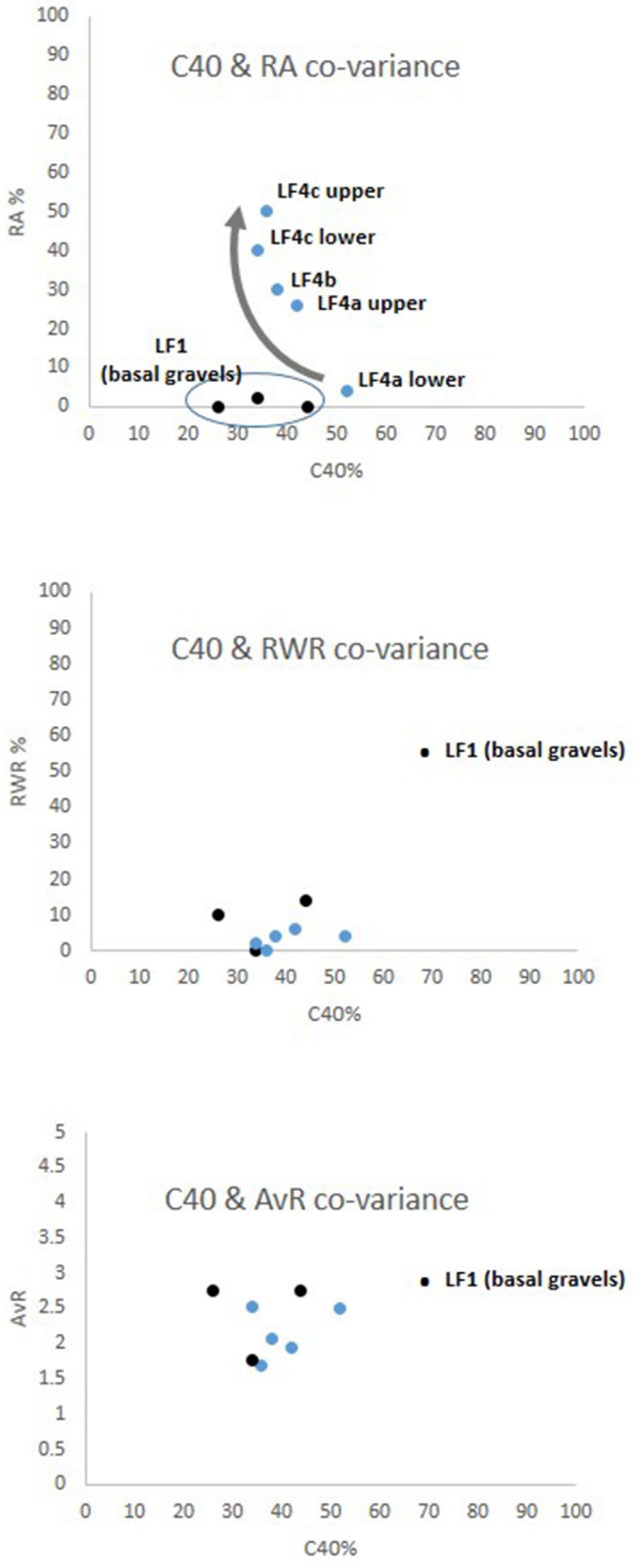

Fig. 19. Clast form C40/RA co-variance graphs for section HR 1 and LF1 gravels from section HR 2. Arrows in each plot show vertical trend in RA, RWR and AvR for lithofacies 1 and 4 in section HR 1.

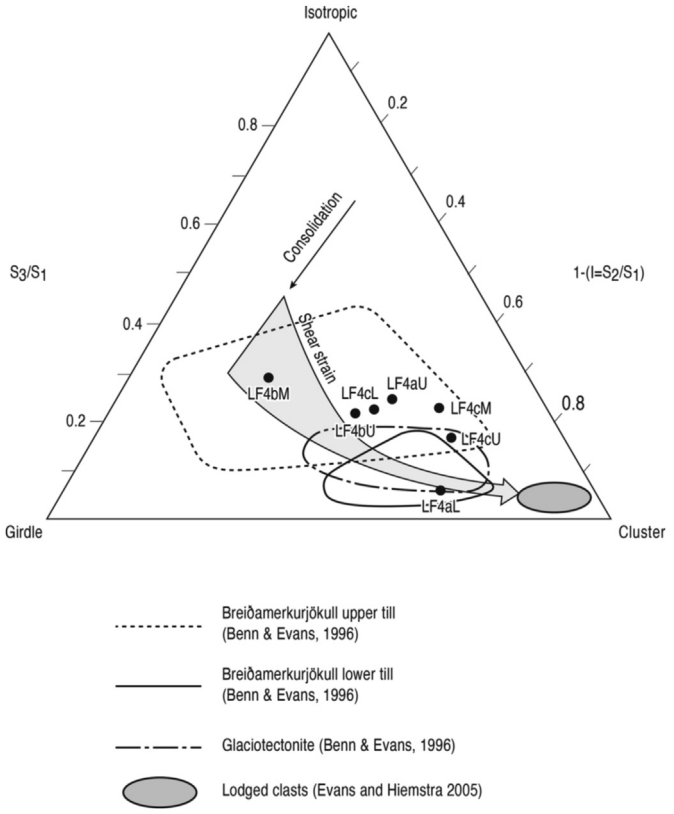

Fig. 20. Clast fabric shape ternary plot (after Benn, 1994) containing envelopes of fabric shapes for lodged clasts, subglacial traction tills (Icelandic upper/A and lower/B horizons) and glacitectonites, as well as the influence trends for consolidation (black arrow) and shear strain (grey arrow) proposed by Iverson et al. (2008). Sample labels identify lithofacies (e.g. LF4b) and location (upper - U, middle - M, lower - L).

Lithologically, clasts from the HR 1 section diamictons are broadly similar to those of the plateau ("Beaufort Formation") gravels, and inspections of the finer clast material reveal that the same range of lithologies are found in each deposit type. There is a difference, however, when comparing the LF4c diamictons with the plateau gravels, which display increased chert and quartz abundances and an accompanying decrease in dolomite and sandstone clasts (Figs. 4a and 13). The plateau gravels also possess a slightly higher average roundness (Figs. 4a and 13). This slight increase in clast rounding, and decrease in less resistant lithologies, supports the interpretation that the plateau gravels are derived from reworked glacial deposits. The plateau gravels were sampled from sites generally north of HR 1 (Fig. 6a), so different ice flow trajectories could account for some differences in clast lithology composition.

4.2.2. Section HR 2 (69.232213°N; −126.994842°W)

4.2.2.1. Description. The base of section HR 2 is composed of 3–6 m of Smoking Hills Formation mudstone. Importantly, this bedrock shows evidence of low strain deformation in the form of locally contorted and asymmetrical open folded bedding, recording a general stress direction from the southeast (140°; Fig. 21). This is unconformably overlain by LF1, which is a 3.2 m thick sequence of horizontally bedded gravels, comprising alternating beds of poorly sorted to sandy matrix-supported pebble to cobble gravels and occasional well sorted granule to pebble gravels (Fig. 21). Clast forms are sub-angular to sub-rounded (AvR = 2.52; RA = 2%) with a C40 of 34% and a total of 4% with striated surfaces. Clast lithologies in LF1 (sample CL1 in Fig. 21) are dominated by chert and quartzite,

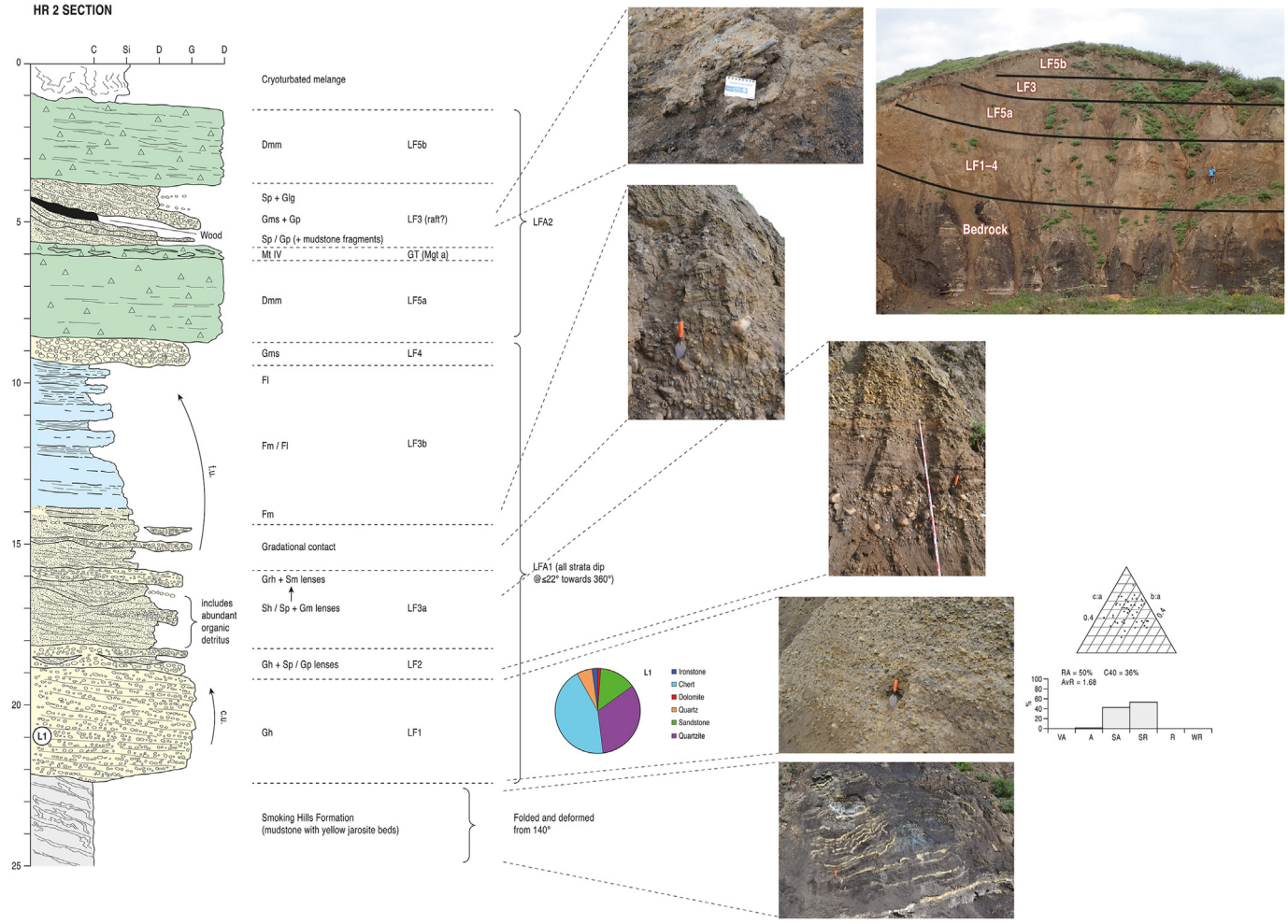

Fig. 21. Vertical profile log of section HR 2 with relevant data and photographs of some typical lithofacies, and a cross-section showing upward deformation of the bedrock through to LF5a.

with lesser amounts of sandstone and quartz. It was also noted that in the fine gravel fraction there was abundant fragmented shale/mudstone clasts. Like the HR 1 section, no granitic material was found in these basal gravels.

The upper 1 m of LF1 coarsens upwards towards the base of LF2, which displays a conformable contact with LF1 and comprises 0.60 m of similar horizontally bedded gravels but also contains lenses of planar cross-bedded sands and fine gravels. Conformably overlying LF2 is a 9 m thick fining upwards sequence, classified as LF3 and sub-divided into two sub-lithofacies (LF3a and 3b) which are separated by a 1.5 m thick gradational contact zone (Fig. 21). LF3a is characterised by cross-bedded and scour fill sequences of horizontally and planar bedded sand with massive, fine to coarse gravel lenses which grade upwards to horizontally bedded granule gravels and massive sand lenses. Included within the base of scour fills in LF3a are significant concentrations of reworked organics, mostly woody detritus, including intact spruce cones. Separating LF3a and 3b is the gradational contact zone, which comprises interbedded units of massive fine gravel and cross-bedded sands, fining upwards to massive fine sands and silts. This fining upward trend then continues with 4.5 m of interbedded units of massive and laminated silts and clays (LF3b), which form weakly developed rhythmites in their upper 3 m (Fig. 21). Importantly, all the strata in LF 1–3 dip consistently at 22° towards the north (360°).

Truncating LF3b is a 0.60 m unit of matrix-supported gravels (LF4) which is in turn truncated by the base of a 7.5 m thick massive, matrix-supported diamicton (Dmm). The diamicton is further sub-divided into LF5a and 5b, due to the occurrence of an intervening, 1.8 m thick unit of sand and gravel. The characteristics of LF5a are a predominantly massive but locally fissile appearance, with some faint pseudo-lamination being imparted by wisps of fine silt. Fissility is more prominent and densely developed in LF5b. The sand and gravel unit that separates LF5a and 5b appears initially to be an *in situ* sequence of planar cross-bedded sands and fine gravels with areas of matrix-supported gravel and gravel lags, and importantly containing mudstone fragments derived from the local Smoking Hills Formation bedrock as well as a substantial bed of woody detritus. These characteristics are identical to those of LF3a. Although these deposits do not appear to have been deformed or displaced, they are separated from underlying LF5a by a significant 0.20 m thick boundary comprising a deformed and attenuated mixture of diamicton and sand typical of a Type IV mélange (*sensu* Cowan, 1985; cf. Evans, 2018).

The uppermost 1.1 m of section HR 2 is characterised by a convolute-bedded mélange composed of highly contorted laminations of fine sands, silts and silty clays. On the land surface above the section these deposits form patterned ground features such as non-sorted hummocks, frost boils and ice wedge polygons.

4.2.2.2. Interpretation. Section HR 2 lies within a valley in which

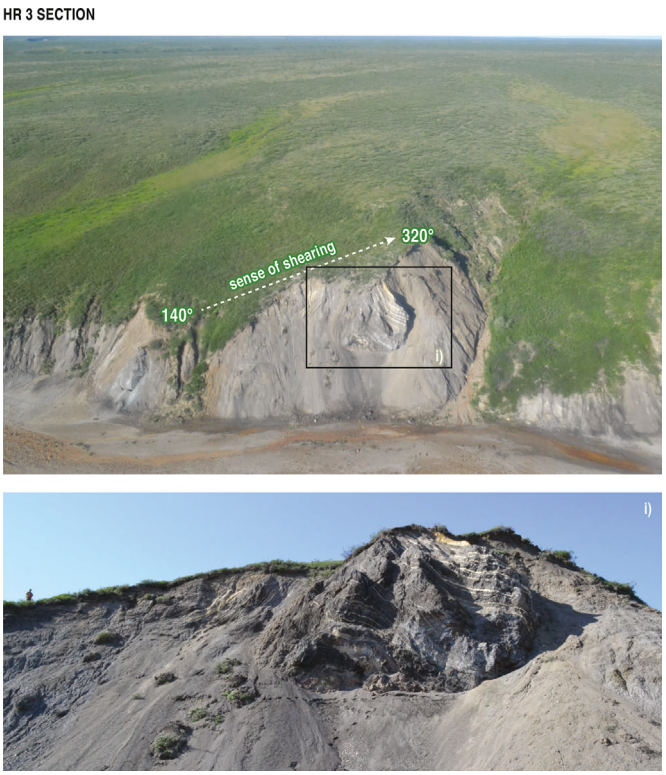

Fig. 22. Annotated photographs of section HR 3.

substantial bedrock contortions are evident in exposed river-side cliffs and hence some interpretations presented here are consistent with the observations made at other locations (see section HR 3). The deformed mudstone at the base of section HR 2 is interpreted as glacitectonically disturbed Smoking Hills Formation bedrock, because there are no known tectonic events that could otherwise account for the folding of horizontally bedded strata in the region (Yorath et al., 1975; Yorath and Cook, 1981). A SE-NW imposed stress direction indicates that the glacier ice responsible for the deformation advanced from the southeast.

The various lithofacies in section HR 2 are grouped into two lithofacies associations. LFA1 comprises LF1-4, which largely constitutes an overall fining-upward sequence, from horizontally bedded fluvial sheet flow gravels (LF1), through cross-bedded and scour fill sequences typical of migrating channels and bars of gravel bed river deposits (LF2-3a), to partly rhythmically bedded massive and laminated silts and clays typical of deeper water sedimentation (LF3b); an abrupt return to higher discharge stream activity is then recorded by the matrix-supported gravels of LF4, which we interpret as a glacifluvial outwash deposit. Organic detritus in scour fills in LF3a indicate that pre-existing, non-glacial peat and woody debris, typical of an arctic boreal forest environment, were reworked by stream erosion (cf. Davies et al., 2014). The predominantly sub-rounded clast forms of LF1 are slightly more rounded and more blocky than those of High Arctic glacifluvial sediments but are identical to those of LF1 and 2 in section HR 1 (Fig. 19) and include small numbers of clasts with striated and faceted surfaces. While there is no evidence for till deposition over the folded bedrock, a proximal glacial advance (like at section HR 1) is still required to supply the erratic clast complement along with the striated and faceted clasts in LF1. We suggest that the fining upward sequence in LFA1 records glacifluvial followed by deeper water sedimentation indicative of impeded drainage and ice-dammed lake formation. The consistent 22° dip of all the LFA1 strata towards the north, especially the rhythmites, indicates that the whole 6 m association has been tilted, likely by glacitectonic disturbance, but shearing direction is difficult to assess. This deformation event could have been responsible for the deeper seated disruption of the mudstone bedrock, whereby a thrust mass comprising LFA1 was displaced over the bedrock whilst being tilted northwards. Like the LFA1 sands and gravels at section HR 1, the palaeo-thalweg of the river depositing these fluvial/glacifluvial sediments appears to broadly conform to the existing drainage pattern eastward towards a proto-lower Horton River.

LFA2 comprises LF5a and 5b together with a separating raft of LF3. The LF5a diamicton represents direct glacigenic deposition in the form of a subglacial traction till, as indicated by its matrix-supported and fissile to pseudo-laminated appearance. Additionally, the 1.8 m thick unit of sand and gravel that resembles LF3 has been emplaced over a Type IV mélange, which is interpreted as a Type A glacitectonite (*sensu* Benn and Evans, 1996; Evans et al., 2006; Evans, 2018), developed as a shear zone between the sands and the diamicton at the top of LF5a. Hence the LF3 sand and gravel unit is not *in situ* but is instead a raft that forms part of a stacked sequence in which the upper till (LF5a) has been glacitectonically thickened.

There is a complex history of glacitectonic deformation preserved in this section that may include multiple events over successive glaciations. A pronounced upward deflection of the western, valley-ward edge of this section carries from the underlying bedrock through LF5a (Fig. 21), suggesting that the formation of the glacitectonite capping LF5a, and the emplacement of the raft of upper LF3 gravels was responsible for the deformation. This deformation appears separate from that which independently inclined the lower LFA1 strata. The uppermost LF5b diamict capping the LF3 gravels appears undeformed.

The uppermost cryoturbated mélange that caps section HR 2 is of periglacial origin. This is demonstrated by its surface representation as patterned ground features that have been constructed by the cryoturbation of what appear to be aeolian deposits.

4.2.3. Section HR 3 (69.226998°N; −126.999056°W)

4.2.3.1. Description. Section HR 3 displays a large deformed Smoking Hills Formation bedrock structure located directly southwest and across the valley from section HR 2 (Figs. 6b and 22). It has been deformed into a ≥20 m high crumpled fold structure with overturned anticlinal crests indicative of stress imposed from the southeast (140°). The structure has been truncated and capped by gravelly and diamictic materials but widespread slumping and vegetation cover restricted assessment of the overlying deposits.

4.2.3.2. Interpretation. As discussed, there is no evidence for regional tectonic events that could account for the folding of the horizontally bedded Smoking Hills Formation strata, thus the deformed mudstone in section HR 3 is also interpreted as glacitectonically disturbed. It is a compressed or polyclinal fold structure that was created by glacier ice flowing into the area from the southeast. The extensively slumped gravels and diamictons that cap the structure likely correlate with those seen in section HR 2. This section is important in that it verifies the significant glacitectonic disruption of bedrock in the region, in this case down to at least 20 m. Such vertical displacements have the potential to construct significant glacitectonic landforms which may be manifest as surface features even when overlain by tills and glacitectonites (e.g. ice-thrust ridges).

4.2.4. Section HR 4 (69.411278°N; −126.601772°W)

4.2.4.1. Description. Section HR 4 is a 38 m thick complex sequence of diamictons and stratified deposits comprising predominantly

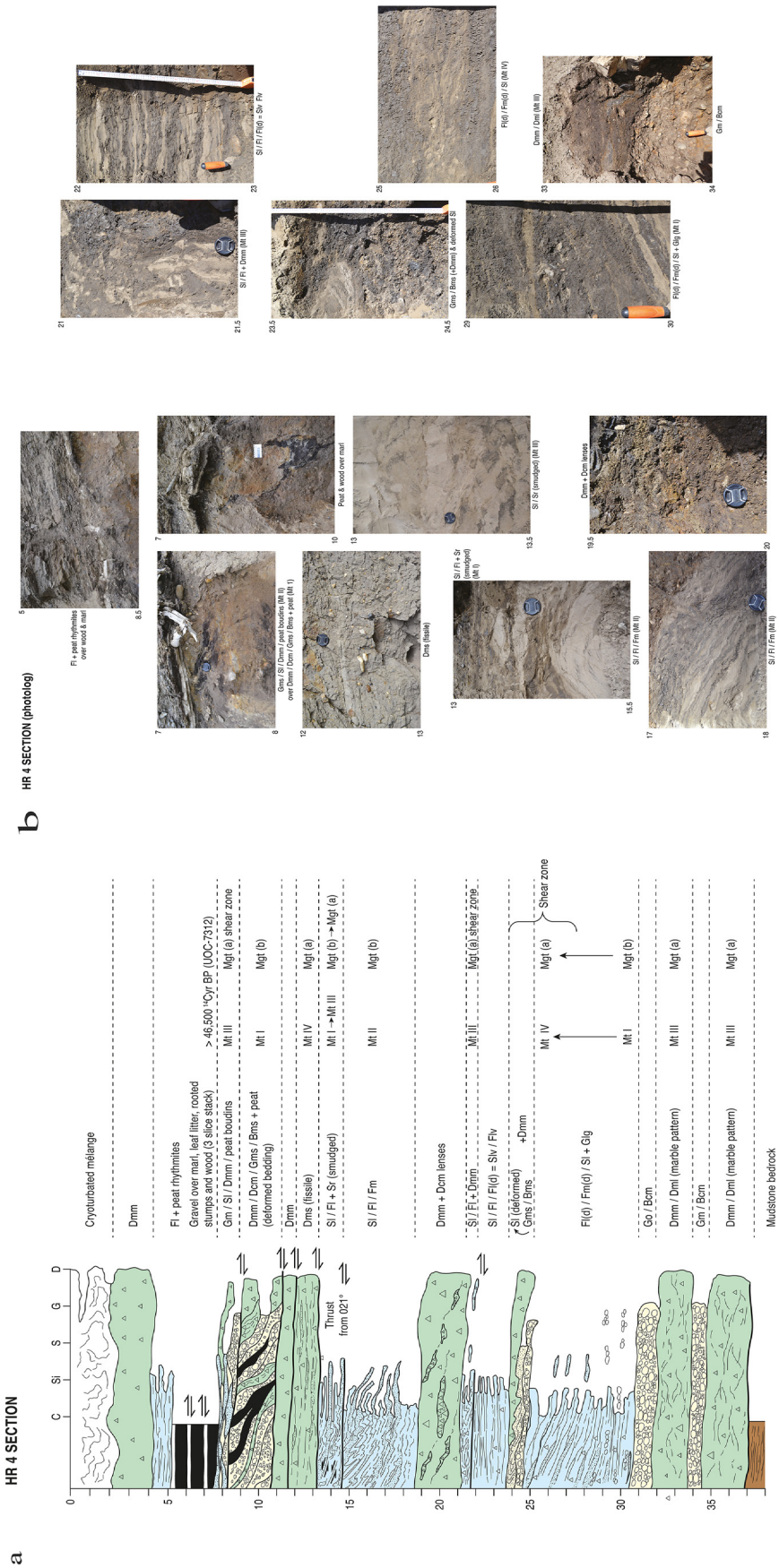

Fig. 23. Details of section HR 4: a) vertical profile log; b) vertical photograph log.

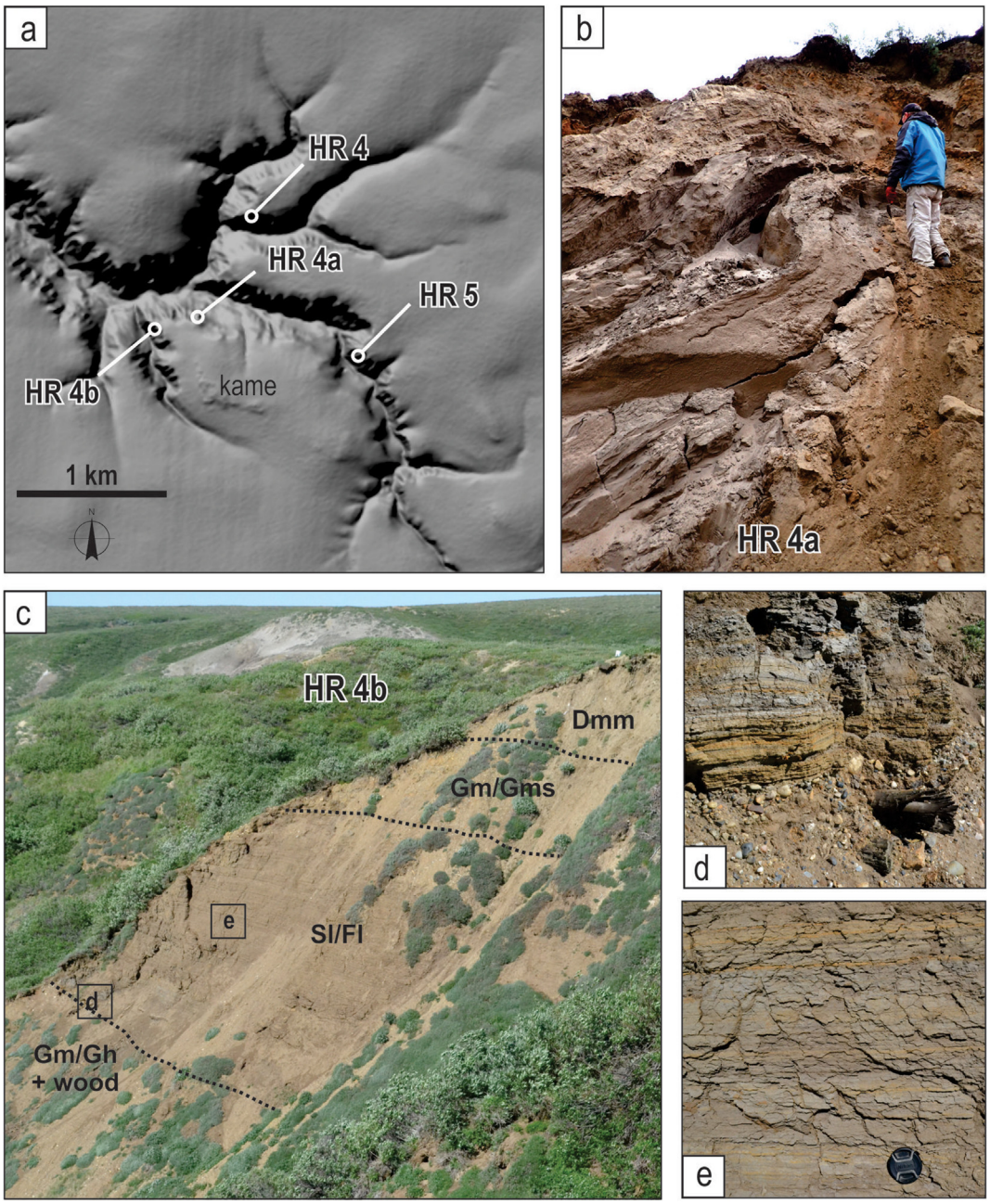

Fig. 24. Northeast field sections: a) locations of sections HR 4, 4a, 4b and 5 (ArcticDEM hillshade base map image); b) section 4a, convolute deformation of >8 m of laminated glacilacustrine sands underlying massive to planar laminated gravels; c) section 4b photographic log; d) detail of lower wood-bearing Gm/Gs – Sl/Fl contact; e) detail of planar laminated glacilacustrine Sl/Fl.

fine grained rhythmites and poorly-sorted gravels (Fig. 23), situated in the upper part of an unnamed eastern tributary to the lower Horton River (Fig. 6). The diamictons are predominantly clast-poor and range from 0.10 to 2.50 m thick, and in some cases pinch out across section. At the base of the section, two massive, matrix-supported to pseudo-laminated diamictons appear to be composed of a clay-rich matrix that varies in colour so that it appears as a marble pattern. In the middle of the section (18.5–21.2 m depth), an otherwise massive, matrix-supported diamicton contains clast-rich diamictic lenses (Dcm) that display boudinage and are inclined consistently towards the east. In the upper middle part of the section (7.5–13.2 m depth), four diamictons and their associated stratified sediments are stacked upon one another, as indicated by erosional and/or sheared boundaries. The lowest, 1.6 m thick, diamicton is stratified but the sorted beds have been highly attenuated and the surrounding matrix appears highly fissile. This is overlain by a 0.80 m thick, massive, matrix-supported diamicton, which is in turn overlain by an internally deformed, 2.2 m thick unit comprising matrix- and clast-supported diamictons that are interbedded with matrix-supported gravels and boulder gravels and peat beds. Finally, the uppermost diamicton in the four-fold stack is a discontinuous lens within a tectonically interbedded 1.5 m thick sequence of massive gravel and laminated sands with peat lenses, all displaying attenuation and boudinage. The top of the section is capped by a 2 m thick massive, matrix-supported diamicton which has been modified by the development of

cryoturbation cells in the active layer.

The stratified deposits of section HR 4 have been largely modified by deformation. The coarsest of these deposits are massive cobble and boulder gravels, which appear to fine abruptly upwards into laminated sands in places. The finest stratified deposits consist of laminated to massive sands, silts and clays, which locally contain dropstones and clast lags; rhythmites with the appearance of varves occur in the middle part of the section. Deformation is apparent, especially in the finer-grained deposits, in the form of polyclinal folds, thrusts and thrust overfolds, the attenuation (boudinage) of bedding and smudged sand ripples (smudged bedforms; Evans, 2018). Relatively large scale folds have been truncated by shallow thrust faults in the stacked diamicton sequence of the upper middle section. A three-fold stacked sequence of 5–20 cm thick beds of marl, overlying lenses of muddy gravels (overbank deposits), 5–15 cm thick undisturbed leaf litter and peat mats atop a layer of vertically-rooted tree stumps (preserving fine rootlets) and wood (≤18 cm diameter trunks) occurs in the upper part of the section and appears to have been sheared over the underlying stacked diamictons, as evidenced by peat boudins in a Type III mélange at the top of the stacked diamictons (*sensu* Cowan, 1985; cf. Evans, 2018). A radiocarbon date on a vertically rooted stump yielded a non-finite age of >46,500 ^{14}C yr BP (UOC-7312; Supplementary data S3).

One kilometre southwest of section HR 4, stream cut exposures of thick Quaternary deposits on opposite sides of a headland reveal both highly deformed (HR 4a) and undeformed (HR 4b) stratigraphic sequences containing lithofacies similar to those in the intensively disturbed stratigraphy of section HR 4 (Fig. 24). In section HR 4a, >8 m of fine to medium sand have been intensely deformed into convolute bedding. These deposits are unconformably overlain by 2 m of massive to planar stratified, matrix-supported gravel and gravelly-sand. In section HR 4b, the base of the sequence (Fig. 24) comprises ≤2.5 m of massive to crudely horizontally bedded, medium to coarse gravels that contain significant quantities of wood detritus including small logs. This is abruptly overlain by ≤15 m of fine sand and silt rhythmites that display clear couplets of relatively fine and coarse laminae. In a coulee to the immediate south, these sand and silt deposits preserve a prominent ice wedge pseudomorph, suggesting periods of both glacilacustrine and subaerial (permafrost) exposure. An erosional contact separates the rhythmites in section HR 4b from an overlying 5 m of massive to matrix-supported, coarse gravel, which is in turn overlain by a 3 m thick massive, matrix-supported diamicton with a cryoturbated surface.

4.2.4.2. Interpretation. Overall the appearance of the stratigraphy in section HR 4 is one of deformed sediment stacks. This is manifest in the numerous apparent thrust fault boundaries, one of which reveals displacement from the north-northeast (021°), as well as the appearance of various mélanges throughout the stratigraphy. The two lowermost diamictons with their marble patterns are defined as Type III mélange, likely derived from underlying mudstone bedrock. Lying above these diamictons, 6 m of deformed laminated sediments reveal a vertical development from Type I to Type IV mélange, which is effectively a change from Type B to Type A glacitectonites (*sensu* Benn and Evans, 1996; Evans et al., 2006; Evans, 2018); the Type IV zone at the top of this unit is associated with a 1 m thick deformed zone of gravels, sands and diamicton, collectively interpreted as a shear zone (Fig. 23). A further shear zone occurs 2 m above this, where a Type III mélange represents a Type A glacitectonite that has been constructed from underlying laminated fines and overlying diamicton; the inclined attenuated gravelly diamict lenses (boudins) in this diamicton have likely been cannibalised from underlying gravel units and sheared from the east. Above this, the 5.25 m thick laminated sediments can be sub-

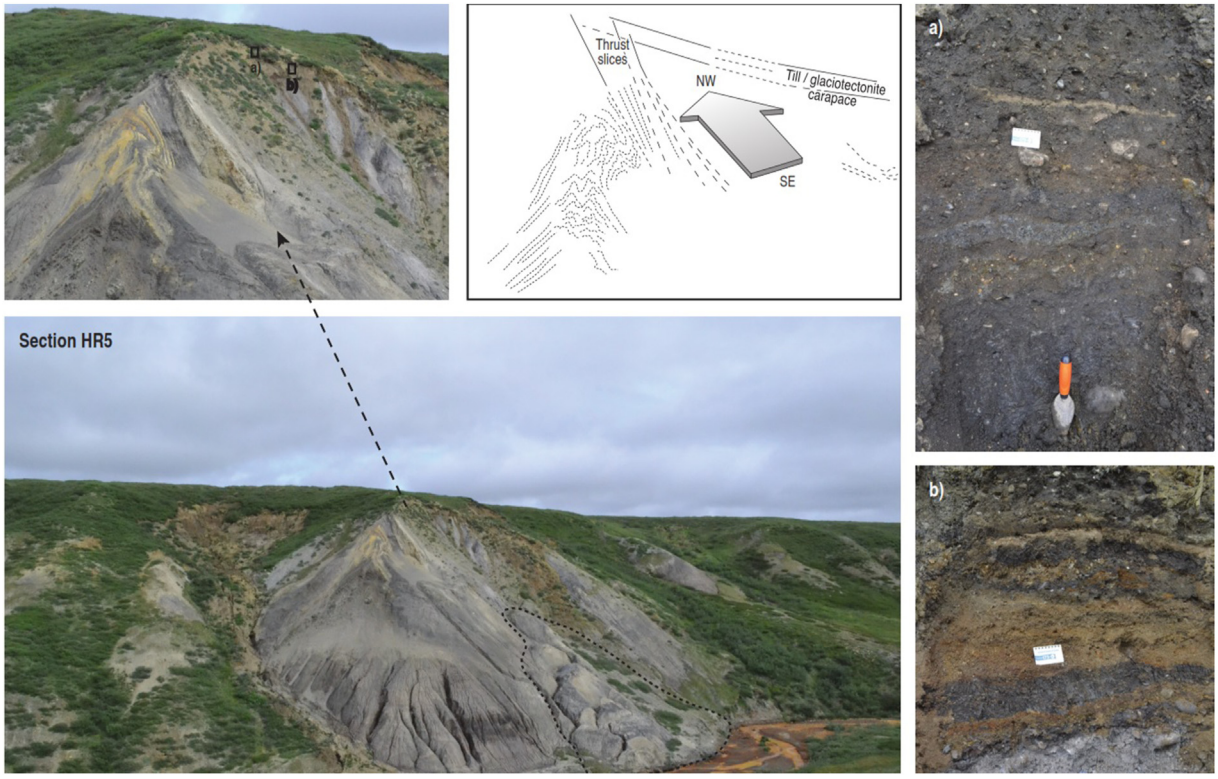

Fig. 25. Annotated photographs of section HR 5 with sketch of main glacitectonic structures. Area outlined by short dashed line is modern mass movement.

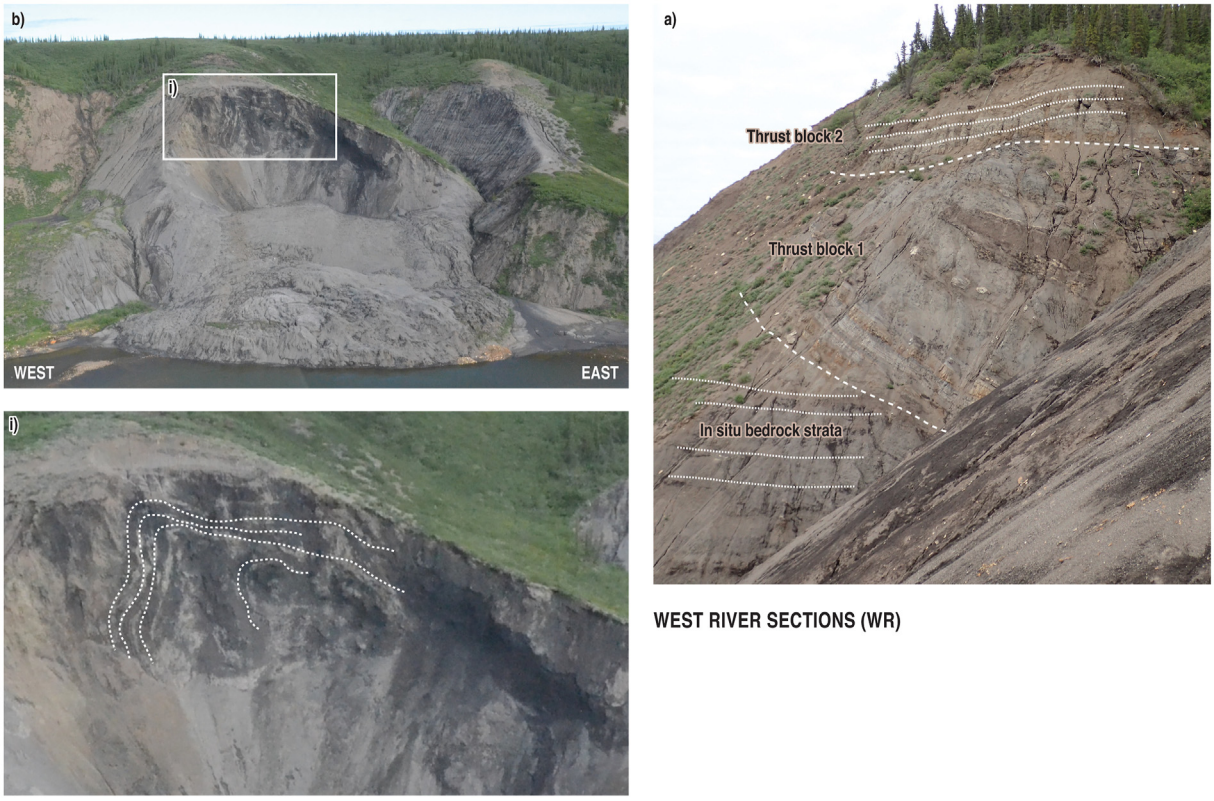

Fig. 26. Annotated photographs of the West River sections, showing main glacitectonic structures: a) blocks of Horton River Formation sandstone and siltstone thrust atop younger Smoking Hills Formation black mudstone; b) isoclinal fold structure in Smoking Hills Formation bedrock.

divided based on their tectonic signatures as well as a thrust fault contact, with the lower 4 m resembling a Type II mélange and the upper 1.25 m containing a range of patterns from Type I-III mélange; these patterns suggest that the lower 4 m is a Type B glacitectonite in which primary sediment structures can still be recognised, whereas the upper 1.25 m displays characteristics of both Type A and B glacitectonites.

The four-fold stacked diamictons and associated stratified sediments of the upper middle section appear to have been largely derived from the deformation of pre-existing stratified deposits. The lowest stratified diamicton is a Type IV mélange in which stratified inclusions have been highly attenuated and shear fissility has been imparted on the unit, and hence this constitutes a Type A glacitectonite. The origin of the overlying thin Dmm is unclear but the complex 2.2 m thick unit of folded diamicton, matrix-supported gravel, boulder gravels and peat interbeds displays the characteristics of a Type I mélange and is interpreted as a Type B glacitectonite (truncated folds) derived from older gravels and diamictons. Peat inclusions are instructive in terms of the wider stratigraphic record in that they are similar to other organic inclusions in gravels and sands in sections HR 1 and HR 2, the implications of which will be discussed below. The uppermost diamicton and stratified sediments of the four-fold stack is a Type III mélange and interpreted as a Type A glacitectonite constructed in a shear zone at the top of the underlying folded beds. The marl overlying peat-litter layer, and rooted stumps and wood couplet then appear to have been internally thrust stacked into three slices together with overlying peat-rich rhythmites, likely during the emplacement of the capping diamicton, which is hence most likely a subglacial traction till. The actual marl-litter layer-rooted stump deposits suggest entrainment and rafting of a former floodplain and possible oxbow lake environment. Marl is unknown from the Smoking Hills area, suggesting this originated from carbonate terrain located a significant distance to the east.

Although section HR 4 comprises a complex stack of glacitectonic rafts, the similarities between individual lithofacies in the sequence and those in sections HR 1 and 2 indicate that this stack is composed of LFA1 and 2 thrust slices. Deformation, at least in the upper part of the sequence, was imparted from the north-northeast by glacier ice advancing from Amundsen Gulf. The laminated fines in section HR 4, 4a and 4b record glacial lake sedimentation and therefore likely represent the presence of an ice-dammed lake that was impounded in the lower Horton River catchment by the advancing ice; inland ice flowing from the east and southeast (see sections HR 1 and 2) as well as lower Great Bear Lake/Liverpool Bay ice were likely also involved in this lake damming (see Discussion). Verification of this sequence of depositional events is provided by the sediments in section HR 4b, wherein the organic-rich gravels at the base of the sequence likely equate to LF 1–3 and the overlying rhythmites to LF3b in sections HR 1 and 2. The erosional upper contacts between the sands in sections 4a and 4b, and the capping Gm/Gms and Dmm, then record glacier advance likely correlative to LFA2 in section HR 2. That the same sand deposits in sections 4a and 4b (~250 m apart; Fig. 24) can record such stark differences in deformation, is an indication of the localised variability in glacitectonic disruption of pre-existing deposits as dictated by site-specific factors, especially location with respect to buried valley margins (e.g. Tsui et al., 1989; Evans et al., 2012; Andriashek and Atkinson, 2007; Atkinson et al., 2013), pre-existing slope failure masses (e.g. Campbell and Evans, 1990; Evans et al., 2012) and patchy development of near-surface taliks in the permafrost (e.g. Mathews and Mackay, 1960; Mackay and Mathews, 1964; Waller and Tuckwell, 2005).

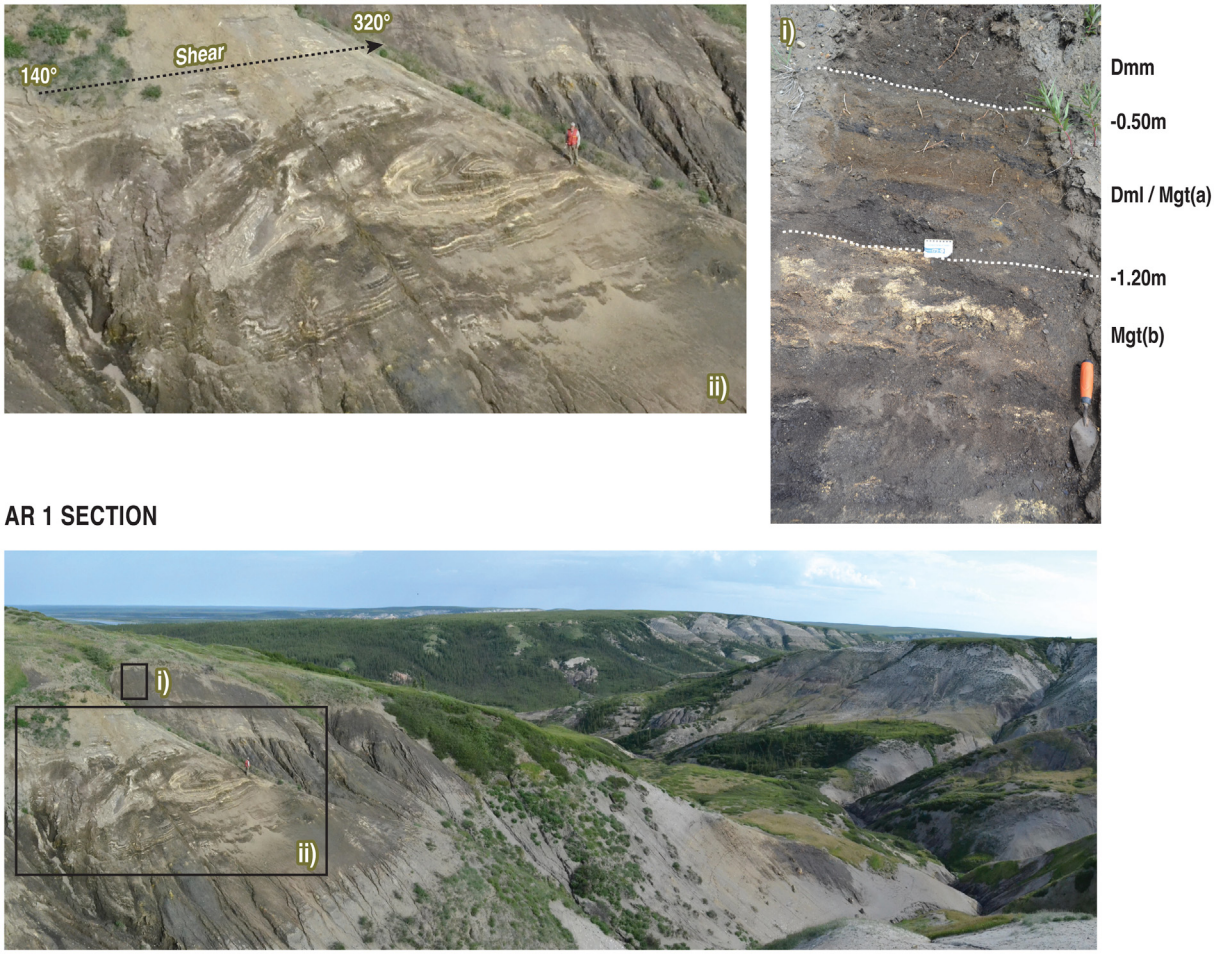

Fig. 27. Annotated photographs of section AR 1, showing main glacitectonic structures and overlying glacitectonite and till carapace.

4.2.5. Section HR 5 (69.406088°N; −126.587893°W)

4.2.5.1. Description. Section HR 5 is located ~1.1 km east of section HR 4 (Fig. 24), and comprises a >30 m high bluff containing highly deformed Smoking Hills Formation bedrock overlain by ≤2.0 m of very poorly-sorted, massive gravel and 1.80 m of interbedded sandy gravels, matrix-supported and clast-supported diamictons and mudstone lenses (Fig. 25). The interbeds are mostly discontinuous and most of them pinch and swell along the outcrop. They also grade upwards from gravel-dominated interbeds in the basal 0.20 m to banded or alternating beds of matrix-rich and clast-rich diamictons in the middle 1.10 m (Fig. 25a and b). This banding gives way in the upper 0.5 m to a massive, matrix-supported diamicton (Dmm), which contains no lenses other than attenuated light coloured shale bands (Dml) at its contact with the underlying banded diamictons (Fig. 25a). The lower 0.20 m is classified as a Type I mélange and the middle 1.10 m as a Type IV mélange (*sensu* Cowan, 1985; cf. Evans, 2018).

The structural components of the underlying deformed bedrock comprise a large, tightly compressed polyclinal fold that is truncated by several sheets of parallel-bedded strata with no apparent internal folding but dipping steeply (≤55°) towards the southeast (Fig. 25). The unconformable contact between the slabs and the truncated fold is marked by strongly developed Type IV mélange that resembles a marble pattern of crushed and variably attenuated fragments of mudstone.

4.2.5.2. Interpretation. Section HR 5 records glacitectonic deformation of the Smoking Hills Formation down to at least 20 m below the present land surface. A large truncated fold and overlying bedrock sheets, separated by a Type IV mélange, represent folding and thrust slice development in the Smoking Hills Formation by ice flowing into the area from the southeast. The exposures through the poorly-sorted massive gravels on the surface of the upper thrust slice indicate that they were also glacitectonically emplaced along with the bedrock. As these thrust slices lie below the present land surface, they must have been derived from a pre-existing (pre-glacial) valley lying approximately at the location of the contemporary valley. The glacitectonised materials are unconformably capped by a 1.8 m thick, vertically grading sequence comprising a lower Type I mélange, a middle Type IV mélange and an upper Dml/Dmm. In combination these deposits are indicative of cannibalisation and homogenization of underlying bedrock and gravels, and are therefore interpreted as a vertical continuum from a Type B to Type A glacitectonite and then to a subglacial traction till. The relative age relationships of the glacitectonized bedrock and overlying glacitectonite and till are unknown but given the southwesterly-directed stress recorded in the uppermost glacitectonic structures in this area (see Section HR 4), it is likely that the subglacial sediment carapace was emplaced during later ice flow phases.

4.2.6. West River Sections (69.021217°N; -126.692501°W)

Two large outcrops have been exposed by slumping and fluvial erosion along the West River and are significant in terms of bedrock

Table 1
Simple burial ages.

Sample ID	Lithofacies	Sample depth (m)	^{10}Be ± 1σ(katom/g)		^{26}Al ± 1σ(katom/g)		^{26}Al/^{10}Be ± 1σ(atom/atom)		Simple burial age ± 1σ		
			conc	unc	conc	unc	ratio	ratio unc	Ma	+Ma	-Ma
18SUV-503-S	LF4b (HR 1)	35.5	32.3	0.8	97.5	14.7	3.02	0.5	1.76	0.40	0.29
18SUV-502-S	LF4b (HR 1)	48.5	45.5	1.0	115.0	20.1	2.54	0.4	2.13	0.49	0.31
18SUV502-2	LF4a (HR 1)	48.5	29.9	1.3	122	20	4.10	0.7	1.09	0.46	0.30
18SUV502-3	LF4a (HR 1)	48.5	625	10	927	214	1.48	0.3	2.95	0.56	0.34
18SUV502-4	LF4a (HR 1)	48.5	34.6	1.0	47.1	8.6	1.36	0.3	3.46	0.52	0.32
18SUV-507-S	LF4a (HR 1)	49.5	76.3	1.6	111	13	1.45	0.2	3.28	0.30	0.21
18SUV507-1	LF4a (HR 1)	49.5	49.3	1.9	89.8	38.2	1.82	0.8	2.82	2.92	0.44
18SUV501-2	LF2 (HR 1)	54.0	16.8	0.5	77.9	13.6	4.63	0.8	0.84	0.50	0.31
18SUV501-5	LF2 (HR 1)	54.0	17.6	0.7	43.4	13.1	2.47	0.8	2.21	1.26	0.44
18SUV501-6	LF2 (HR 1)	54.0	19.5	0.8	59.4	24.3	3.04	1.2	1.77	2.96	0.46
18SUV-525-S	LF1 (HR 2)	20.0	20.8	0.7	56.9	10.1	2.74	0.5	1.94	0.54	0.29

Notes: Italicized samples with -S are sand, all others are cobbles. Concentration and ratio uncertainties are total analytical error.
Katom is 1000 atoms. Refer to Figs. 13 and 21 for section and lithofacies information and sample positions.

disturbance due to glaciation (Fig. 26). Although there are no exposures through the capping Quaternary deposits, it is clear that both locations lie below at least 5 m of diamictic material. At both sites, the undisturbed Smoking Hills Formation bedrock is visible as horizontally bedded strata. At the western section (Fig. 26a), horizontally bedded Smoking Hills Formation strata is cross-cut by a ≤20 m block of Horton River Formation sandstone and siltstone dipping 20–30° towards the east. This tilted block is then in turn truncated by ≤5 m of largely horizontal lying Horton River Formation strata, while to the east and west of this exposure, Smoking Hills Formation bedrock outcrops from river level to the top of slope (Fig. 26b). Clearly the upper c. 25 m of bedrock at this location (thrust blocks 1 and 2, Fig. 26a) has been glacitectonically dislocated from outcrops of Horton River Formation immediately south and east of here (Fig. 1b) and displaced westward and stacked by westerly flowing ice. At the West River eastern section (Fig. 26b) the Smoking Hills Formation mudstone strata have been crumpled into a weakly isoclinal fold structure with an axial plane dipping towards the southeast and therefore indicative of glacitectonic deformation by northwesterly flowing ice.

4.2.7. Section AR 1 (69.221034°N; −128.244391°W)

Located in the lower Anderson River, section AR 1 is an exposure through highly deformed Smoking Hills Formation bedrock on a deeply incised valley wall in an eastern tributary (Figs. 6a and 27). The deformation structure in the bedrock penetrates up to 15 m downwards into the otherwise horizontally bedded strata and comprises an asymmetric overfold with an axial plane dipping to the southeast (140°), recording glacitectonic shear from that direction. The top of the fold is truncated by a 1.70 m thick, matrix-supported diamicton comprising lower laminated or Type IV mélange (Dml; *sensu* Cowan, 1985; cf. Evans, 2018) and upper massive (Dmm) components (Fig. 27). The Dml lies abruptly but conformably over a Type III/IV mélange developed in the top ≤1 m of the underlying bedrock. This intensely deformed carapace over the fold structure is interpreted as a vertical continuum from a Type B (Mgt(b)) to Type A (Mgt(a)) glacitectonite and then to a subglacial traction till (Dmm), wherein the mixing of bedrock and further travelled erratic clasts appears in the Type A zone. Consequently, this continuum is regarded as a product of cannibalisation and homogenization of the folded bedrock by a subglacial deforming layer, generated by glacier ice flowing into the area from the southeast.

4.3. Chronostratigraphy

4.3.1. Radiocarbon dating

The five bivalve mollusc shell fragments and gastropod recovered from diamictons LF4b and 4c in section HR 1 all yielded non-finite radiocarbon ages (Supplementary data S3). The absence of a finite age cannot therefore be used to constrain the LF4c diamictons atop section HR 1 as Wisconsinan as we surmise them to be. It does not, however, rule it out. Laurentide ice advancing westwards through Amundsen Gulf and other inter-island marine channels could as well entrain and redeposit non-finite shells as they could a finite, pre-Late Wisconsinan age (cf. England et al., 2009; Lakeman and England, 2012). Regional compilations of radiocarbon dated shells and other organic materials point to an extensive area of northern mainland Canada and the southern Canadian Arctic Archipelago devoid of such sub-fossil remains (McMartin et al., 2019). Indeed some glaciological models (Stokes et al., 2012) have suggested that the central Canadian Arctic, including the Smoking Hills area, may have been subsumed by ice (through various waxing and waning glacial cycles) since at least OIS 5d (~110 ka). It is also noted that the local Cretaceous bedrock contains rare shell fragments (Yorath et al., 1975; and seen in scans of the A-23 well cuttings), and

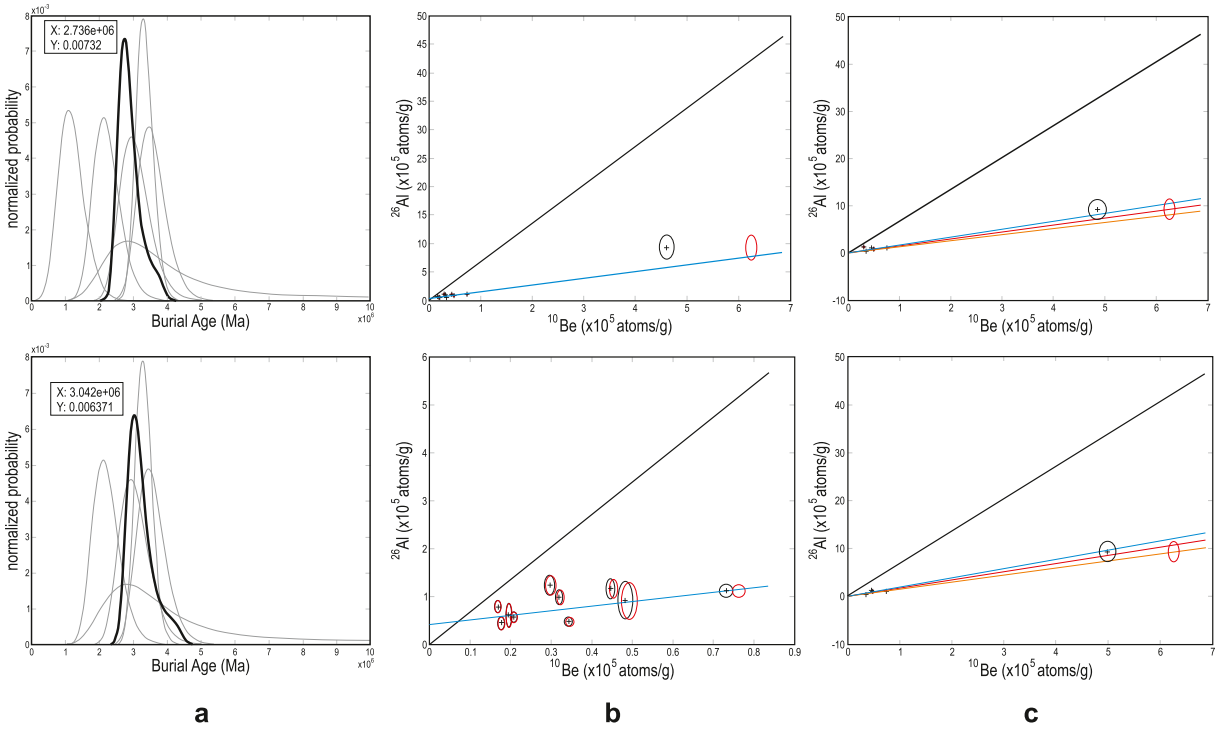

Fig. 28. Cosmogenic dating analytical graphs: a) convolved probability function distributions for $^{26}Al/^{10}Be$ simple burial ages. Upper - convolution of PDFs for all samples in LF4a (samples 502 and 507). Lower - convolution of all samples except sample 18SUV502-2 which yielded a significantly lower simple burial age beyond the 1σ confidence of this convolved age; b) ^{26}Al vs ^{10}Be isochron burial plots. Data is illustrated with different colour error ellipses (1σ); pale blue line is line of best fit from which burial age is inferred; black line has a slope of 6.75, defined by the production ratio of $^{26}Al/^{10}Be$ at surface. Upper - isochron based on all samples in Table 1. Lower - same as upper except the sample with high ^{26}Al and ^{10}Be concentrations (18SUV502-2) was removed to show a close-up of the remaining samples; c) ^{26}Al vs ^{10}Be isochron burial plots for LF4a based on samples at sites 18SUV502 and -507. Upper - isochron based on all samples from LF4a. Lower - same as upper except the sample with the high $^{26}Al/^{10}Be$ ratio (18SUV502-2) was removed. (For interpretation of the references to colour in this figure legend, the reader is referred to the Web version of this article.)

so non-finite radiocarbon ages could be from reworking of these shell remains too.

Klassen's non-finite peat date (>41 000 ^{14}C yr BP; GSC-1100; Lowdon et al., 1971) was likely from re-deposited organics found within the upper bedrock raft of HR 1, which appears to be the same stratigraphic location where Duk-Rodkin and Barendregt (2011) noted a 13 cm diameter log they identify as *Larix* sp. embedded in the section. *Larix* trees today are found 200 km to the southwest along the Mackenzie River, or almost 600 km southward, south of Great Bear Lake, suggesting a significant period of climatic amelioration, if the log was locally derived. Vincent (1988) also recovered a log (unknown species) within the upper part of our LF4c laminated diamict, just north of the main exposure and at the same location that we logged the uppermost sediments and also noted wood remains (Fig. 17). The stacked rafts of overbank deposits, rooted stumps, litter layers and marl in section HR 4 (Fig. 23) contain logs up to 18 cm diameter (species unknown), but similarly suggest a locally warmer climate than present. While it is tempting to suggest a Sangamonian (OIS 5e) interglacial age for these materials, additional methods, such as OSL dating, and rigorous palynological and macrofossil analyses will be required to resolve this. Regardless, intra- and sub-till wood and organic remains are uncharacteristically abundant within the Smoking Hills field area for which there may well be multiple populations of ages. Just as we see definitive evidence of bedrock rafts, it is likely that re-worked wood debris and peat from the basal sands and gravels of sections HR 1 and HR 2 could be successively re-deposited through time in later glacial deposits, as could interglacial forest remains. To the east, in the Melville Hills (Fig. 1a), Veillette (2004) has suggested large accumulations of woody debris could relate to unidentified Beaufort Formation-aged deposits. While we argue against the existence of Beaufort Formation deposits in the Smoking Hills area, we share Veillette's (2004) observations of abundant, old wood.

4.3.2. Cosmogenic burial dating

4.3.2.1. Simple burial ages. We first present simple burial ages for each sample which consists of a single large cobble, multiple smaller cobbles, or a bag of sand (Table 1; Supplementary data S4). There is a wide range of burial ages, including stratigraphic inversions. At the base of section HR 1, simple burial ages from three samples from LF2 range from 0.8 to 2 Ma (Table 1). In the equivalent stratigraphic position at section HR 2, a single sample (18SUV525 – LF1) has a better precision than any of the HR 1 basal gravel samples, and its 1.94 (+0.54/−0.29) Ma age overlaps samples from section HR 1.

Lithofacies 4a has the most samples per unit (n = 6). Convolving the probability distribution functions for the four HR 1 18SUV502 (CL4) and two 18SUV507 (CL5) samples from LF4a (Fig. 13) indicates a most probable age of 2.7 +0.6/−0.5 Ma (Fig. 28a upper graph). The single burial age of 1.76 +0.40/−0.29 Ma for stratigraphically higher LF4b (18SUV503) is younger than the most probable age for LF4a but they agree at 1σ.

Overall, most of the samples had low concentrations of order 10^4 atom/g ^{10}Be and ^{26}Al, indicating not only a prolonged burial but possibly a high erosion rate in the palaeo-catchment and little post-depositional exposure (consistent with the lack of palaeosols), so that the clasts began *in situ* burial with relatively low concentrations. Large age uncertainties are attributed to measurement error in ^{26}Al, which may be related to a combination of the low $^{26}Al/^{27}Al$, the

difficulty of obtaining high purity quartz from the small samples, and possibly incomplete calcination (Bunsen burner at >950 °C for 4 min has been a standard procedure but we have recently discovered that longer time may remove H_2O more completely). If the samples experienced prolonged periods of post-depositional exposure, their age is an underestimation of the actual burial duration. However, considering the depth of samples, bulk density of the diamictons, and the likelihood of the additional shielding by glacier ice during at least one additional glaciation, muonic production and gradual surface erosion at the section sites would not significantly affect their age or explain the variability in ages within a single layer. On the other hand, if the clasts were re-worked and had different previous burial histories before their final deposition, which would explain some or all of the variability among ages within a lithofacies, the simple burial ages may be over-estimates. Based on the large uncertainties in the ^{26}Al measurement and simple burial ages, we recommend ignoring all of the simple burial ages from 18SUV501 samples and sample 18SUV507-1.

4.3.2.2. Isochron burial ages. While this method usually uses cobble samples to maximize the probability that the nuclide concentration among the samples will span a sufficient range to reliably define a best-fit curve, we used one supplementary sand sample from each lithofacies unit because many of the cobbles collected had insufficient quartz. Using all samples (assuming that all units were deposited synchronously) the isochron mean age is 3.6 ± 0.2 Ma (Fig. 28b upper graph). The isochron slope is significantly controlled by one sample (18SUV502-3) with concentrations of ^{10}Be and ^{26}Al that are about one order of magnitude higher than the other samples. Such a significant difference in concentration may indicate that the samples originated from sources with different exposure histories. Removing that one sample increases the isochron age to 4.1 ± 0.1 Ma (Fig. 28b lower graph). However, we have no measurement or geological reason to discard that sample. As discussed above, we have less confidence in the 18SUV501 series samples (HR 1, LF2) owing to their high measurement uncertainty. We therefore computed an isochron age based solely on the six samples from LF4a (Fig. 28c upper graph) which yields a most probable burial age of 3.2 ± 0.3 Ma. When we remove sample 18SUV502-2 which has relatively high ^{26}Al/^{10}Be, the isochron burial age for LF4a lowers slightly to 2.9 ± 0.3 Ma. We favour this age as it disregards the anomalous sample 18SUV502-2.

4.3.2.3. Interpretation. The variability of ^{26}Al and ^{10}Be concentrations and isotopic ratio among samples within a lithofacies suggests that at least some of the individual cobbles or amalgamated sands may have had different or complex burial histories. Three samples in the lower gravel unit (LF2 from HR 1; Fig. 13a) had high uncertainty in the ^{26}Al concentration, perhaps suggesting that this unit was sourced differently from the other units and had the lowest ^{10}Be concentration, which suggests it may have been buried for significantly longer than the stratigraphically younger units, which is consistent with the geological interpretation. We only have one dated sample from LF4b (an amalgamated sand), yielding a simple burial age 1.76 + 0.40−0.29 Ma. Our most robust chronology derives from LF4a (section HR 1), which yields a simple burial age of 3.0 + 0.7−0.4 Ma and an isochron burial age of 2.9 ± 0.3 Ma. These ages are within the Gauss Chron normal but given their uncertainty could fall within the earliest Matuyama Chron reversal (2.58 Ma), or the Kaena (3.05−3.13 Ma) and possibly Mammoth (3.22−3.33 Ma) subchron reversals.

4.3.3. Magnetostratigraphy

In light of revisions to the stratigraphic interpretations of section HR 1, and the derivation of a cosmogenic isochron burial age of 2.9 ± 0.3 Ma from the lower LF4a stratigraphy (Figs. 18 and 28), aspects of the established magnetostratigraphies need to be critically reviewed. Note, palaeomagnetic records from the Smoking Hills employed the natural remanent magnetism (NRM) methodology, wherein declination is measured relative to the magnetic field (north/south) and inclination is measured relative to the geocentric axial dipole (cf. Eyles et al., 1987; Easterbrook, 1988; Jackson, 1991a; Barendregt et al., 1996). Vincent (1988) included approximate stratigraphic location and declination measures of samples (3 per location). Duk-Rodkin et al. (2004) and Duk-Rodkin and Barendregt (2011) presented only normal/reverse (N)/(R) polarity assignations for units but provide no actual measurements. Neither of the two magnetostratigraphic records include precision parameter (K) and mean direction dispersion (circle of confidence; α_{95}) measures of magnetic strength and sample reliability. Sampling locations are illustrated by Duk-Rodkin and Barendregt (2011) in photographs (which allowed us in some cases to make comparisons to stratigraphy that we were able to inspect in the field), but are lacking any sedimentological descriptions. In what Vincent interpreted to be his lowermost till (our LF4a) his field data indicate that three locations were normally magnetized (1 m above the base, the center, and 1 m below the top; declinations of 43-47-51°, 63-56-62°, 78-88-77°, respectively). This was overlain by a normally magnetized "transition" deposit (what we confirmed through palynology and the presence of selenite nodules as a Horton River Formation bedrock raft − see Supplementary data S5, Figure S5.2; Figs. 14f and 18) which had normally magnetized declinations of 15-28-02° measured at the centre of the deposit. As the till above this was indicated to be reversed, this would suggest a possible Gauss Chron age (3.04−2.58 Ma) for Vincent's lowermost till (our LF4a). In contrast, Duk-Rodkin and Barendregt (2011) indicated that all of the lower stratigraphy, including the basal sand and gravel (equivalent to our LF1 through LF4b), is reversely magnetized, placing it within a probable Matuyama Chron (0.78−2.58 Ma).

Given the complex mixture of bedrock rafts and diamict layers we describe from LF4a (Figs. 13 and 14d-g), and the tendency for palaeomagnetic samples to be collected from finer-grained and less compacted materials, we suspect that many of the samples from both authors were collected in bedrock rafts or stringers, as opposed to glacigenic diamictons or sorted sediments. Duk-Rodkin and Barendregt's (2011) five samples collected from the uppermost part of our LF4a (their Unit 2; Fig. 18) appear to have been collected in what we describe as a pseudo-laminated, fissile diamict, but we cannot be certain that they did not target pockets or stringers of unconsolidated Cretaceous bedrock (e.g. Fig. 14d, g). Above their Unit 2, Duk-Rodkin and Barendregt (2011) predominantly sampled the silt lamina in what we identify as a Horton River Formation bedrock raft (Fig. 14f), and reported a reverse polarity. However, the Albian-aged Horton River Formation would have been deposited within the Cretaceous Normal Superchron (120-83 Ma), and therefore should plot as normal. While we recognize the prevalence of bedrock slumping as a likely major contributor to glacial rafting of intact bedrock, we do not see how this could result in a diametric (180°) change in polarity. However, it may be possible that smaller degrees of rotation (60°?) may be sufficient to change the interpretation of declination, although this would also require an accompanying tilting of the strata to account for changes in inclination. In large, coherent blocks of rafted bedrock, perhaps this is tenable; we find the notion less convincing for highly deformed and attenuated bedrock stringers and wisps that may have been a focus of sample collection. Note, aside from the large, coherent Horton River Formation bedrock raft, the Smoking Hills and Mason River formations potentially contain both magnetically normal and reversed signatures, and these too could comprise various bedrock

Fig. 29. Compilation map of main glacial landforms for the Smoking Hills study area and the wider region. Flowsets are compiled from the flutings identified in Fig. 6 and major moraine limits represent the outermost ridges of inset sequences of hummocky terrain belts.

stringers and rafts.

It is clearly understood that magnetostratigraphy does not provide an absolute age determination independent of other geochronological controls (e.g. tephrochronology and isotopic age determinations; Easterbrook, 1988; Barendregt et al., 2012). Our cosmogenic burial age of 2.9 ± 0.3 Ma (Fig. 18) places the LF4a diamicton most likely within the Gauss Chron normal. This corroborates Vincent's (1988) measurements for this stratigraphic unit, but contradicts that reported by Duk-Rodkin and Barendregt (2011), although the Kaena subchron reversal (3.05–3.13 Ma) does occur within the cosmogenic age error bounds. This prompts a critical question about the process through which glacial diamictons can actually preserve a palaeomagnetic signature, and whether our sedimentological conclusions on their formation under high shear strain in particular could alter the detrital remanent magnetism (DRM) signature. First, shallowing of elongate grains during compaction may cause magnetic inclination shallowing of the DRM (e.g., Jackson et al., 1991). Second, it is well established that anisotropy of magnetic susceptibility (AMS) can be used to record shear strain patterns in tills, and from this deduce ice flow directions (cf. Hrouda, 1982; Eyles et al., 1987; Easterbrook, 1988; Tarling and Hrouda, 1993; Hooyer et al., 2008). However, it is

considered that strain and viscous flow-related reorientation of the larger silt-sized particles (17–180 μm) measured by AMS do not affect the fine silt and clay-sized particles (<10 μm) which tend to dominate the DRM signal, and thus AMS and DRM can have distinctly different orientations (Gravenor and Stupavsky, 1974; Easterbrook, 1983, 1988). Larger grains can also produce a random, self-cancelling component of remanence that does not affect the remanence of smaller particles (Easterbrook, 1983). Instead, these

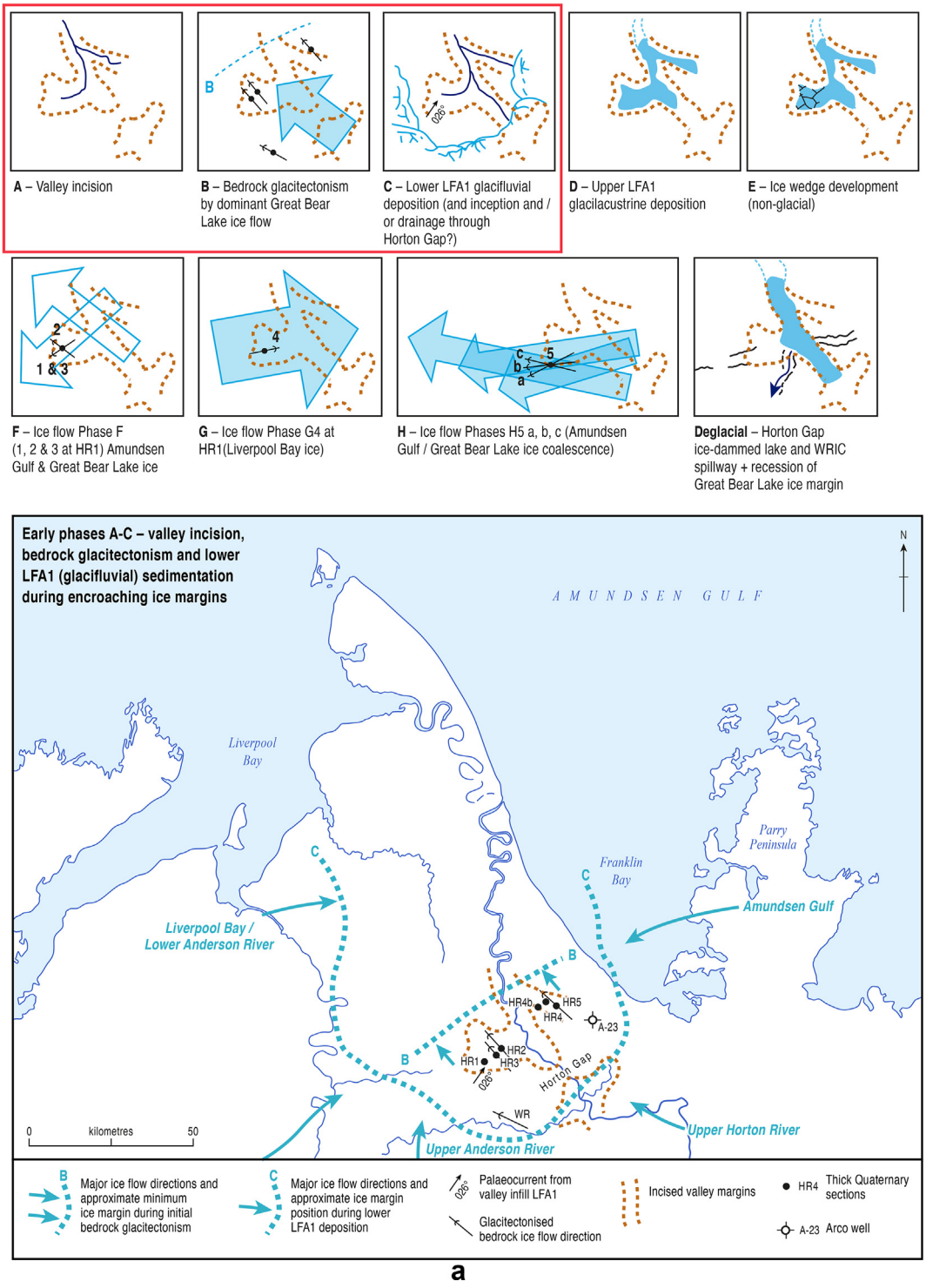

Fig. 30. Regional palaeogeographic event reconstructions based on the glacial landforms depicted in Figs. 6 and 29 and the stratigraphic details from the section logs in the study area. Ice margins and flow patterns are approximate and inferred from the stratigraphic and landform evidence: a) early Phases A-C; b) early Phases D and E; c) early flow Phase F; d) later flow Phases G and H. Note that ice flow direction H5a recorded by clast macrofabric in lower LF4c at section HR 1 appears not to be represented in surface flutings; e) deglacial and topographically confined ice flow directions and recessional ice margins. Light red flowsets record earliest deglacial flow and light green flowsets represent later, valley-confined flows. In the absence of evidence for additional glaciations, the intervening period between phases A-E and F-deglacial could be up to 2.8 million years. (For interpretation of the references to colour in this figure legend, the reader is referred to the Web version of this article.)

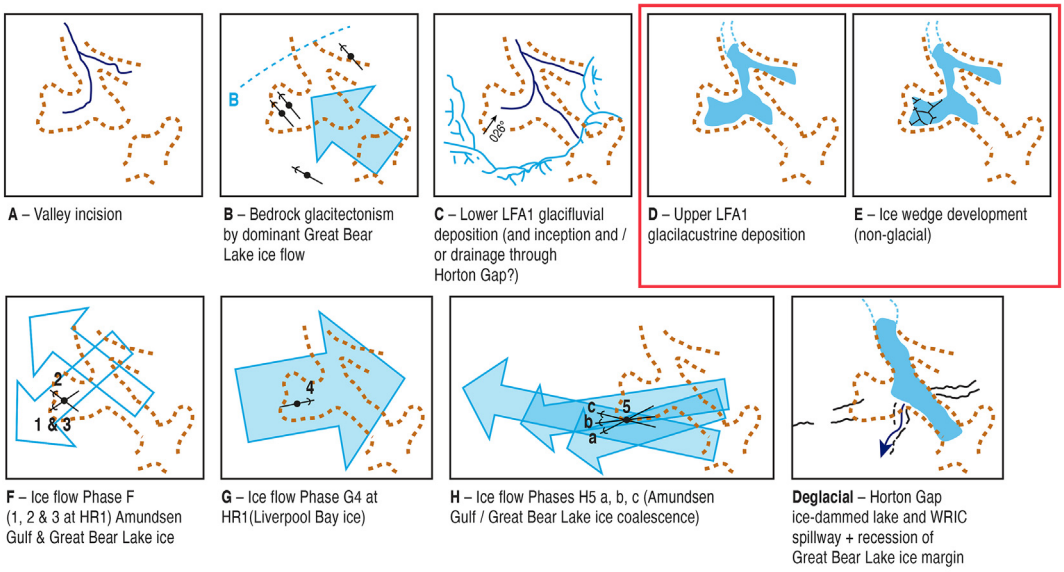

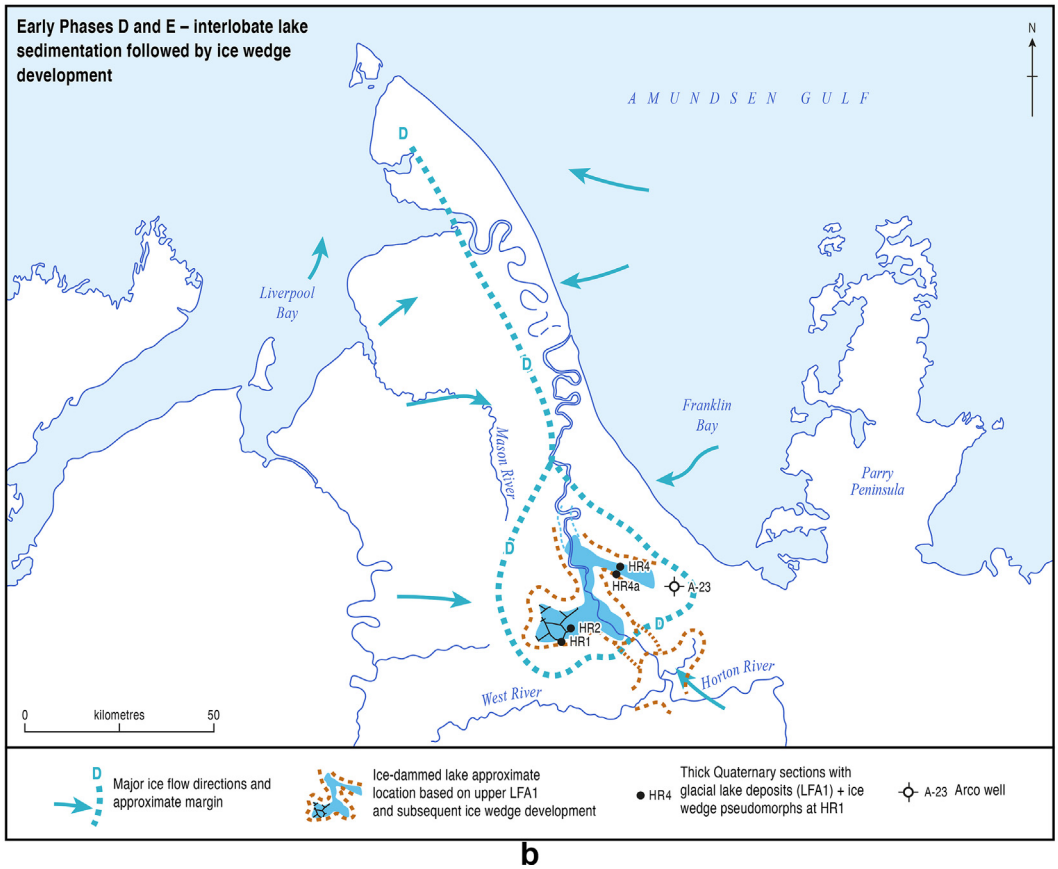

b

Fig. 30. (*continued*).

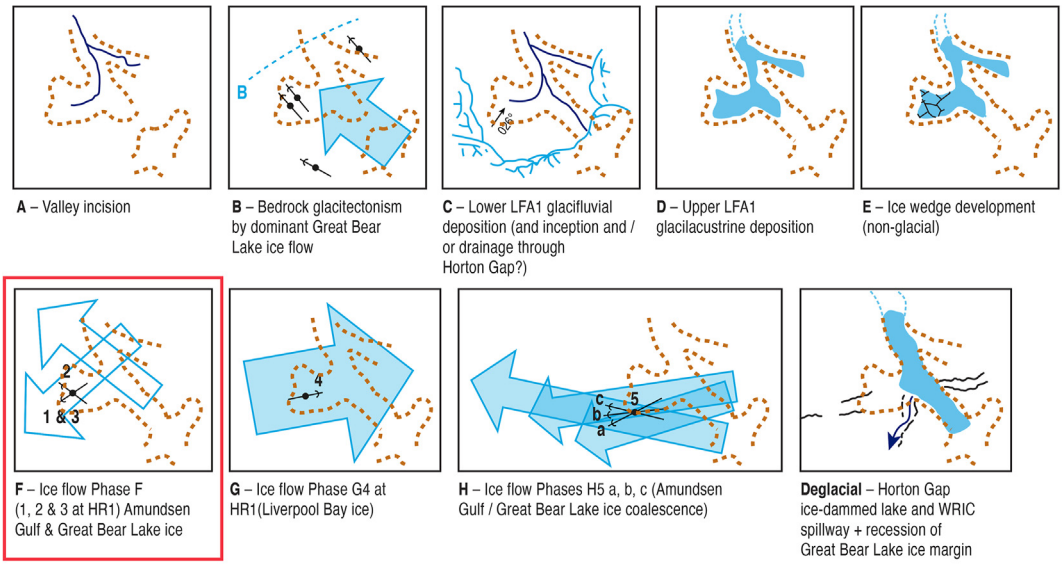

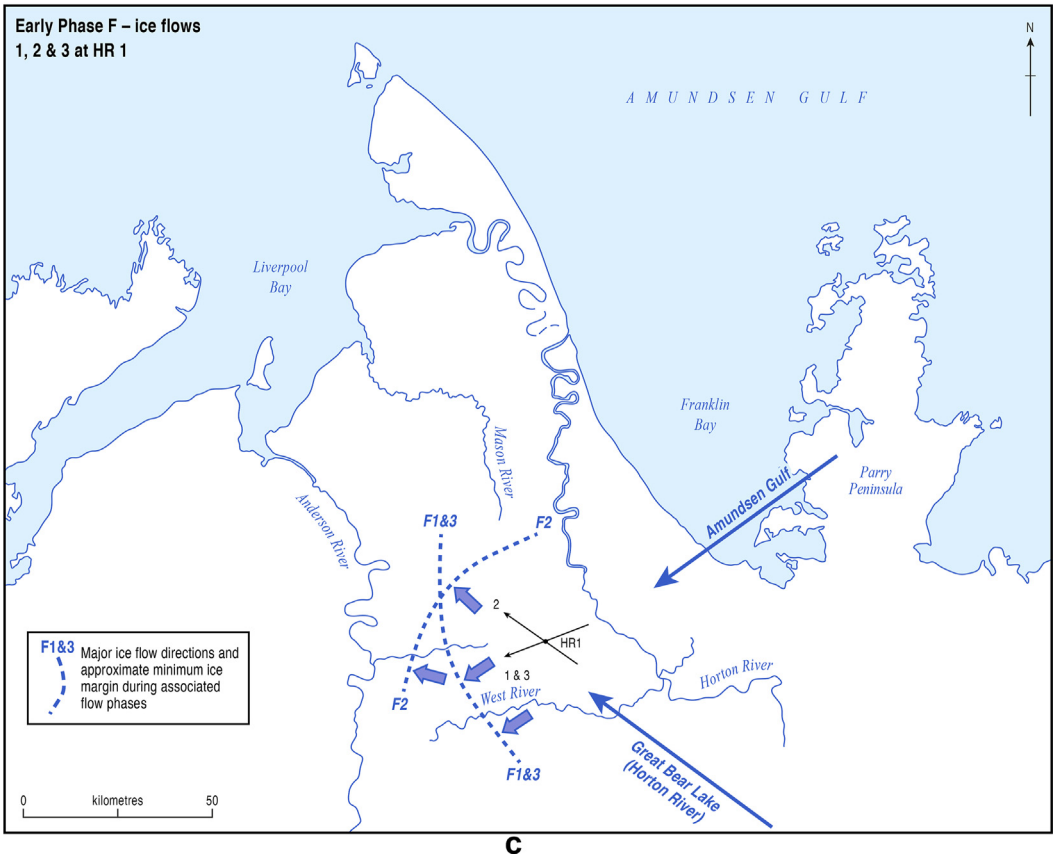

C

Fig. 30. (*continued*).

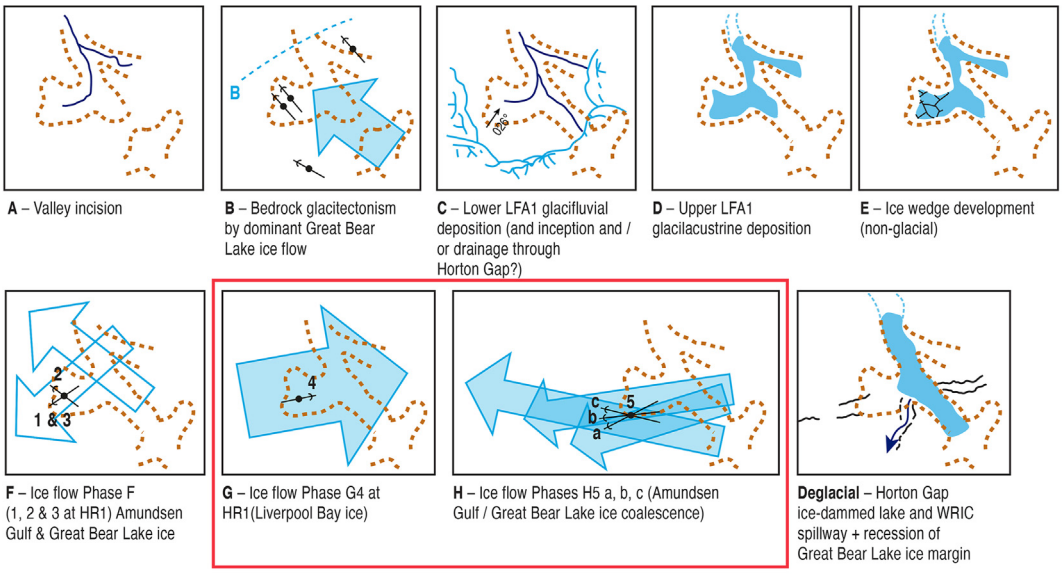

d

Fig. 30. (*continued*).

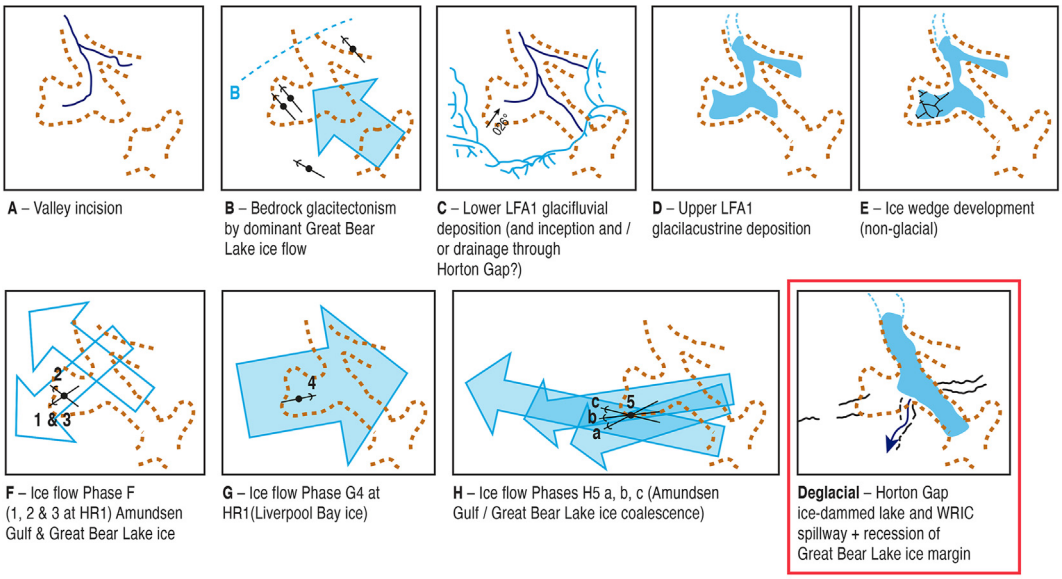

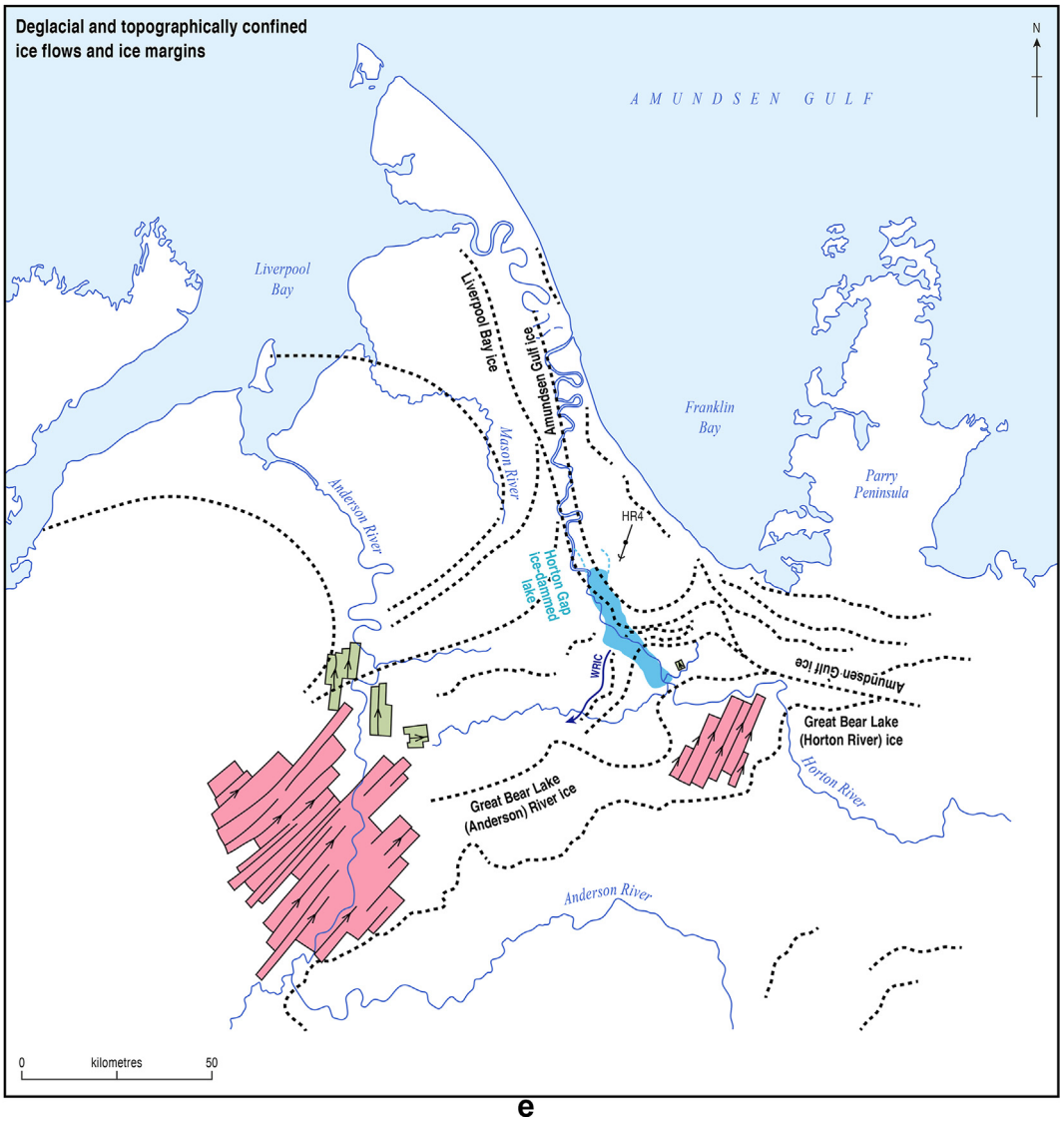

e

Fig. 30. (*continued*).

finest-sized magnetic particles are considered to magnetically align themselves within pore waters at the waning phases of sediment dewatering (Denham and Chave, 1982; Easterbrook, 1983, 1988). While pore fluids are not considered to transmit shear stress, and therefore should not affect particle magnetic alignment (Easterbrook, 1988), Eyles et al. (1987) demonstrated that DRM fabrics in lodgement tills can display a girdle distortion (transverse or parallel to ice flow direction) around the geomagnetic pole (in contrast to "rain-out" diamictons) in tills that experienced compaction but relatively low glacigenic strain. As summarized by Eyles et al. (1987), the process of final particle alignment can be complicated by a range of conditions, including intensity of the Earth's magnetic field, magnetic moment of grains, grain size, shape and roughness, size and geometry of voids, deposition rate, moisture content, and disturbance by traction currents and re-sedimentation, all of which can introduce "bedding" errors (Blow and Hamilton, 1978). Chemical precipitation of magnetic minerals through time can also occur, as can viscous remanent magnetism (VRM), and Barendregt et al. (1991, 1998, 2012) have indicated that generally 50% of samples (even up to 68% in one of their examples) are rejected in palaeomagnetic analysis of tills because of weak or unstable magnetizations or incoherent remanence directions held by randomly oriented sand or pebbles within the sample. Where samples have weak overall DRM, characteristics like VRM (acquired over long periods of time in response to changes in the direction or intensity of the natural magnetic field) must also be addressed through stepwise alternating field demagnetization. As discussed, no information on sample magnetic properties is provided by Duk-Rodkin and Barendregt (2011), but we note that in the bulk sample processing from this study, separation of ferromagnetic sand grains (0.25–2 mm) shows very low concentrations of 0.02 g/1 kg of sample (<2 mm), which is generally 1–2 orders of magnitude less than tills collected on Banks Island (Smith, 2020). While this does not give a measure of the total magnetic susceptibility of the samples (nor that which DRM is detecting), it does suggest that the Smoking Hills diamictons have very low concentrations of magnetic material, which could impair their reliability in preserving a palaeomagnetic signature. Given the disparity between the original palaeomagnetic measurements of Vincent (1988) and those of Duk-Rodkin and Barendregt (2011), the absence of detailed sample measurements and sedimentology, the cosmogenic isochron burial age, and a measure of reversed polarity in what should be a normally magnetized bedrock raft(s), we are uncertain as to the reliability and accuracy of the palaeomagnetic record from the Smoking Hills stratigraphy, and thus choose to disregard it until such time or opportunity arises to critically analyse the data and sedimentological records of the collected samples.

5. Discussion - implications for glacial landsystems of the NW Laurentide Ice Sheet

The interpretations developed above are now used to reconstruct the dynamics of glacier ice over the Smoking Hills and wider regional study area. A compilation of glacial landform and stratigraphic evidence is presented in Fig. 29 and then employed to produce a sequential palaeoglaciological reconstruction, as portrayed in the various stages in Fig. 30a-e. Subglacial streamlined bedforms (flutings), widespread till veneer and rare blanket (>2 m thick), and substantial till units preserved in isolated valleys are indicative of warm-based ice conditions, which appear to have dominated over parts of the region during phases of vigorous ice flow (ice streaming) and then given way to cold-based glacier submarginal conditions, as indicated by controlled moraine construction during final deglaciation (Dyke and Savelle, 2000; Evans, 2009). This glacial geomorphological signature is collectively regarded as diagnostic of a polythermal ice sheet marginal landsystem (Dyke and Evans, 2003).

A paucity of evidence for clear overprinting of subglacial streamlined bedforms in the region makes it difficult to decipher the sequence of flowset production, and indicates, in the context of multiple glaciations (cf. Batchelor et al., 2019), that only the most recent glaciation(s) may be widely preserved in the surface geomorphological record. Evidence of older glaciations may be preserved only within the marine stratigraphic record (cf. Stashin, 2021), but it is likely that successive glaciations have cannibalised/removed much of the pre-existing record. Based upon flowset locations relative to one another, their alignment with likely ice sources, and their interpreted relationships with till macrofabrics and glacitectonic deformation signatures, the flowsets depicted in Fig. 29 are assigned a relative chronology. This chronology is likely short (i.e. related to the last (Wisconsinan) glaciation) because of the low preservation potential of subglacial bedforms dating to older glaciations. Three sources of ice dispersal are recognised from the flowset imprints and the pattern of ice-marginal recession demarcated by controlled moraine belts: a) Amundsen Gulf ice flowing through Franklin Bay from the east; b) Liverpool Bay ice flowing from the southwest; and c) Great Bear Lake ice flowing from the south and southeast. The latter two ice flows originated from a migrating ice divide in and around the Great Bear Lake region, and the northwest-extension of the Mackenzie lobe (cf. Dyke and Prest, 1987).

Following upon Mathews et al. (1989), we have demonstrated that the purported oldest deposits in the Smoking Hills region, the "plateau-cap fluvial sediments" of Yorath et al. (1969, 1975), are clearly not Neogene Beaufort Formation equivalents, but instead record Pleistocene glacial and glacifluvial processes. Further, we have documented that they have a far less extensive coverage than depicted or would be compatible with sedimentation in a regional river network. Instead, isolated gravel deposits mostly reflect deposition in glacifluvial depo-centres dictated by local interactions of receding ice margins with topography (i.e. kame and outwash terraces). Flutings imprinted on glacial drift that discontinuously mantles the plateau surfaces indicate that in some areas the isolated gravel deposits may pre-date at least the last glaciation. The outwash and kame terrace deposits running parallel with the lower Horton River valley are likely to have been deposited between the receding margins of Liverpool Bay and Amundsen Gulf ice during deglaciation.

5.1. Palaeogeographic event phases A through C

Interpretations of the Pliocene-Quaternary stratigraphy of the study area necessitate a palaeoglaciological reconstruction that involves an interlobate zone of ice confluence centred over the upland regions, created by ice flowing into the area from the west (Liverpool Bay ice), east (Amundsen Gulf ice) and south (Great Bear Lake ice moving through the upper Horton River and Anderson River basins; Fig. 30a), with ice flow dominance varying spatially over time. The eastward verging bedrock (glacitectonic) deformation noted by Yorath and Cook (1981) in the Mason River basin, and both east and west verging glacitectonic bedrock deformation on either side of the lower Horton River valley (our observations and Mathews et al., 1989), confirms this confluence. Bedrock glacitectonic deformation in the study area extends to depths generally $\leq$25 m. In order to explain the glacitectonic disturbance of bedrock at altitudes similar to those of the present-day valley floors, we argue that the first glacial advance encountered a landscape with existing fluvial dissection, but not necessarily one in which the Horton Gap had formed (Phase A, Fig. 30a). Importantly, in the case of sections HR 1, 2 and 3, it implies that a major side valley was

already draining eastward into a northward-flowing proto lower Horton River with a base level ±210 m asl (base of deformed bedrock at section HR 2 + 20 m; Fig. 30a). Bedrock deformation at section HR 5 indicates that a further side valley drained westwards into the proto lower Horton River. To the south of the uplands, drainage including the upper Horton River flowed across a low divide (~165 m asl; "topographic low" of Mathews et al., 1989) into the Anderson River. As ice flowed into the region from the south-east, over-topping the upland regions, bedrock on the incised valley floors and margins was then glacitectonically disturbed. Ice margins attained a position located at least as far north as ice margin Phase B on Fig. 30a. A subsequent recession to around or further south of the location of ice margin Phase C is required to explain the deposition of LFA1 valley infill as glacifluvial outwash draining north-northwestwards down the proto-lower Horton River. Southward retreat of ice and impoundment of regional drainage against the uplands likely initiated the incision of the Horton Gap, though by how much is uncertain. That the basal LFA1 gravels contain facetted and striated clasts, but no Canadian Shield-derived granitic material, perhaps supports Barendregt and Duk-Rodkin (2004) and Duk-Rodkin and Barendregt's (2011) notion of a Horton (Melville Hills) ice cap source (i.e. north and west of Canadian Shield outcrops; Fig. 1b). However, it may well be that the first glaciation into this area encountered such a deeply weathered bedrock regolith, that farther travelled Canadian Shield lithologies were diluted even more than their rare (<1–2%) occurrence in what are interpreted as Laurentide (continental) tills above, and that these basal glacifluvial gravels are also a Laurentide deposit.

5.2. Palaeogeographic event phases D and E

Following on from the above depositional events, it is clear from the glacilacustrine sediments of upper LFA1 at section HR 2 that a substantial glacial lake occupied at least this side valley, if not much of the lower Horton River valley (see also the undeformed and heavily glacitectonised upper LFA1 in Sections HR 4, 4a and 4b). This required coalescence of the Liverpool Bay and Amundsen Gulf ice over what is now the northernmost reach of the lower Horton River (Phase D, Fig. 30b). The development of ground ice during a periglacial period, as recorded by the ice wedge pseudomorph in LFA1 glacifluvial gravels in section HR 1, likely took place after the lake emptied (Phase E, Fig. 30b), based on the fact that the conformable and gradational contacts between LF1-LF3 and LF3a-LF3b, respectively (sections HR 2, HR 4b), indicate no break between glacifluvial and glacilacustrine environments.

5.3. Palaeogeographic event Phase F; last glaciation early flows

Till sequences and clast macrofabrics together with glacitectonic shearing directions then record the oscillatory dominance of the three main LIS ice flow sources. The earliest of these switching ice flow directions are classified as Phases F1-3 (Fig. 30c) based upon the sequencing recorded in LF4a and middle LF4b in section HR 1. Amundsen Gulf ice appears to have been dominant during Phases 1 and 3 (LFs 4a lower and 4b middle, respectively), based upon west-southwesterly directed flow indicators (Fig. 30c). Ice flowing north from the Great Bear Lake ice divide area through the Horton River basin appears to have been dominant during Phase 2 (LF4a upper), based on west-northwesterly directed flow indicators, which presumably forced Amundsen Gulf ice to also flow north-northwestwards after crossing the Parry Peninsula from east to west (Fig. 30c). Tills and glacitectonites emplaced during these ice flow phases were nourished by the cannibalisation of pre-existing deposits and continued bedrock rafting from partially filled valley margins.

5.4. Palaeogeographic event Phases G and H; last glaciation late flows

The dominance of fabrics indicative of Amundsen Gulf and Great Bear Lake ice sources during Phases F1-3 was superimposed in the construction of upper LF4b in section HR 1 by an easterly directed stress signature. This represents dominance of ice flowing from the Liverpool Bay area, nourished by vigorous flow from the Mackenzie lobe to the southwest of the region and appears to be the first stratigraphic ice flow indicator that is manifest also in surface flutings; hence this is classified Phase G4 (Fig. 30d). These flutings form the prominent and extensive flowsets that converge on the Mason River and lower Horton River area. This prominent Phase G4 flow imprint is used by Margold et al. (2015) to identify the Anderson River ice stream, although its origin is to the southwest of the Anderson River drainage basin.

The final set of ice flow phases is recorded in the uppermost tills and glacitectonites in the study area. At section HR 1 these are reflected in clast macrofabrics from LF4c, which indicate a reversion to Amundsen Gulf ice dominance. Bedrock and pre-existing glacigenic sediments were heavily glacitectonised and cannibalised during this renewed westerly directed stress regime. Subtle changes in ice flow trajectory are recorded in flow Phases H5a, b and c, sequentially directed towards southwest, then west-southwest, and finally towards the west, respectively (Fig. 13a). These latter flow phases appear to be recorded in flowsets, specifically on the north Parry Peninsula (H5b) and most prominently in a regional signature (H5c) that reflects the late stage arcuate drawdown of coalesced Amundsen Gulf and Great Bear Lake ice masses (Fig. 30d). Interestingly, it appears that Phase H5c was responsible for the final deformation signature imparted on the buried glacier ice in section AR 2 in the Anderson River area. Changes in lithological, matrix geochemical, particle size and colour characteristics of the section HR 1 upper LF4c diamicts (Phase H5; Supplementary data S2), from earlier Amundsen Gulf-centred ice flows (Phases F1 and 3) likely reflects progressive shifts in ice divides over the southern Arctic Archipelago and northern mainland during build-up and retreat of the LIS.

5.5. Deglacial ice flows

The final stages of deglaciation of the region are recorded by the development of inset sequences of ice-cored (controlled) moraine, whose arcuate assemblages demarcate the margins of ice lobes receding westwards into Liverpool Bay, eastwards into Franklin Bay (Amundsen Gulf) and southwards into the upper Horton/Anderson rivers and Great Bear Lake basins (Fig. 30e). Flowsets formed at this time were largely fragmentary and spatially restricted, recording local topographic confinement. Ice-marginal thrusting of materials was likely intensified during recession as glacier sub-marginal thermal conditions turned strongly polythermal (cf. Ó Cofaigh et al., 1999, 2003; Dyke and Savelle, 2000; Dyke and Evans, 2003; Evans, 2009) and this appears to be manifest in the late stage thrust stacking at section HR 4 by ice flowing from the north-northeast (Fig. 30e). An important feature that developed during the final stages of deglaciation is the Horton Gap ice-dammed lake, as evidenced by the extensive lake sediment and shorelines in the area. The existence of this lake indicates that the lower Horton River was occupied by coalescent Liverpool Bay and Amundsen Gulf ice margins (Fig. 30e), a palaeoglaciological reconstruction of some significance because it implies that the region was completely overrun by glacier ice during the last glaciation in contrast to the more restricted ice marginal reconstructions depicting the Smoking Hills as an unglaciated enclave (Rampton, 1981, 1988; Hughes, 1987; Vincent, 1984; Dyke and Prest, 1987; Mathews et al., 1989;

Barendregt and Duk-Rodkin, 2004; Duk-Rodkin et al., 2004; Stokes et al., 2006, 2009; Brown et al., 2011; Duk-Rodkin and Barendregt, 2011; Batchelor et al., 2013a, b, 2014; MacLean et al., 2015; Margold et al., 2015).

With the exception of non-finite radiocarbon ages indicative of non-glacial accumulation of organic materials at some stage, our only absolute dating constraints for the glacial events depicted in Fig. 30 derive from an isochron burial age of 2.9 ± 0.3 Ma for LF4a (section HR 1). The chronology of emplacement of all subsequent deposits is hence relative, but the ice flow events since and including the deformation signature in upper LF4b are thought to be related entirely to the last glacial cycle due to their compatibility with surface flowsets, and the absence of inter-till units with a clear interglacial record. Of relevance here in this context, there has been a tendency for the most recent LGM ice sheet reconstructions for the region to depict a vigorous Amundsen Gulf ice stream reaching the continental shelf edge to the southwest of Banks Island but failing to make incursions into the Smoking Hills area (cf. Stokes et al., 2006, 2009; Brown et al., 2011; Batchelor et al., 2013a, b, 2014; MacLean et al., 2015; Margold et al., 2015), perhaps in deference to the earlier reconstructions of Mackay (1958), Klassen (1971), Rampton (1981, 1988), Vincent (1984), Dyke and Prest (1987), Hughes (1987) and Mathews et al. (1989). However, flowsets mfs-9 and -11 of Stokes et al. (2006) clearly record vigorous Amundsen Gulf ice flow across Franklin Bay and outer Liverpool Bay, equated with our Phase H5 regional ice flow (Fig. 30d) and thereby operating over the Smoking Hills. Moreover, the pattern of inset, ice-cored recessional moraine sequences are indicative of Late Wisconsinan deglaciation of the Smoking Hills, during which ice would also have had to occupy the lower Horton River area in order to create the Horton Gap ice-dammed lake (Fig. 30e). On the question of multiple glaciations in the area, we acknowledge that the Anderson River buried old glacier ice and deformed ice wedges site (AR 2) likely record at least two glacial periods; moreover, widespread glacitectonized bedrock at valley floor level as well as reworked, striated and faceted clasts in the basal glacifluvial gravels of LFA1 in section HR 1, which are also superimposed by an ice wedge pseudomorph, record a glaciation that either pre-dates the emplacement of LF4a (i.e. potentially $\geq$2.9 Ma), or is accordant with oscillating ice margins during the same glacial cycle.

5.6. Glacial chronologies

Although multiple diamictons, when interpreted as tills, are potential records of multiple glaciations, their designation as such is inherently problematic and potentially erroneous in the Smoking Hills area due to two critical factors: 1) the lack of a robust chronostratigraphic framework; and 2) the extensive evidence of glacitectonic disturbance, raft emplacement and hence facies repetition due to folding and thrust stacking. The latter factor is particularly marked in poorly consolidated (soft) bedrock terrains and can result in disproportionately thicker glacigenic sequences for the most recent (i.e. Late Wisconsinan) glaciations relative to older events, especially in ice sheet-marginal settings (cf. Evans et al., 2012). However, notwithstanding our re-interpretation of previously identified inter-till lacustrine and mass flow deposits and palaeosols as bedrock rafts, a magnetostratigraphy has previously been constructed that suggests significant age differences between glacigenic diamictons (Fig. 18). This is important, because it has been confidently employed in regional reconstructions of multiple ice sheet extents throughout the Quaternary (e.g. Duk-Rodkin et al., 2004; Batchelor et al., 2019). The continued use of magnetostratigraphy in this way (i.e. in glacitectonised and glacigenic deposits) requires critical evaluation and further study.

Although the majority of the glacigenic sediment in the study area may equate to the last (Wisconsinan) glaciation, we have reported here a potentially pre-Quaternary glaciation(s). The ages derived from LF4a lie within the Gauss Chron normal but could relate also to the earliest Matuyama Chron reversal (<2.58 Ma) or the Kaena (3.05–3.13 Ma), and possibly the Mammoth (3.22–3.33 Ma) subchron reversals. Evidence for such Pliocene (5.33–2.58 Ma) glaciations has largely been derived from marine isotopic records that reflect changes in global ice volume (cf. Lisiecki and Raymo, 2005), sea level records (e.g. Dwyer and Chandler, 2009; Miller et al., 2011), and marine records of ice-rafted detritus (IRD; e.g. Jansen et al., 2000; Bailey et al., 2013; De Schepper et al., 2014; Knies et al., 2014). From such studies, glacial modelling exercises have focussed on changes in global CO_2 concentrations and sea level changes to reconstruct various glacial configurations ranging from alpine glacial expansion to continental ice sheets (De Schepper et al., 2014; Dolan et al., 2015; Berends et al., 2019). The major cooling event during Marine Isotope Stage (MIS) M2 (3.3 Ma; during the Mammoth reversed polarity subchron; Lisiecki and Raymo, 2005) has been a focus for many of the earliest Pliocene glaciations, while others have been linked to later MIS excursions, including the establishment of prominent northern hemispheric glaciation cycles accordant with the Pliocene – Pleistocene cooling event (~2.75 Ma; Lisiecki and Raymo, 2005). Terrestrial records of large scale Pliocene glaciations in northern Canada include the buried till of Gao et al. (2012) from northwestern James Bay lowland (palaeomagnetic and proxy-dated ~3.5 Ma, although this age is not strongly constrained), and a late Pliocene (~2.64 Ma) glaciation in the Yukon Cordillera that was both the earliest and the historically most extensive Cordilleran Ice Sheet (Duk-Rodkin et al., 2004; Barendregt et al., 2010; Hidy et al., 2013). In acknowledging the uncertainties in our HR 1 section burial ages, our evidence for an expansive continental glaciation in the Smoking Hills area is broadly coeval with the latest Pliocene (2.64 Ma) Yukon Cordillera Ice Sheet record (Hidy et al., 2013), but would pre-date the 2.4 Ma age of the first extension of the Laurentide Ice Sheet south of 39°N, close to its maximum all time limit identified by Balco and Rovey (2010).

With respect to the construction of a fuller chronostratigraphy that is independent of the problematic magnetostratigraphic framework, it is clear that significant quantities of intra- and subtill wood and organic remains are available within the Smoking Hills field area but the employment of only radiocarbon dating has so far resulted in a failure to elucidate on the likelihood of multiple populations of ages. Also critical in this respect is the widespread evidence for glacitectonic displacement and intercalation of wood debris and peat that has been cannibalised from older deposits, potentially Neogene, as has been demonstrated by Evans et al. (2014) and Vaughan et al. (2014) for sites on Banks Island.

6. Conclusions

Detailed sedimentological, stratigraphic and structural analysis of the main Quaternary section (our HR 1) and several other newly identified sections, along with cosmogenic burial dating, fundamentally revise the previous reconstructions of Pliocene – Pleistocene glacial history for the Smoking Hills area. The basal sand and gravel deposits, containing what are considered broadly Neogene-aged reworked plant and organic remains, are made up of lithologies that could not be sourced from the local catchment, and include glacially faceted and striated clasts. Previously misconstrued as possible Beaufort Formation and plateau gravel equivalents, we identify these instead as glacifluvial deposits formed within a Pliocene landscape exhibiting modest fluvial dissection. Glacitectonic deformation and displacement of coherent, poorly-consolidated bedrock masses was found

throughout the study area, particularly within the Smoking Hills Formation mudrock. Depths of bedrock deformation are generally ≤25 m, and examples of this deformation are found at altitudes similar to present-day tributary valley floors, suggesting these lie close to the preglacial landscape morphology. The exception to this is the lower Horton River valley, and particularly the "gap" which bisects the upland region (>200 m incision), and formed at the interlobate confluence of westward flowing Amundsen Gulf and north and eastward flowing Great Bear and Liverpool Bay ice, likely over successive glaciations. A cosmogenic isochron burial date of 2.9 ± 0.3 Ma derived from quartzite clasts and a bulk quartz sand separate from a lower diamicton/glacitectonite sequence (LF4a, containing Canadian Shield-derived granites) provides evidence of the earliest dated Laurentide (continental) glaciation of the region. This age is broadly coeval with the documented earliest and most extensive northern Cordilleran glaciation. An ice-wedge pseudomorph in the underlying glacifluvial gravels (Duk-Rodkin and Barendregt, 2011; unobserved by us due to slumping) records a period of periglacial conditions following on from glacifluvial and glacilacustrine sedimentation after bedrock glacitectonism, thereby representing a pre-2.9 Ma glaciation, or oscillating ice margins within the same glacial period. The lower LF4a assemblage contains both diamictons and formally unrecognized rafts and intraclasts of poorly-consolidated Cretaceous bedrock. Indeed the ~3 m thick unit overlying LF4a, which has been noted by all previous researchers investigating this site and described as lacustrine or other non-glacial fine-grained laminated rhythmites, is instead revealed through sedimentology, palynology, and the presence of large siderite concretions as a coherent raft of Horton River Formation bedrock. The overlying LF4b and 4c assemblages of massive to laminated diamictons (separated by a 2–6 m thick, highly glacitectonised bedrock raft) is interpreted as a stacked facies of glacitectonic thrust and folded Laurentide diamictons and Cretaceous bedrock intraclasts. The sequence of deposits, clast macrofabrics, and glacitectonic shearing directions in the various sections inspected are used to decipher a relative chronology of ice flow history, which for the most recent deposits and structures is matched to surface geomorphological mapping of ice flowsets, controlled moraines, and deglacial ice margins. With respect to regional ice stream evolution, the changes in ice flow trajectory of flow Phases H5a, b and c incorporate those of flowsets mfs-9 to mfs-11 of Stokes et al. (2006), which record vigorous Amundsen Gulf ice flow across Franklin Bay and outer Liverpool Bay and appear to reconcile with flowsets in the Anderson River catchment, thereby demonstrating Late Wisconsinan ice flow over the Smoking Hills and the final deformation signature imparted on the buried glacier ice in section AR 2. That the overriding ice was able to deform the underlying "old" ice and ice wedges, and produce the adjacent ice-cored flutings, yet not melt more of this buried ice beyond the shallow thermal unconformity, suggests transient shear zone development, and possibly only a brief period of glacial inundation. Further evidence of Late Wisconsinan glaciation of the Smoking Hills is the former existence of the Horton Gap ice-dammed lake, which required the occupation of the lower Horton River by coalescent Liverpool Bay and Amundsen Gulf ice margins. The uncoupling of these ice masses and the Great Bear Lake ice margin to the south during the final stages of deglaciation is recorded by inset sequences of ice-cored (controlled) moraine.

Declaration of competing interest

The authors declare that they have no known competing financial interests or personal relationships that could have appeared to influence the work reported in this paper.

Acknowledgements

This study was funded under Natural Resources Canada's Geomapping for Energy and Minerals Program (NRCan contribution #20200754). The Department of Geography, Durham University provided financial assistance to DJAE for his participation in fieldwork. Our project was supported by the Paulatuk and Tuktoyaktuk Hunters and Trappers committees, and operated under Inuvialuit Land Administration licence ILA17TO-028, and NWT Scientific Research Licence 16210. Polar Continental Shelf Program provided logistical assistance. G. Yang, N. Whelan, and S. Des Roches completed the mineral separation and target chemistry for the cosmogenic nuclide burial ages at CRISDal Lab, with partial support from Canadian Foundation for Innovation-Major Science Initiatives Fund 35432 and NSERC-Discovery Grant 06785-19 to JCG. Chris Orton of Durham University compiled most of the figures; C. Deblonde (GSC Calgary) is thanked for assistance with GIS and DEM imagery. An internal GSC review by I. McMartin, and formal reviews by M. Ross and an anonymous reviewer, helped us improve the clarity and scope of this paper.

Author statement

David J A Evans - Conceptualization; Data curation; Formal analysis; Investigation; Methodology; Software; Validation; Visualization; Writing – 65% original draft; Writing – review & editing, I Rod Smith - Conceptualization; Data curation; Formal analysis; Funding acquisition; Investigation; Methodology; Project administration; Resources; Validation; Visualization; Roles/Writing – 35% original draft; Writing – review & editing, Jennifer M Galloway - Data curation; Formal analysis; Investigation; Methodology; Validation; Writing – review & editing, John C Gosse - Formal analysis; Methodology; Resources; Validation; Visualization; Writing – review & editing.

Appendix A. Supplementary data

Supplementary data to this article can be found online at https://doi.org/10.1016/j.quascirev.2021.106958.

References

Andriashek, L.D., Atkinson, N., 2007. Buried channels and glacial-drift aquifers in the Fort McMurray region, northeast Alberta. Earth Sciences Report 2007-01. Alberta Geological Survey. Alberta Energy Utilities Board 160.

Astakhov, V.I., Isayeva, L.L., 1988. The 'ice-hill': an example of 'retarded deglaciation' in Siberia. Quat. Sci. Rev. 7, 29–40.

Astakhov, V.I., Kaplyanskaya, F.A., Tarnogradskiy, V.D., 1996. Pleistocene permafrost of West Siberia as a deformable glacier bed. Permafrost Periglac 7, 165–191.

Atkinson, N., Andriashek, L.D., Slattery, S.R., 2013. Morphological analysis and evolution of buried tunnel valleys in northeast Alberta, Canada. Quat. Sci. Rev. 65, 53–72.

Bailey, I., Hole, G.M., Foster, G.L., Wilson, P.A., Storey, C.D., Trueman, C.N., Raymo, M.E., 2013. An alternative suggestion for the Pliocene onset of major northern hemisphere glaciation based on the geochemical provenance of North Atlantic Ocean ice-rafted debris. Quat. Sci. Rev. 75, 181–194.

Balco, G., Rovey, C.W., II, 2008. An isochron method for cosmogenic-nuclide dating of buried soils and sediments. Am. J. Sci. 308, 1083–1114.

Balco, G., Rovey, C.W., II, 2010. Absolute chronology for major Pleistocene advances of the Laurentide ice sheet. Geology 38, 795–798.

Balkwill, H.R., Bustin, R.M., 1975. Stratigraphic and structural studies, central Ellesmere Island and eastern Axel Heiberg Island, District of Franklin. Geological Survey of Canada, pp. 513–517. Paper 75-1A.

Barendregt, R.W., Duk-Rodkin, A., 2004. Chronology and extent of late Cenozoic ice sheets in North America: a magnetostratigraphic assessment. In: Ehlers, J., Gibbard, P.L. (Eds.), Quaternary Glaciations – Extent and Chronology, Part II. Elsevier, Amsterdam, pp. 1–7.

Barendregt, R.W., Vincent, J.-S., 1990. Late cenozoic paleomagnetic record of Duck Hawk Bluffs, Banks Island, Canadian Arctic Archipelago. Can. J. Earth Sci. 27, 124–130.

Barendregt, R.W., Thomas, F.F., Irving, E., Baker, J., Stalker, A.M., Churcher, C.S., 1991. Stratigraphy and paleomagnetism of the Jaw Face section, Wellsch Valley site,

Saskatchewan. Can. J. Earth Sci. 28, 1353–1364.
Barendregt, R.W., Enkin, J.E., Duk-Rodkin, A., Baker, J., 1996. Paleomagnetic evidence for late Cenozoic glaciations in the Mackenzie Mountains of the Northwest Territories, Canada. Can. J. Earth Sci. 33, 896–903.
Barendregt, R.W., Irving, E., Christiansen, E.A., Sauer, E.K., Schreiner, B.T., 1998. Stratigraphy and paleomagnetism of Late Pliocene and Pleistocene sediments from Wellsch Valley and Swift Current Creek areas, southwestern Saskatchewan, Canada. Can. J. Earth Sci. 35, 1347–1361.
Barendregt, R.W., Enkin, J.E., Tessler, D.L., 2012. Magnetostratigraphy of late Neogene glacial, interglacial, and preglacial sediments in the Saskatoon and Regina areas, Saskatchewan, Canada. Stud. Geophys. Geod. 56, 705–724.
Batchelor, C.L., Dowdeswell, J.A., Pietras, J.T., 2013a. Seismic stratigraphy, sedimentary architecture and palaeo-glaciology of the Mackenzie Trough: evidence for two Quaternary ice advances and limited fan development on the western Canadian Beaufort Sea margin. Quat. Sci. Rev. 65, 73–87.
Batchelor, C.L., Dowdeswell, J.A., Pietras, J.T., 2013b. Variable history of Quaternary ice-sheet advance across the Beaufort Sea margin. Arctic Ocean. Geology 41, 131–134.
Batchelor, C.L., Dowdeswell, J.A., Pietras, J.T., 2014. Evidence for multiple Quaternary ice advances and fan development from the Amundsen Gulf cross-shelf trough and slope, Canadian Beaufort Sea margin. Mar. Petrol. Geol. 52, 125–143.
Batchelor, C.L., Margold, M., Krapp, M., Murton, D.K., Dalton, A.S., Gibbard, P.L., Manica, A., 2019. The configuration of Northern Hemisphere ice sheets through the Quaternary. Nat. Commun. 10, 1–10.
Benn, D.I., 1994. Fabric shape and the interpretation of sedimentary fabric data. J. Sediment. Res. 64, 910–915.
Benn, D.I., 2004a. Macrofabric. In: Evans, D.J.A., Benn, D.I. (Eds.), A Practical Guide to the Study of Glacial Sediments. Arnold, London, pp. 93–114.
Benn, D.I., 2004b. Clast morphology. In: Evans, D.J.A., Benn, D.I. (Eds.), A Practical Guide to the Study of Glacial Sediments. Arnold, London, pp. 77–92.
Benn, D.I., Ballantyne, C.K., 1993. The description and representation of clast shape. Earth Surf. Process. Landforms 18, 665–672.
Benn, D.I., Ballantyne, C.K., 1994. Reconstructing the transport history of glacigenic sediments: a new approach based on the co-variance of clast form indices. Sediment. Geol. 91, 215–227.
Benn, D.I., Evans, D.J.A., 1996. The interpretation and classification of subglacially-deformed materials. Quat. Sci. Rev. 15, 23–52.
Benn, D.I., Evans, D.J.A., Phillips, E.R., Hiemstra, J.F., Walden, J., Hoey, T.B., 2004. The research project – a case study of Quaternary glacial sediments. In: Evans, D.J.A., Benn, D.I. (Eds.), A Practical Guide to the Study of Glacial Sediments. Arnold, London, pp. 209–234.
Berends, C.J., de Boer, B., Dolan, A.M., Hill, D.J., van de Wal, R.S.W., 2019. Modelling ice sheet evolution and atmospheric CO_2 during the Late Pliocene. Clim. Past 15, 1603–1619.
Blow, R.A., Hamilton, N., 1978. Effect of compaction on the acquisition of a detrital remanent magnetization in fine-grained sediments. Geophys. J. 52, 13–23.
Boulton, G.S., Dobbie, K.E., Zatsepin, S., 2001. Sediment deformation beneath glaciers and its coupling to the subglacial hydraulic system. Quatern. Int. 86, 3–28.
Brown, V.H., Stokes, C.R., Ó Cofaigh, C., 2011. The glacial geomorphology of the north-west sector of the Laurentide Ice Sheet. J. Maps 7, 409–428.
Burn, C.R., 1988. The development of near-surface ground ice during the Holocene at sites near Mayo, Yukon Territory, Canada. J. Quat. Sci. 3, 31–38.
Bustin, R.M., 1982. Beaufort Formation, eastern Axel Heiberg Island, Canadian Arctic Archipelago. Bull. Can. Petrol. Geol. 30, 140–149.
Campbell, I.A., Evans, D.J.A., 1990. Glaciotectonism and Landsliding in Little Sandhill Creek, Alberta. Geomorphology 4, 19–36.
Clark, C.D., 1997. Reconstructing the evolutionary dynamics of former ice sheets using multi-temporal evidence, remote sensing and GIS. Quat. Sci. Rev. 16, 1067–1092.
Coulombe, S., Fortier, D., Lacelle, D., Kanevskiy, M., Shur, Y., 2019. Origin, burial and preservation of late Pleistocene-age glacier ice in Arctic permafrost (Bylot Island, NU, Canada). Cryosphere 13, 97–111.
Cowan, D.S., 1985. Structural styles in Mesozoic and Cenozoic mélanges in the western Cordillera of North America. Geol. Soc. Am. Bull. 96, 451–462.
Craig, B.J., Fyles, J.G., 1960. Pleistocene Geology of Arctic Canada. Geological Survey of Canada, p. 21. https://doi.org/10.4095/101191. Paper 60-10.
Craig, B.J., Fyles, J.G., 1965. Quaternary of arctic Canada. In: Anthropegene Period in Arctic and Subarctic, vol. 143. Scientific Research Institute of the Geology of the Arctic, Transactions, State Geological Committee, USSR, Moscow, pp. 5–33 (In Russian, with English summary).
Crickmay, C.H., 1967. A note on the term bocanne. Am. J. Sci. 265, 626–627.
Dalton, A.S., Margold, M., Stokes, C.R., Tarasov, L., Dyke, A.S., 66 others, 2020. An updated radiocarbon-based ice margin chronology for the last deglaciation of the North American Ice Sheet Complex. Quat. Sci. Rev. 234, 106223.
Davies, N.S., Gosse, J.C., Rybczynski, N., 2014. Cross-bedded woody debris from a Pliocene forested river system in the high arctic: Beaufort Formation, Meighen Island, Canada. J. Sediment. Res. 84, 19–25.
Dawson, G.M., 1881. Report on an Exploration from Port Simpson on the Pacific Coast, to Edmonton on the Saskatchewan, Embracing a Portion of the Northern Part of British Columbia and the Peace River Country, 1879. Geological Survey of Canada, pp. 1–142. https://doi.org/10.4095/302782. Report of Progress 1879-1880, Part B.
De Schepper, S., Gibbard, P.L., Salzmann, U., Ehlers, J., 2014. A global synthesis of the marine and terrestrial evidence for glaciations during the Pliocene Epoch. Earth Sci. Rev. 135, 83–102.
Denham, C.R., Chave, A.D., 1982. Detrital remanent magnetization: Viscosity theory of the lock-in zone. J. Geophys. Res. 87, 7126–7130.
Devaney, J.R., 1991. Clastic sedimentology of the Beaufort Formation, Prince Patrick Island, Canadian Arcic Islands: Late Tertiary sandy braided river deposits with woody detritus beds. Arctic 4, 206–216.
Dolan, A.M., Haywood, A.M., Hunter, S.J., Tindall, J.C., Dowsett, H.J., Hill, D.J., Pickering, S.J., 2015. Modelling the enigmatic Late Pliocene Glacial Event – Marine Isotope Stage M2. Global Planet. Change 128, 47–60.
Duk-Rodkin, A., Barendregt, R.W., 2011. Stratigraphical record of glacials/interglacials in northwest Canada. In: Ehlers, J., Gibbard, P.L. (Eds.), Quaternary Glaciations – Extent and Chronology, Developments in Quaternary Science, vol. 15. Elsevier, Amsterdam, pp. 661–698.
Duk-Rodkin, A., Hughes, O.L., 1994. Tertiary-Quaternary drainage of the pre-glacial Mackenzie Basin. In: Ager, T.A., White, J.M., Matthews Jr., J.V. (Eds.), Tertiary Quaternary Boundaries, 22/23. Quatern. Int., pp. 221–241
Duk-Rodkin, A., Barendregt, R.W., Froese, G.D., Weber, F., Enkin, R., Smith, I.R., Waters, P., Klassen, R., 2004. Timing and extent of Plio-Pleistocene glaciations in north-western Canada and east-central Alaska. In: Ehlers, J., Gibbard, P.L. (Eds.), Quaternary Glaciations – Extent and Chronology, Part II. Elsevier, Amsterdam, pp. 313–345.
Dwyer, G.S., Chandler, M.A., 2009. Mid-Pliocene sea level and continental ice volume based on coupled benthic Mg/Ca palaeotemperatures and oxygen isotopes. Philos. T R Soc. A 367, 157–168.
Dyke, A.S., 1993. Landscapes of cold-centred Late Wisconsinan ice caps, Arctic Canada. Prog. Phys. Geogr. 17, 223–247.
Dyke, A.S., Evans, D.J.A., 2003. Ice-marginal terrestrial landsystems: northern Laurentide and Innuitian ice sheet margins. In: Evans, D.J.A. (Ed.), Glacial Landsystems. Hodder Arnold, pp. 143–165.
Dyke, A.S., Prest, V.K., 1987. Late Wisconsinan and Holocene history of the Laurentide Ice Sheet. Geog. Phys. Qutern. 41, 237–263.
Dyke, A.S., Savelle, J.M., 2000. Major end moraines of Younger Dryas age on Wollaston Peninsula, Victoria Island, Canadian Arctic: implications for palaeoclimate and for formation of hummocky moraine. Can. J. Earth Sci. 37, 601–619.
Easterbrook, D.J., 1983. Remanent magnetism in glacial tills and related diamictions. In: Evenson, E.G., Schluchter, C., Rabassa, J. (Eds.), Tills and Related Deposits, pp. 303–313. Rotterdam, The Netherlands, Balkema.
Easterbrook, D.J., 1988. Paleomagnetism of Quaternary deposits. In: Easterbrook, D.J. (Ed.), Quaternary, vol. 227. Geological Society of America, Special Paper, pp. 111–122.
England, J.H., Furze, M.F.A., Doupé, J.P., 2009. Revision of the NW Laurentide Ice Sheet: implications for paleoclimate, the northeast extremity of Beringia, and Arctic Ocean sedimentation. Quat. Sci. Rev. 28, 1573–1596.
Erlanger, E.D., Granger, D.E., Gibbon, R.J., 2012. Rock uplift rates in South Africa from isochron burial dating of fluvial and marine terraces. Geology 40, 1019–1022.
Evans, D.J.A., 2000a. A gravel outwash/deformation till continuum, Skalafellsjokull, Iceland. Geogr. Ann. 82A, 499–512.
Evans, D.J.A., 2000b. Quaternary geology and geomorphology of the Dinosaur Provincial Park area and surrounding plains, Alberta, Canada: the identification of former glacial lobes, drainage diversions and meltwater flood tracks. Quat. Sci. Rev. 19, 931–958.
Evans, D.J.A., 2009. Controlled moraine: origins, characteristics and palaeoglaciological implications. Quat. Sci. Rev. 28, 183–308.
Evans, D.J.A., 2010. Controlled moraine development and debris transport pathways in polythermal plateau icefields: examples from Tungnafellsjokull, Iceland. Earth Surf. Process. Landforms 35, 1430–1444.
Evans, D.J.A., 2018. Till – A Glacial Process Sedimentology. Wiley-Blackwell, p. 390.
Evans, D.J.A., Benn, D.I., 2004. Facies description and the logging of sedimentary exposures. In: Evans, D.J.A., Benn, D.I. (Eds.), A Practical Guide to the Study of Glacial Sediments. Arnold, London, pp. 11–51.
Evans, D.J.A., Phillips, E.R., Hiemstra, J.F., Auton, C.A., 2006. Subglacial till: formation, sedimentary characteristics and classification. Earth Sci. Rev. 78, 115–176.
Evans, D.J.A., Twigg, D.R., Rea, B.R., Shand, M., 2007. Surficial geology and geomorphology of the Brúarjökull surging glacier landsystem. J. Maps 2007, 349–367.
Evans, D.J.A., Hiemstra, J.F., Boston, C.M., Leighton, I., Ó Cofaigh, C., Rea, B.R., 2012. Till stratigraphy and sedimentology at the margins of terrestrially terminating ice streams: case study of the western Canadian prairies and high plains. Quat. Sci. Rev. 46, 80–125.
Evans, D.J.A., England, J.H., LaFarge, C., Coulthard, R.D., Lakeman, T.R., Vaughan, J.M., 2014. Quaternary geology of the Duck Hawk Bluffs, southwest Banks Island, Arctic Canada: a re-investigation of a critical terrestrial type locality for glacial and interglacial events bordering the Arctic Ocean. Quat. Sci. Rev. 91, 82–123.
Evans, D.J.A., Roberts, D.H., Evans, S.C., 2016. Multiple subglacial till deposition: a modern exemplar for Quaternary palaeoglaciology. Quat. Sci. Rev. 145, 183–203.
Eyles, N., Eyles, C.H., Miall, A.D., 1983. Lithofacies types and vertical profile models; an alternative approach to the description and environmental interpretation of glacial diamict and diamictite sequences. Sedimentology 30, 393–410.
Eyles, N., Day, T.E., Gavican, A., 1987. Depositional controls on the magnetic characteristics of lodgement tills and other glacial diamict facies. Can. J. Earth Sci. 24, 2436–2458.
Froese, D.G., Westgate, J.A., Reyes, A.V., Enkin, R.J., Preece, S.J., 2008. Ancient permafrost and a future, warmer Arctic. Science 321, 1648.
Fulton, R.J., Klassen, R.W., 1969. Quaternary Geology, Northwest District of Mackenzie. Geological Survey of Canada, Report of Activities, Part A, pp. 193–194.

https://doi.org/10.4095/105991. Paper 69-1.
Fyles, J.G., 1989. High terrace sediments, probably of Neogene age, west-central Ellesmere Island, Northwest Territories. Geological Survey of Canada, Current Research, Part D, pp. 101–104. Paper 89-1D. https://doi.org/10.4095/126702.
Fyles, J.G., 1990. Beaufort Formation (late Tertiary) as seen from Prince Patrick Island, Arctic Canada. Arctic 43, 393–403.
Fyles, J.G., Hills, L.V., Matthews Jr., J.V., Barendregt, R., Baker, J., Irving, E., Jette, H., 1994. Ballast Brook and Beaufort Formations (Late Tertiary) on Northern Banks Island, Arctic Canada. Quat. Int. 22/23, 141–171.
Gao, C., McAndrews, J.H., Wang, X., Menzies, J., Turton, C.L., Wood, B.D., Pei, J., Kodors, C., 2012. Glaciation of North America in the James Bay Lowland, Canada, 3.5 Ma. Geology 40, 975–978.
Glasser, N.F., Hambrey, M.J., 2003. Ice-marginal terrestrial landsystems: Svalbard polythermal glaciers. In: Evans, D.J.A. (Ed.), Glacial Landsystems. Arnold, London, pp. 65–88.
Gosse, J.C., Philips, F.M., 2001. Terrestrial in situ cosmogenic nuclides: theory and application. Quat. Sci. Rev. 20, 1475–1560.
Grasby, S.E., Smith, I.R., Galloway, J.M., Bringué, M., 2019. Burning shales and extreme acidity – toxic stew in the Smoking Hills. In: Gervais, S.D., Irwin, D., Terlaky, V. (Eds.), (compilers), 47th Annual Yellowknife Geoscience Forum Abstracts; Northwest Territories Geological Survey, pp. 34–35. Yellowknife, NT.
Gravenor, C.P., Stupavsky, M., 1974. Magnetic susceptibility of the surface tills of southern Ontario. Can. J. Earth Sci. 11, 658–663.
Heim, D., 1983. Glaziare Entwasserung und Sanderbildung am Kotlujökull, Südisland. Polarforschung 53, 17–29.
Heim, D., 1992. Sandergenese und Gletscherentwasserung am Kotlujökull (Hofðabrekkujökull), Südisland. Polarforschung 62, 95–128.
Hicock, S.R., Dreimanis, A., 1992a. Sunnybrook drift in the Toronto area, Canada: reinvestigation and reinterpretation. In: Clark, P.U., Lea, P.D. (Eds.), The Last Interglacial–Glacial Transition in North America, vol. 270. Geol. S. Am. S., pp. 139–161
Hicock, S.R., Dreimanis, A., 1992b. Deformation till in the Great Lakes region: implications for rapid flow along the south-central margin of the Laurentide Ice Sheet. Can. J. Earth Sci. 29, 1565–1579.
Hidy, A.J., Gosse, J.C., Froese, D.G., Bond, J.D., Rood, D.H., 2013. A latest Pliocene age for the earliest and most extensive Cordilleran Ice Sheet in northwestern Canada. Quat. Sci. Rev. 61, 77–84.
Hills, L.V., 1969. Beaufort Formation, northwestern Banks Island, District of Franklin. Geological Survey of Canada, pp. 204–207. Report of Activities, Part A, Paper 69-1A. https://doi.org/10.4095/106000.
Hodgson, D.A., Vincent, J.-S., Fyles, J.G., 1984. Quaternary geology of central Melville Island, Northwest Territories. Geological Survey of Canada, p. 25. Paper 83-16. https://doi.org/10.4095/119784.
Hooyer, T.S., Iverson, N.R., Lagroix, F., Thomason, J.F., 2008. Magnetic fabric of sheared till: a strain indicator for evaluating the bed deformation model of glacier flow. J. Geophys. Res. 113, F02002.
Hrouda, F., 1982. Magnetic anisotropy of rocks and its application in geology and geophysics. Geophys. Surv. 5, 37–82.
Hughes, O.L., 1987. Late Wisconsinan Laurentide glacial limits of northwestern Canada: the Tutsieta Lake and Kelly Lake phases. Geological Survey of Canada, p. 19. https://doi.org/10.4095/122385. Paper 85-25.
Ingólfsson, O., Lokrantz, H., 2003. Massive ground ice body of glacial origin at Yugorski Peninsula, arctic Russia. Permafr. Periglac. Process. 14, 199–215.
Iverson, N.R., Hooyer, T.S., Thomason, J.F., Graesch, M., Shumway, J.R., 2008. The experimental basis for interpreting particle and magnetic fabrics of sheared till. Earth Surf. Process. Landforms 33, 627–645.
Jackson, M., 1991. Anisotropy of magnetic remanence: a brief review of mineralogical sources, physical origins, and geological applications, and comparison with susceptibility anisotropy. Pure Appl. Geophys. 136, 1–28.
Jackson, M.J., Banerjee, S.K., Marvin, J.A., Lu, R., Gruber, W., 1991. Detrital remanence inclination errors, and anhysteretic remanence anisotropy: quantitative model and experimental results. Geophys. J. Int. 104, 95–103.
Jakobsson, M., Mayer, L.A., Coakley, B., Dowdeswell, J.A., Forbes, S., Fridman, B., Hodnesdal, H., Noormets, R., Pedersen, R., Rebesco, M., Schenke, H.-W., Zarayskaya, Y., Accettella, A.D., Armstrong, A., Anderson, R.M., Bienhoff, P., Camerlenghi, A., Church, I., Edwards, M., Gardner, J.V., Hall, J.K., Hell, B., Hestvik, O.B., Kristoffersen, Y., Marcussen, C., Mohammad, R., Mosher, D., Nghiem, S.V., Pedrosa, M.T., Travaglini, P.G., Weatherall, P., 2012. The international bathymetric chart of the arctic ocean (IBCAO) version 3.0. Geophys. Res. Lett. 39, L12609. https://doi.org/10.1029/2012GL052219.
Jansen, E., Fronval, T., Rack, F., Channell, J.E.T., 2000. Pliocene-Pleistocene ice rafting history and cyclicity in the Nordic Seas during the last 3.5 Ma. Paleooceanography 15, 709–721.
Kaplyanskaya, F.A., Tarnogradskiy, V.D., 1986. Remnants of the Pleistocene ice sheets in the permafrost zone as an object for paleoglaciological research. Polar Geogr. Geol. 10, 257–266.
Kjaer, K.H., Sultan, L., Krüger, J., Schomacker, A., 2004. Architecture and sedimentation of outwash fans in front of the Myrdalsjökull Ice Cap. Iceland. Sediment. Geol. 172, 139–163.
Klassen, R.W., 1968. Unpublished Geological Survey of Canada Field Notebook.
Klassen, R.W., 1971. Surficial geology, Franklin Bay and brock river, district of Mackenzie, northwest territories. Geological Survey of Canada, Open File 48. https://doi.org/10.4095/129145, 2 sheets, scale 1:250 000.
Knies, J., Mattingsdal, R., Fabian, K., Grøsfjeld, K., Baranwal, S., Husum, K., De Schepper, S., Vogt, C., Andersen, N., Matthiessen, J., Andreassen, K., Jokat, W., Nam, S.-I., Gaina, C., 2014. Effect of early Pliocene uplift on the late Pliocene cooling the Arctic-Atlantic gateway. Earth Planet Sci. Lett. 387, 132–144.
Kokelj, S.V., Kokoszka, J., van der Sluijs, J., Rudy, A.C.A., Tunnicliffe, J., Shakil, S., Tank, S., Zolkos, S., 2020. Permafrost thaw couple slopes with downstream systems and effects propagate through Arctic drainage networks. Cryosphere Discuss. https://doi.org/10.5194/tc-2020-218 [preprint].
Kozarski, S., Kasprzak, L., 1994. Dynamics of the last Scandinavian ice sheet and glacio-dislocation metamorphism of unconsolidated deposits in west central Poland: a terminological approach. Z. Geomorphol. 95, 49–58.
Krüger, J., 1984. Clasts with stoss-lee form in lodgement tills: a discussion. J. Glaciol. 30, 241–243.
Krüger, J., 1997. Development of minor outwash fans at Kotlujökull, Iceland. Quat. Sci. Rev. 16, 649–659.
Kuc, M., Hills, L.V., 1971. Fossil mosses, Beaufort Formation (Tertiary), northwestern Banks Island, western Canada Arctic. Can. J. Bot. 49, 1089–1094.
Lacelle, D., Lauriol, B., Clark, I.D., Cardyn, R., Zdanowicz, C., 2007. Nature and origin of a Pleistocene-age massive ground ice body exposed in the Chapman Lake moraine complex, central Yukon Territory, Canada. Quat. Res. 68, 249–260.
Lacelle, D., Fisher, D.A., Coulombe, S., Fortier, D., Frappier, R., 2018. Buried remnants of the Laurentide Ice Sheet and connections to its surface elevation. Sci. Rep. 8, 13286.
Lakeman, T.R., England, J.H., 2012. Paleoglaciological insights from the age and morphology of the Jesse moraine belt, western Canadian Arctic. Quat. Sci. Rev. 47, 82–100.
Lakeman, T.R., England, J.H., 2013. Late Wisconsinan glaciation and postglacial relative sea level change on western Banks Island, Canadian Arctic Archipelago. Quat. Res. 80, 99–112.
Lakeman, T.R., England, J.H., 2014. Facies and stratigraphical analyses of glacial and interglacial sediments at Morgan Bluffs, Banks Island, Canadian Arctic Archipelago. Boreas 43, 895–913.
Lakeman, T.R., Pieńkowski, A.J., Nixon, F.C., Furze, M.F.A., Blasco, S., Andrews, J.T., King, E.L., 2018. Collapse of a marine-based ice stream during the early Younger Dryas chronozone, western Canadian Arctic. Geology 46, 211–214.
Lisiecki, I.E., Raymo, M., 2005. A Pliocene-Pleistocene stack of 57 globally distributed benthic δ18O records. Paleoceanography 20, PA1003.
Lowdon, J.A., Robertson, I.M., Blake Jr., W., 1971. Geological Survey of Canada Radiocarbon Dates XI. Radiocarbon 13, 255–324. https://doi.org/10.4095/102432. Geological Survey of Canada, Paper 71-7, 74.
Lukas, S., Benn, D.I., Boston, C.M., Brook, M., Coray, S., Evans, D.J.A., Graf, A., Kellerer-Pirklbauer, A., Kirkbride, M.P., Krabbendam, M., Lovell, H., Machiedo, M., Mills, S.C., Nye, K., Reinardy, B.T.I., Ross, F.H., Signer, M., 2013. Clast shape analysis and clast transport paths in glacial environments: a critical review of methods and the role of lithology. Earth Sci. Rev. 121, 96–116.
Mackay, J.R., 1958. The Anderson River map-area, vol. 5. Geographical Branch, Memoir, p. 137. N.W.T.
Mackay, J.R., 1972. The world of underground ice. Ann. Assoc. Am. Geogr. 62, 1–22.
Mackay, J.R., 1981. Dating of the Horton River breakthrough, District of Mackenzie. Current Research, Part B. Geological Survey of Canada, pp. 129–132. Paper 81-1B.
Mackay, J.R., 1990. Some observations on the growth and deformation of epigenetic, syngenetic and anti-syngenetic ice wedges. Perm. Periglac. 1, 15–29.
Mackay, J.R., Mathews, W.H., 1964. The role of permafrost in ice thrusting. J. Geol. 72, 378–380.
MacLean, B., Blasco, S., Bennet, R., Lakeman, T., Hughes-Clarke, J., Kuus, P., Patton, E., 2015. New marine evidence for a Late Wisconsinan ice stream in Amundsen Gulf, Arctic Canada. Quat. Sci. Rev. 114, 149–166.
Margold, M., Stokes, C.R., Clark, C.D., Kleman, J., 2015. Ice streams in the Laurentide Ice Sheet: a new mapping inventory. J. Maps 11, 380–395.
Mathews, W.H., Bustin, R.M., 1984. Why do the Smoking Hills smoke? Can. J. Earth Sci. 21, 737–742.
Mathews, W.H., Mackay, J.R., 1960. Deformation of Smoking by glacier ice and the influence of pore pressures and permafrost. T. Roy. Soc. Can., Section 3 (54), 27–36.
Mathews, W.H., Mackay, J.R., Rouse, G.E., 1989. Pleistocene geology and geomorphology of the Smoking Hills upland and lower Horton River Arctic coast of mainland Canada. Can. J. Earth Sci. 26, 1677–1687.
Matthews Jr., J.V., Ovenden, L.E., 1990. Late Tertiary plant macrofossils from localities in Arctic/Subarctic North America: a review of the data. Arctic 43, 364–392.
McClenaghan, M.B., Plouffe, A., McMartin, I., Campbell, J.E., Spirito, W.A., Paulen, R.C., Garrett, R.G., Hall, G.E.M., 2013. Till sampling and geochemical analytical protocols used by the Geological Survey of Canada. Geochem. Explor. Environ. Anal. 13, 285–301.
McMartin, I., Campbell, J.E., Dredge, L.A., 2019. Middle Wisconsinan marine shells near Repulse Bay, Nunavut, Canada: implications for Marine Isotope Stage 3 ice-free conditions and Laurentide Ice Sheet dynamics in north-west Hudson Bay. J. Quat. Sci. 34, 64–75.
Miall, A.D., 1979. Mesozoic and Tertiary geology of Banks Island, Arctic Canada: the history of an unstable craton margin, 387. Geological Survey of Canada, Memoir, p. 235. https://doi.org/10.4095/105620.
Miller, K.G., Mountain, G.S., Wright, J.D., Browning, J.V., 2011. A 180-million-year record of sea level and ice volume variations from continental margin and deep-sea isotopic records. Oceanography 24, 40–53.
Murton, J.B., Waller, R.I., Hart, J.K., Whiteman, C.A., Pollard, W.H., Clark, I.D., 2004. Stratigraphy and glaciotectonic structures of a relict deformable bed of

permafrost at the northwestern margin of the Laurentide ice sheet, Tuktoyaktuk Coastlands, Canada. J. Glaciol. 50, 399–412.
Murton, J.B., Whiteman, C.A., Waller, R.I., Pollard, W.H., Clark, I.D., Dallimore, S.R., 2005. Basal ice facies and supraglacial melt-out till of the Laurentide ice sheet, Tuktoyaktuk coastlands, western arctic Canada. Quat. Sci. Rev. 24, 681–708.
Norris, D.K., 1981. Geology, Aklavik, District of Mackenzie. Geological Survey of Canada. https://doi.org/10.4095/109706. Map 1517A, scale 1:250 000.
Ó Cofaigh, C., Lemmen, D.S., Evans, D.J.A., Bednarski, J., 1999. Glacial landform-sediment assemblages in the Canadian High Arctic and their implications for late Quaternary glaciation. Ann. Glaciol. 28, 195–201.
Ó Cofaigh, C., Evans, D.J.A., England, J., 2003. Ice-marginal terrestrial landsystems: sub-polar glacier margins of the Canadian and Greenland high arctic. In: Evans, D.J.A. (Ed.), Glacial Landsystems. Arnold, London, pp. 44–64.
Okulitch, A.V., Irwin, D., 2017. Geological compilation of the Western Mainland and Arctic Islands of the Northwest Territories. NWT Open File 2016-09.
Porter, C., Morin, P., Howat, I., Noh, M.-J., Bates, B., Peterman, K., Keesey, S., Schlenk, M., Gardiner, J., Tomko, K., Willis, M., Kelleher, C., Cloutier, M., Husby, E., Foga, S., Nakamura, H., Platson, M., Wethington Jr., M., Williamson, C., Bauer, G., Enos, J., Arnold, G., Kramer, W., Becker, P., Doshi, A., D'Souza, C., Cummens, P., Laurier, F., Bojesen, M., 2018. ArcticDEM. https://doi.org/10.7910/DVN/OHHUKH. Harvard Dataverse, vol. 1 accessed 06-01-18.
Powers, M.C., 1953. A new roundness scale for sedimentary particles. J. Sediment. Petrol. 23, 117–119.
Rainbird, R.H., 2019a. Bedrock geology, Erly Lake, Northwest Territories-Nunavut, NTS 97-A. Canadian Geoscience Map 378. https://doi.org/10.4095/313540 scale 1:250 000.
Rainbird, R.H., 2019b. Bedrock geology, Brock River, Northwest Territories-Nunavut, NTS 97-D. Geological Survey of Canada. Canadian Geoscience Map 407. https://doi.org/10.4095/314723 scale 1:250 000.
Rampton, V.N., 1981. Surficial Geology, Malloch Hill (Parts of 97F and 107E). Geological Survey of Canada. https://doi.org/10.4095/109692. Map 30-1979. scale 1:250 000.
Rampton, V.N., 1988. Quaternary Geology of the Tuktoyaktuk Coastlands, Northwest Territories, vol. 423. Geological Survey of Canada, Memoir, p. 98. https://doi.org/10.4095/126937.
Richardson, J., 1828. Narrative of the eastern detachment of the expedition. In: Franklin, J. (Ed.), Narrative of a Second Expedition to the Shores of the Polar Sea in the Years 1825, 1826, 1827. Murray, London, pp. 187–283.
Rudy, A.C.A., Lamoureux, S.F., Kokelj, S.V., Smith, I.R., England, J.H., 2017. Accelerating thermokarst transforms ice-cored terrain triggering a down-stream cascade to the ocean. Geophys. Res. Lett. 44 (11), 080-11,087.
Schomacker, A., Kruger, J., Kurth, K., 2006. Ice-cored drumlins at the surge-type glacier Bruarjökull, Iceland: a transitional-state landform. J. Quat. Sci. 21, 85–93.
Segal, R.A., Lantz, T.C., Kokelj, S.V., 2016. Acceleration of thaw slump activity in glaciated landscapes of the western Canadian Arctic. Environ. Res. Lett. 11, 034025.
Selwyn, A.E.C., 1877. Report on exploration in the Yukon and Mackenzie basins, Northern Territories. Geological Survey of Canada, Annual Report, Part D, pp. 1–163.
Sharp, M.J., 1982. Modification of clasts in lodgement tills by glacial erosion. J. Glaciol. 28, 475–481.
Smith, I.R., 2020. Kimberlite indicator mineral studies on Banks Island, Northwest Territories: assessing the potential for diamond-bearing kimberlite. Geological Survey of Canada, Open File 8726, 45. https://doi.org/10.4095/326157.
Smith, I.R., Evans, D.J.A., 2018. Kimberlite indicator minerals and glacial reconstructions in Tertiary Beaufort Formation and Quaternary glacial deposits, Smoking Hills, NT. Geological Survey of Canada, pp. 22–40. Open File 8482.
Smith, I.R., Lesk-Windfield, K., 2012. An updated assessment of ground ice and permafrost geology-related observations based on seismic shothole drillers' log records, Northwest Territories and northern Yukon. Geological Survey of Canada, p. 1. https://doi.org/10.4095/290974. Open File 7061, 1 .zip file.
Spedding, N., Evans, D.J.A., 2002. Sediments and landforms at Kviarjokull, southeast Iceland: a reappraisal of the glaciated valley landsystem. Sediment. Geol. 149, 21–42.
St-Onge, D.A., McMartin, I., 1995. Quaternary geology of the Inman River area, Northwest Territories. Geol. Surv. Can. Bull. 446, 59. https://doi.org/10.4095/203578.
St-Onge, D.A., McMartin, I., 1999. La moraine de Lac Bluenose (Territoires du Nord-Ouest), une moraine à noyau de glace de glacier. Géogr. Phys. Quaternaire 53, 287–295.
Stashin, S.A., 2021. Late Cenozoic Basin Evolution of the Western Canadian Arctic Archipelago: the Beaufort Formation and Iperk Sequence. M.Sc. thesis. Dalhousie University, Halifax, NS, p. 172.
Stokes, C.R., Clark, C.D., Winsborrow, M., 2006. Subglacial bedform evidence for a major palaeo-ice stream in Amundsen Gulf and its retreat phases, Canadian Arctic Archipelago. J. Quat. Sci. 21, 300–412.
Stokes, C.R., Clark, C.D., Storrar, R., 2009. Major changes in ice stream dynamics during deglaciation of the north-western margin of the Laurentide Ice Sheet. Quat. Sci. Rev. 28, 721–738.
Stokes, C.R., Tarasov, L., Dyke, A.S., 2012. Dynamics of the north American ice sheet complex during its inception and build-up to the last glacial maximum. Quat. Sci. Rev. 50, 86–104.
Tarasov, L., Dyke, A.S., Neal, R.M., Peltier, W.R., 2012. A data-calibrated distribution of deglacial chronologies for the North American ice complex from glaciological modelling. Earth Planet Sci. Lett. 315–316, 30–40.
Tarling, D.H., Hrouda, F., 1993. The Magnetic Anisotropy of Rocks. Chapman and Hall, London, p. 218.
Thorsteinsson, R., 1961. History and geology of Meighen Island. Geol. Surv. Can. Bull. 75, 19.
Thorsteinsson, R., Tozer, E.T., 1962. Banks, Victoria and Stefansson islands, Arctic Archipelago, 330. Geological Survey of Canada, Memoir, p. 85.
Tozer, E.T., 1956. Geological reconnaissance, Prince Patrick, eglinton, and western Melville islands, arctic archipelago, northwest territories. Geological Survey of Canada, p. 32. https://doi.org/10.4095/101290. Paper 55-5.
Tozer, E.T., 1960. Summary account of Mesozoic and Tertiary stratigraphy, Canadian Arctic Archipelago. Geological Survey of Canada, p. 25. Paper 60-5.
Tozer, E.T., 1970. Geology of the arctic archipelago. In: Douglas, R.J.W. (Ed.), Geology and Economic Minerals of Canada. Geological Survey of Canada, Economic Geology Report No. 1, fifth ed., pp. 547–589. https://doi.org/10.4095/106153.
Traverse, A., 2007. Palynological Laboratory Techniques. Paleopalynology, Second Edition. Topics in Geobiology Series, vol. 28. Springer-Verlag, New York, pp. 615–772.
Tsui, P.C., Cruden, D.M., Thomson, S., 1989. Ice thrust terrains and glaciotectonic settings in central Alberta. Can. J. Earth Sci. 26, 1308–1318.
Vaughan, J.M., England, J.H., Evans, D.J.A., 2014. Glaciotectonic deformation and reinterpretation of the Worth Point stratigraphic sequence: Banks Island, NT, Canada. Quat. Sci. Rev. 91, 124–145.
Veillette, J.J., 2004. Surficial Geology and Glacial History of Tuktut Nogait National Park, District of Mackenzie, N.W.T. Technical Report 04-01, Parks Canada.
Vincent, J.-S., 1983. La géologie du Quaternaire et la géomorphologie de l'île Banks, Arctique canadien, 405. Geological Survey of Canada, Memoir, p. 118. https://doi.org/10.4095/119517 map 1565A, scale 1:500 000.
Vincent, J.-S., 1984. Quaternary stratigraphy of the western Canadian Arctic archipelago. In: Fulton, R.J. (Ed.), Quaternary Stratigraphy of Canada - A Canadian Contribution to IGCP Project 24. Geological Survey of Canada, pp. 87–100. https://doi.org/10.4095/119761. Paper 84-10.
Vincent, J.-S., 1988. Unpublished GSC Field Notebook.
Vincent, J.-S., 1990. Late Tertiary and Early Pleistocene deposits and history of Banks Island, southwestern Canadian Arctic Archipelago. Arctic 43, 339–363.
Vincent, J.-S., 1991. Unpublished GSC Field Notebook.
Vincent, J.-S., Occhietti, S., Rutter, N.W., Lortie, G., Guilbault, J.P., Boutray, B.De, 1983. The late Tertiary-Quaternary stratigraphic record of the Duck Hawk Bluffs, Banks Island, Canadian Arctic Archipelago. Can. J. Earth Sci. 20, 1694–1712.
Waller, R.I., Tuckwell, G.W., 2005. Glacier-permafrost interactions and glaciotectonic landform generation at the margins of the Leverett Glacier, West Greenland. In: Harris, C., Murton, J.B. (Eds.), Cryospheric Systems: Glaciers and Permafrost, vol. 242. Geological Society of London Special Publication, pp. 39–50.
Waller, R.I., Murton, J.B., Whiteman, C.A., 2009. Geological evidence for subglacial deformation of Pleistocene permafrost. Proc. Geol. Assoc. 120, 155–162.
Williams, C.J., Mendell, E.K., Murphy, J., Wesley, M.C., Johnson, A.H., Richter, S.L., 2008. Paleoenvironmental reconstruction of a Middle Miocene forest from the western Canadian Arctic. Palaeogeogr. Palaeocl. 261, 160–176.
Wilson, D.G., 1976. Eureka sound and Beaufort Formation, yelverton Bay, Ellesmere island, district of Franklin. Geological Survey of Canada, pp. 453–455. https://doi.org/10.4095/104244. Paper 76-1A.
Yorath, C.J., Cook, D., 1981. Cretaceous and Tertiary Stratigraphy and Plaeogeography, Northern Interior Plains. District of Mackenzie, vol. 398. Geological Survey of Canada Memoir, Ottawa, p. 76. https://doi.org/10.4095/109299.
Yorath, C.J., Balkwill, H.R., Klassen, R.W., 1969. Geology of the eastern part of the northern interior and arctic coastal plains, northwest territories. Geological Survey of Canada, p. 29. https://doi.org/10.4095/101454. Paper 68-27.
Yorath, C.J., Balkwill, H.R., Klassen, R.W., 1975. Franklin Bay and Malloch Hill Map-Areas, District of Mackenzie. Geological Survey of Canada. https://doi.org/10.4095/102527. Paper 74-36, 35 p., map 1403A, scale 1:250 000.